

Topics in Fluid Mechanics

G. P. Benham

These lecture notes are largely based on the notes by A. C. Fowler.
Some sections have been removed and a few have been added.

Mathematical Institute, Oxford University

November 25, 2022

Chapter 1

Thin film flows

1.1 Lubrication theory

Lubrication theory refers to a class of approximations of the Navier–Stokes equations which are based on a large *aspect ratio* of the flow. The aspect ratio is the ratio of two different directional length scales of the flow, as for example the depth and the width. Typical examples of flows where the aspect ratio is large (or small, depending on which length is in the numerator) are lakes, rivers, atmospheric winds, waterfalls, lava flows, and in an industrial setting, oil flows in bearings (whence the term lubrication theory). Lubrication theory forms a basic constituent of a viscous flow course and will not be dwelt on here.

In brief the Navier–Stokes equations for an incompressible take the form

$$\begin{aligned}\nabla \cdot \mathbf{u} &= 0, \\ \rho[\mathbf{u}_t + (\mathbf{u} \cdot \nabla)\mathbf{u}] &= -\nabla p + \mu \nabla^2 \mathbf{u},\end{aligned}\tag{1.1}$$

at least in Cartesian coordinates. It should be recalled that the actual definition of $\nabla^2 \equiv \nabla \cdot \nabla - \nabla \times \nabla \times$, and the components of $\nabla^2 \mathbf{u} = \nabla^2 u_i \mathbf{e}_i$ (we use the summation convention) is only applicable in Cartesian coordinates. For other systems, one can for example consult the appendix in Batchelor (1967).

We begin by non-dimensionalising the equations by choosing scales

$$\mathbf{x} \sim l, \quad t \sim \frac{l}{U}, \quad \mathbf{u} \sim U, \quad p - p_a \sim \frac{\mu U}{l};\tag{1.2}$$

this is the usual way to scale the equations, except that we have chosen to balance the pressure with the viscous terms. The pressure p_a is an ambient pressure, commonly atmospheric pressure. The resulting dimensionless equations are

$$\begin{aligned}\nabla \cdot \mathbf{u} &= 0, \\ Re \dot{\mathbf{u}} \equiv Re [\mathbf{u}_t + (\mathbf{u} \cdot \nabla)\mathbf{u}] &= -\nabla p + \nabla^2 \mathbf{u},\end{aligned}\tag{1.3}$$

where

$$Re = \frac{\rho U l}{\mu}\tag{1.4}$$

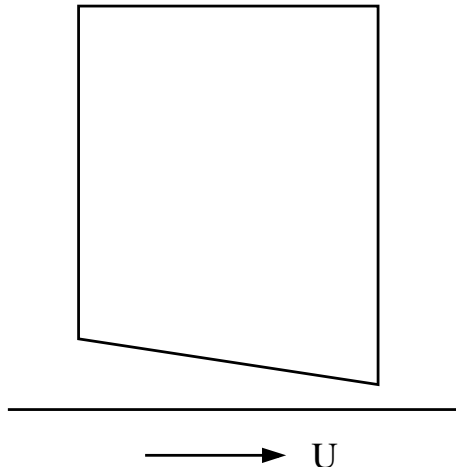


Figure 1.1: A slider bearing.

is the Reynolds number; the overdot denotes the material derivative. For $Re \ll 1$ we have Stokes flow, where the inertial terms can be neglected, and for $Re \gg 1$, boundary layers generally occur (and the pressure would be rescaled to balance the inertia terms, thus $p \sim Re$).

Lubrication theory describes a situation where the geometry of the flow allows the neglect of the inertial terms, even if the Reynolds number is not small. Suppose for example that l measures the extent of the flow in the x direction, but the fluid thickness in the (say) z direction is small. A simple example is the slider bearing, shown in figure 1.1, in which the fluid is confined between two surfaces, which we might take to be $z = 0$ and $z = h(x)$, and one of the surfaces moves at speed U relative to the other. To be specific, we assume a two-dimensional flow in which the coordinates are (x, z) , the velocity components are (u, w) , the bearing ($z = h$) is of finite length l and lies above a flat surface $z = 0$ which moves at speed U ; the bearing is open to the atmosphere at each end, and the gap width $h \sim d \ll l$. We define the small parameter

$$\varepsilon = \frac{d}{l}, \quad (1.5)$$

so that in non-dimensional terms, the bearing is at $z = \varepsilon h(x)$ (where we scaled the dimensional h with d , so that the dimensionless h is $O(1)$). It is then appropriate to rescale the variables as follows:

$$z \sim \varepsilon, \quad w \sim \varepsilon, \quad p \sim \frac{1}{\varepsilon^2}, \quad (1.6)$$

and the equations then take the form

$$\begin{aligned} u_x + w_z &= 0, \\ \varepsilon^2 Re \dot{u} &= -p_x + u_{zz} + \varepsilon^2 u_{xx}, \\ \varepsilon^4 Re \dot{w} &= -p_z + \varepsilon^2 (w_{zz} + \varepsilon^2 w_{xx}), \end{aligned} \quad (1.7)$$

with boundary conditions

$$\begin{aligned} u = 1, \quad w = 0 \quad \text{at} \quad z = 0, \\ u = w = 0 \quad \text{at} \quad z = h, \\ p = 0 \quad \text{at} \quad x = 0, 1. \end{aligned} \tag{1.8}$$

At leading order we then have $p = p(x, t)$, and thus, integrating, we obtain

$$u = \frac{z}{h} - \frac{1}{2}p_x(hz - z^2). \tag{1.9}$$

The final part of the solution comes from integrating the mass conservation equation from $z = 0$ to $z = h$. This gives

$$0 = -[w]_0^h = -\int_0^h w_z dz = \int_0^h u_x dz = \frac{\partial}{\partial x} \int_0^h u dz, \tag{1.10}$$

where we can take the differentiation outside the integral because u is zero at $z = h$. In fact we can write down (1.10) directly since it is an expression of conservation of mass across the layer; and this applies more generally, even if the base is not flat, and indeed even if both surfaces depend on time, and the result can be extended to three dimensions; see question 1.2. Calculating the flux from (1.9), we obtain

$$\int_b^s u dz = \frac{1}{2}h - \frac{1}{12}h^3 p_x = K \tag{1.11}$$

is constant. Given h , the solution for p can be found as a quadrature, and is

$$p = 6 \left[f_2(x) - \frac{f_2(1)f_3(x)}{f_3(1)} \right], \quad f_n(x) = \int_0^x \frac{dx}{h^n}. \tag{1.12}$$

In three dimensions, exactly the same procedure leads to the equation

$$\frac{1}{12} \nabla_H \cdot (h^3 \nabla_H p) = \frac{1}{2} h_x, \tag{1.13}$$

where the plate flow direction is taken along the x axis; derivation of this is left as an exercise.

1.2 Droplet dynamics

When one of the surfaces is a free surface (meaning it is free to deform), such as a droplet of liquid resting on a surface, or a rivulet flowing down a window pane, there are two differences which must be accounted for in formulating the problem. One is that the free surface is usually a material surface, so that a kinematic condition is appropriate. In three dimensions, this takes the form

$$w = s_t + us_x + vs_y - a. \tag{1.14}$$

Here, $z = s$ is the free surface, and (u, v, w) is the velocity; the term a is normally absent, but a non-zero value describes surface accumulation (which might for example be due to condensation); if $a < 0$ it describes ablation due for example to evaporation.

The other difference is that the boundary conditions at the free surface are generally not ones of prescribed velocity but of prescribed stress. In the common case of a droplet of liquid with air above, these conditions take the form

$$\sigma_{nn} = -p_a, \quad \sigma_{nt} = 0, \quad (1.15)$$

representing the fact that the atmosphere exerts a constant pressure on the surface, and no shear stress. Commonly the pressure is taken as *gauge* pressure, i. e., measured relative to atmospheric pressure, which is equivalent to taking $p_a = 0$ in (1.15). To unravel these conditions, we will consider the case of a two-dimensional incompressible flow. In this case, the components of the stress tensor are

$$\sigma_{11} = -p + \tau_1, \quad \sigma_{13} = \sigma_{31} = \tau_3, \quad \sigma_{33} = -p - \tau_1, \quad (1.16)$$

where

$$\tau_1 = 2\mu u_x, \quad \tau_3 = \mu(u_z + w_x), \quad (1.17)$$

and then with

$$\mathbf{n} = \frac{(-s_x, 1)}{(1 + s_x^2)^{1/2}}, \quad \mathbf{t} = \frac{(1, s_x)}{(1 + s_x^2)^{1/2}}, \quad (1.18)$$

we have

$$\begin{aligned} \sigma_{nn} = \sigma_{ij}n_i n_j &= -p - \frac{[\tau_1(1 - s_x^2) + 2\tau_3 s_x]}{1 + s_x^2}, \\ \sigma_{nt} = \sigma_{ij}n_i t_j &= \frac{[\tau_3(1 - s_x^2) - 2\tau_1 s_x]}{1 + s_x^2}. \end{aligned} \quad (1.19)$$

The dimensionless equations are virtually the same, as we initially scale $p - p_a$, τ_1 and τ_3 with $\mu U/l$, and then when the rescaling in (1.6) is done (note that consequently we rescale $\tau_3 \sim 1/\varepsilon$), the surface boundary conditions become

$$\begin{aligned} p + \frac{\varepsilon^2[\tau_1(1 - \varepsilon^2 s_x^2) + 2\tau_3 s_x]}{1 + \varepsilon^2 s_x^2} &= 0, \\ \tau_3(1 - \varepsilon^2 s_x^2) - 2\varepsilon^2 \tau_1 s_x &= 0, \end{aligned} \quad (1.20)$$

where

$$\tau_1 = 2u_x, \quad \tau_3 = u_z + \varepsilon^2 w_x. \quad (1.21)$$

Putting $\varepsilon = 0$, we thus obtain the leading order conditions

$$p = \tau_3 = 0 \quad \text{on} \quad z = s. \quad (1.22)$$

We can then integrate $u_{zz} = p_x$, assuming also a no slip base at $z = b$, to obtain an expression for the flux

$$\int_b^s u dz = -\frac{1}{3}h^3 p_x, \quad (1.23)$$

and the conservation of mass equation then integrates (see question 1.2) to give the evolution equation for $h = s - b$ in the form

$$h_t = \frac{1}{3} \frac{\partial}{\partial x} [h^3 p_x]. \quad (1.24)$$

1.2.1 Gravity

The astute reader will notice that something is missing. Unlike the slider bearing, nothing is driving the flow! Indeed, since $p = p(x, t)$ and $p = 0$ at $z = s$, $p = 0$ everywhere. Related to this is the fact that there is nothing to determine the velocity scale U . Commonly such droplet flows are driven by gravity. If we include gravity in the z momentum equation, then it takes the dimensional form $\dots = -p_z - \rho g \dots$, and since in the rescaled model all the other terms are negligible, the pressure will be hydrostatic, $p \approx p_a + \rho g(s - z)$, and this gives a natural scale for $p - p_a \sim \rho g d$, and equating this with the eventual pressure scale $\mu U l / d^2$ determines the velocity scale as

$$U = \frac{\rho g d^3}{\mu l}. \quad (1.25)$$

The dimensionless pressure then becomes $p = s - z$, so that $p_x = s_x$, and (1.24) now takes the form of a nonlinear diffusion equation,

$$h_t = \frac{1}{3} \frac{\partial}{\partial x} [h^3 s_x]. \quad (1.26)$$

One might wonder how the length scales l and d should be chosen; the answer to this, at least if the base is flat, is that it can be taken from the initial condition for s . The reason for this is that, since (1.26) is a diffusion equation, the drop will simply continue to spread out: there is no natural length scale in the model. Associated with this is the consequent fact that for an initial concentration of liquid at the origin (again on a flat base), the solution takes the form of a similarity solution (see question 1.6). On the other hand, if b is variable, then it provides a natural length scale. Indeed, for a basin shaped b (for example x^2 , dimensionlessly), the initial volume (or cross-sectional area) determines the eventual steady state as a lake with s constant, and both d and l prescribed.

1.2.2 Surface tension

Another way in which a natural length scale can occur in the model is through the introduction of surface tension at the interface. Let us digress for a moment to consider how surface tension arises. Surface tension is a property of interfaces, whereby they have an apparent strength. This is most simply manifested by the ability of small objects which are themselves heavier than water to float on the interface. The experiment is relatively easily done using a paper clip, and certain insects (water striders) have the ability to stay on the surface of a pond.

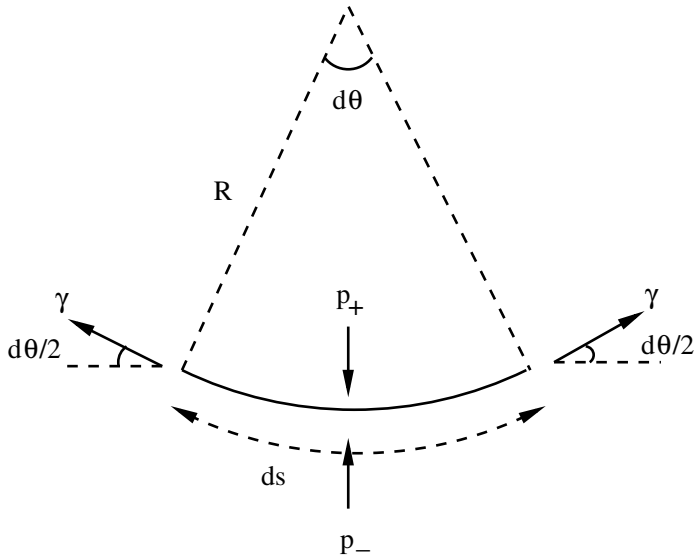


Figure 1.2: The simple mechanical interpretation of surface tension.

The simplest way to think about surface tension is mechanically. The interface between two fluids has an associated tension, such that if one draws a line in the interface of length l , then there is a force of magnitude γl which acts along this line: γ is the surface tension, and is a force per unit length. The presence of a surface tension causes an imbalance in the normal stress across the interface, as is indicated in figure 1.2, which also provides a means of calculating it. Taking ds as a short line segment in an interface subtending an angle $d\theta$ at its centre of curvature, a force balance normal to the interface leads to the condition

$$p_+ - p_- = \frac{\gamma}{R}, \quad (1.27)$$

where

$$R = \frac{ds}{d\theta} \quad (1.28)$$

is the *radius of curvature*, and its inverse $1/R$ is the curvature.

For a two-dimensional surface, the curvature is described by two *principal radii of curvature* R_1 and R_2 , the mean curvature is defined by

$$\kappa = \frac{1}{2} \left(\frac{1}{R_1} + \frac{1}{R_2} \right), \quad (1.29)$$

and the pressure jump condition is

$$p_+ - p_- = 2\gamma\kappa = \gamma \left(\frac{1}{R_1} + \frac{1}{R_2} \right), \quad (1.30)$$

although this is not much use to us unless we have a way of calculating the curvature of a surface. This leads us off into the subject of differential geometry, and we do not want to go there. A better way lies along the following path.

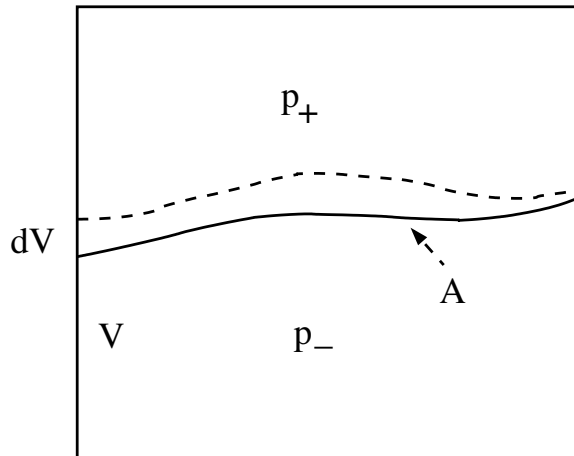


Figure 1.3: The energetic basis of surface tension.

The sceptical reader will in any case wonder what this surface tension actually is. It manifests itself as a force, but along a *line*? And what is its physical origin? The answer to this question veers towards the philosophical. We think we understand force, after all it pops up in Newton's second law, but how do we measure it? Pressure, for example, we conceive of as being due to the collision of molecules with a surface, and the measure of the force they exert is due to the momentum exchange at the surface. We pull on a rope, exerting a force, but the measure of the force is in the extension of the rope via Hooke's law. Force is apparently something we measure via its effect on momentum exchange, or on mechanical displacement; we can actually define force through these laws.

The more basic quantity is energy, which has a direct interpretation, whether as kinetic energy or internal energy (the vibration of molecules). And in fact Newton's second law for a particle is equivalent to the statement that the rate of change of energy is equal to the rate of doing work, and this might be taken as the fundamental law.

The meaning of surface tension actually arises through the property of an interface, which has a surface energy γ with units of energy per unit area. The interfacial condition then arises through the (thermodynamic) statement that in equilibrium the energy of the system is minimised.

To be specific, consider the situation in figure 1.3, where two fluids at pressures p_- and p_+ are separated by an interface with area A . Consider a displacement of the interface causing a change of volume dV as shown. Evidently the work done on the upper fluid is $p_+ dV$, which is thus its change of energy, and correspondingly the change for the lower fluid is $-p_- dV$. If the change of interfacial surface area is dA , then the total change of energy¹ is

$$dF = (p_+ - p_-) dV + \gamma dA, \quad (1.31)$$

¹This energy is the *Helmholtz free energy*.

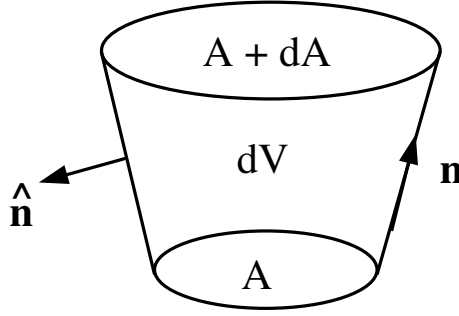


Figure 1.4: Calculation of $\frac{\partial A}{\partial V}$.

and at equilibrium this must be zero (since F is minimised). The equilibrium interfacial boundary condition is therefore

$$p_+ - p_- = -\gamma \frac{\partial A}{\partial V}, \quad (1.32)$$

which, it turns out, is equivalent to (1.30).

Computation of $\frac{\partial A}{\partial V}$ can be done as follows. We consider a displacement of the interface as shown in figure 1.4. An element of surface A is displaced to $A + dA$, and we can form a connecting volume dV such that the normal \mathbf{n} to the interface is always parallel to the connecting surface between the end faces A and $A + dA$. We need to distinguish between the normal $\hat{\mathbf{n}}$ to the surface of the connecting volume and the normal to the interfacial surface. Evidently we have $\mathbf{n} = \hat{\mathbf{n}}$ at the end faces, but $\mathbf{n} \cdot \hat{\mathbf{n}} = 0$ on the connecting cylindrical surface.

Applying the divergence theorem, we see that the change in area is

$$dA = \int_{\partial(dV)} \mathbf{n} \cdot \hat{\mathbf{n}} dS = \int_{dV} \nabla \cdot \mathbf{n} dV, \quad (1.33)$$

and thus

$$\frac{\partial A}{\partial V} = \nabla \cdot \mathbf{n}. \quad (1.34)$$

For example, if the interface is represented as $z = s(x, y, t)$, then

$$\nabla \cdot \mathbf{n} = -\nabla \cdot \left[\frac{\nabla s}{(1 + |\nabla s|^2)^{1/2}} \right], \quad (1.35)$$

where on the right hand side $\nabla = \nabla_H = \left(\frac{\partial}{\partial x}, \frac{\partial}{\partial y} \right)$, and for small interfacial displacement, this may be linearised to obtain

$$2\kappa = -\frac{\partial A}{\partial V} = -\nabla \cdot \mathbf{n} = \nabla \cdot \left[\frac{\nabla s}{(1 + |\nabla s|^2)^{1/2}} \right] \approx \nabla^2 s. \quad (1.36)$$

1.2.3 The capillary droplet

Now we use this in the droplet equation. Again we restrict attention to two-dimensional droplets. For three-dimensional droplets, see question 1.7. The surface boundary condition is now approximately $p - p_a = -\gamma s_{xx}$, and non-dimensionally

$$p = -\frac{1}{B}s_{xx} \quad \text{on} \quad z = s, \quad (1.37)$$

where B (commonly also written Bo) is the Bond number, given by

$$B = \frac{\rho g l^2}{\gamma}. \quad (1.38)$$

This gives a natural length scale for the droplet, by choosing $B = 1$, thus

$$l = \left(\frac{\gamma}{\rho g}\right)^{1/2}; \quad (1.39)$$

in this case the dimensionless pressure is $p = s - z - s_{xx}$, and thus mass conservation leads to

$$h_t = \frac{1}{3} \frac{\partial}{\partial x} [h^3(s_x - s_{xxx})], \quad (1.40)$$

and the surface tension term acts as a further stabilising term.²

Surface tension acts to limit the spread of a droplet. Indeed there is a steady state of (1.40) which is easily found. Suppose the base is flat, so $s = h$. We prescribe the cross-sectional area of the drop, A . In dimensionless terms, we thus require

$$\int h \, dx = 2\alpha = \left(\frac{\rho g}{\gamma}\right)^{1/2} \frac{A}{d}. \quad (1.41)$$

Let us choose d so that the maximum depth is one (note that the value of d remains to be determined). We can suppose that the drop is symmetric about the origin, and that its dimensionless half-width is λ , also to be determined. Thus

$$h(\pm\lambda) = 0, \quad h(0) = 1, \quad (1.42)$$

as well as (1.41), and both α and λ are to be determined.

A further condition is necessary at the margins. This is the prescription of a contact angle, which can be construed as arising through a balance of the surface tension forces at the three interfaces at the contact line: gas/liquid, liquid/solid, and solid/gas. All three interfaces have a surface energy, and minimisation of this corresponds to prescription of a contact angle. Specifically, if θ is the angle between the

²This can be seen by considering small perturbations about a uniform solution $h = s = 1$ (with a flat base), for which the linearised equation has normal mode solutions $\propto \exp(\sigma t + ikx)$, with $\sigma = -\frac{1}{3}(k^2 + k^4)$.

gas/liquid and liquid/solid interfaces, then resolution of the surface tension tangential to the wall leads to

$$\gamma_{\text{SL}} + \gamma \cos \theta = \gamma_{\text{SG}}, \quad (1.43)$$

where γ_{SL} is the solid/liquid surface energy, and γ_{SG} is the solid/gas surface energy. Defining $S = l \tan \theta / d$, this implies that

$$h_x = \mp S \quad \text{at} \quad x = \pm \lambda. \quad (1.44)$$

The steady state of (1.40) is easily found. The flux is zero, so $h_x - h_{xxx}$ is zero, and integration of this leads to

$$h = 1 - \left(\frac{\cosh x - 1}{\cosh \lambda - 1} \right), \quad (1.45)$$

and then (1.41) and (1.44) yield

$$\alpha = \frac{\lambda \cosh \lambda - \sinh \lambda}{\cosh \lambda - 1}, \quad \frac{\sinh \lambda}{\cosh \lambda - 1} = S. \quad (1.46)$$

$S(\lambda)$ is a monotonically decreasing function of λ (why?), and tends to one as $\lambda \rightarrow \infty$, and therefore the second relation determines λ providing $S > 1$. It seems there is a problem if $S < 1$, but this is illusory since both α and S depend on the unknown d , so it is best to solve

$$\frac{\alpha}{S} = \frac{A}{2l^2 \tan \theta} = \frac{\lambda \cosh \lambda - \sinh \lambda}{\sinh \lambda}; \quad (1.47)$$

the right hand side increases monotonically from 0 to ∞ as λ increases, and therefore provides a unique solution for λ for any values of A and θ ; d is then determined by either expression in (1.46).

It is of interest to see when the assumption $d \ll l$ is then valid. From (1.46),

$$\varepsilon = \tan \theta \left(\frac{\cosh \lambda - 1}{\sinh \lambda} \right). \quad (1.48)$$

The expression in λ increases monotonically from 0 to 1 as λ increases. Thus $\varepsilon \ll 1$ if either $\theta \ll 1$, or (if $\tan \theta \sim O(1)$) $\lambda \ll 1$. From (1.47), this is the case provided $A \ll l^2$, i. e., $\frac{\rho g A}{\gamma} \ll 1$. For air and water, this implies $A \ll 7 \text{ mm}^2$.

1.2.4 Stability

We now consider the stability of steady solutions of (1.40), which we take in the form

$$h_t = \left[\frac{1}{3} h^3 (h_x - h_{xxx}) \right]_x. \quad (1.49)$$

Before doing so, we comment on the meaning of the fourth derivative term, which is present due to surface tension. The gravity term is clearly diffusive (with a nonlinear diffusion coefficient $\frac{1}{3}h^3$), but what does the surface tension term represent? In other

contexts it is referred to as a long-range or non-local diffusion (or dispersion) term. To understand such a reference, suppose that the flux of a quantity having density ρ is given not by Fick's law $\mathbf{J} = -D\nabla\rho$, but by

$$\mathbf{J} = -D\nabla W, \quad W = \int_{\mathbf{R}^3} \rho(\mathbf{x} + \boldsymbol{\xi}, t) K(\boldsymbol{\xi}) d\boldsymbol{\xi}, \quad (1.50)$$

where the kernel function $K = K(\xi)$ (here $\xi = |\boldsymbol{\xi}|$) is spherically symmetric in an isotropic medium, and can be taken (by choice of D) to have integral over all space equal to one. If K is a delta function, $K = \delta(\mathbf{x} - \boldsymbol{\xi})$, then we regain Fick's law, but more generally we might suppose it is a Gaussian, for example. (1.50) allows a diffusive motion due to non-local concentrations. An example of such dependence might be in traffic flow, where the motion of individual 'molecules' (cars) is affected by the observation of conditions further ahead. Another example might be in herd migration.

If we suppose that K is delta function-like, in the sense that it varies rapidly with $\boldsymbol{\xi}$, then it is appropriate to approximate (1.50) by Taylor expansion of ρ , and this leads to

$$\mathbf{J} = -D\nabla\rho - D_2\nabla\nabla^2\rho + \dots, \quad (1.51)$$

where

$$D_2 = \frac{1}{6}D \int_{\mathbf{R}^3} \xi^2 K(\xi) d\boldsymbol{\xi} = \frac{2}{3}\pi D \int_0^\infty \xi^4 K(\xi) d\xi. \quad (1.52)$$

Solutions of the conservation law $\rho_t = -\nabla \cdot \mathbf{J}$, using the truncated expression in (1.51), have the normal mode form

$$\rho = e^{i\mathbf{k} \cdot \mathbf{x} + \sigma t}, \quad \sigma = -Dk^2 + D_2k^4, \quad (1.53)$$

and we see that the well-posedness ($\sigma < 0$ as $k \rightarrow \infty$) in this truncated form requires $D_2 < 0$, which seems unlikely, unless K becomes negative at large ξ .

If we use the full expression in (1.50), then we find that (1.53) is replaced by

$$\sigma = -4\pi k D I(k), \quad I(k) = \int_0^\infty r K(r) \sin kr dr \quad (1.54)$$

(use spherical polar coordinates and take the z axis in the direction of \mathbf{k}). For example, the (normalised) Gaussian

$$K(\xi) = \frac{1}{(\pi\nu)^{3/2}} e^{-\xi^2/\nu} \quad (1.55)$$

leads to

$$\sigma = -k^2 D e^{-\frac{1}{4}\nu k^2}, \quad (1.56)$$

and expansion of this for small ν (or k) leads to the truncated version above. Note that for the full expression, the limits $\nu \rightarrow 0$ and $k \rightarrow \infty$ do not commute.

Returning to the matter at hand (equation (1.49)), we first consider the case of an infinite uniform layer of fluid, with constant solution $h = 1$. In this case we write $h = 1 + h_1$ and linearise on the basis that $h_1 \ll 1$. This simply gives

$$h_{1t} = \frac{1}{3}(h_{1xx} - h_{1xxx}), \quad (1.57)$$

which has the normal mode solutions $h_1 = e^{ikx+\sigma t}$, and

$$\sigma = -\frac{1}{3}(k^2 + k^4), \quad (1.58)$$

and the steady solution is stable.

For the case of a finite droplet with solution $h_0(x)$ given by (1.45), we write $h = h_0 + h_1$, and again supposing $h_1 \ll h_0$, we linearise as before, which leads (since $h_0''' = h_0'$) to

$$h_{1t} = \left[\frac{1}{3} h_0^3 (h_{1x} - h_{1xxx}) \right]_x, \quad (1.59)$$

and normal mode solutions are of the form $h_1 = H(x)e^{\sigma t}$, and then

$$\sigma H = \left[\frac{1}{3} h_0^3 (H_x - H_{xxx}) \right]_x. \quad (1.60)$$

This equation requires boundary conditions, but there are issues. If the margins move, then the linearisation must become invalid, since it requires the assumption that $h_1 \ll h_0$, which cannot in general be true if the margins move. Consideration of this case requires a more subtle approach, which uses the method of strained coordinates, but will be foregone here.

Let us suppose, then, that the margins do not move. In this case we should prescribe

$$H = H' = 0 \quad \text{at} \quad x = \pm\lambda. \quad (1.61)$$

This provides four conditions, the gradient condition occurring because of the prescribed contact angle. However, we note that the equation is degenerate since $h_0(\pm\lambda) = 0$, so that the full complement of boundary conditions may not be able to be satisfied. Often in such singular problems (think of Bessel's equation), one only needs to suppress singular solutions. If (1.61) can be satisfied, then automatically $H \ll h_0$ as $x \rightarrow \pm\lambda$, which is required for the validity of the analysis.

Perhaps an ingenious exact solution of (1.60) can be found, but failing that, we resort to an energy-type argument. If we multiply both sides of the equation by $H - H_{xx}$ and integrate, then we find

$$\sigma = \frac{-\int_{-\lambda}^{\lambda} \frac{1}{3} h_0^3 (H_x - H_{xxx})^2 dx}{\int_{-\lambda}^{\lambda} (H^2 + H_x^2) dx}, \quad (1.62)$$

and thus $\sigma < 0$: the droplet is stable. (1.62) actually provides a variational principle for σ : see question 1.3.

Coming back to the issue of the behaviour of H at the end points, we put, for example, $X = x + \lambda$, so that

$$-\alpha H \approx [X^3 (H_X - H_{XXX})]_X, \quad \alpha = \frac{3|\sigma|}{S^3}, \quad (1.63)$$

and we find possible solution behaviours as $X \rightarrow 0$ of the form

$$\begin{aligned} H &\sim X^2 + cX^3 + \dots, \\ H &\sim 1 - bX \ln X, \end{aligned} \tag{1.64}$$

where b and c are specific constants (see exercise 1.3). Therefore it seems in fact that only one condition can be applied at each end, in keeping with the degenerate nature of the equation, but that in fact the extra gradient condition in (1.61) is satisfied automatically.

It should be mentioned that when droplets move, there are issues both with the viability of prescribing a constant contact angle, because of experimentally observed *contact angle hysteresis*, and also with the application of the no-slip condition, which causes a contact line singularity. So the above discussion of stability is slightly inaccurate.

1.2.5 Advance and retreat

When a droplet is of finite extent, it is possible to describe the behaviour near the margins by a local expansion. Typically the surface approaches the base with local power law behaviour, and this depends on whether the droplet is advancing or retreating. Consider, for example, the gravity-driven droplet with an accumulation or ablation term:

$$h_t = \frac{1}{3} (h^3 h_x)_x + a, \tag{1.65}$$

where $a > 0$ for accumulation, and $a < 0$ for ablation. (1.65) represents a simple model for the motion of an ice sheet such as Antarctica, where $a > 0$ represents accumulation due to snowfall. If we suppose that near the margin $x = x_s$ in a two-dimensional motion, $h \sim C(x_s - x)^\nu$, then a local expansion shows that if the front is advancing, $\dot{x}_s > 0$, then $\nu = \frac{1}{3}$ and $\dot{x}_s \sim \frac{1}{9}C^3$; in advance the front is therefore steep. On the other hand, if the front is retreating, then this can only occur if $a < 0$ (as is in fact obvious), and in that case $\nu = 1$ and $\dot{x}_s \sim -|a|/C$. The fact that the front slope is infinite in advance and finite in retreat is associated with ‘waiting time’ behaviour, which occurs when the front has to ‘fatten up’ before it can advance.

We can try and carry out the same analysis for the droplet with gravity and surface tension. If the left hand margin is $x = x_s(t)$, we put $x = x_s + X$, so that in the (X, t) coordinates,

$$h_t - \dot{x}_s h_X = \left[\frac{1}{3} h^3 (h_X - h_{XXX}) \right]_X; \tag{1.66}$$

however, finding a local expansion is not so easy. Trying various choices, it seems that retreat ($\dot{x}_s > 0$) can be described by

$$h \sim aX(-\ln X)^{1/3}, \quad \dot{x}_s \sim \frac{1}{9}a^3, \tag{1.67}$$

but no such simple (!) behaviour describes advance. However, a balance is possible when there is a non-zero flux at the front q_s , and then

$$h \sim aX^{3/4}, \quad q_s = \frac{5}{64}a^4. \tag{1.68}$$

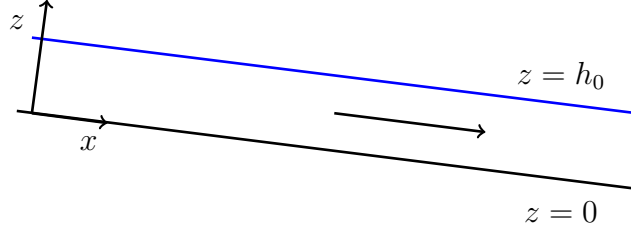


Figure 1.5: Schematic of a falling film e.g. rain flowing down a windshield.

But both these behaviours provide an infinite gradient at the margin, which is inconsistent with the prescription of a finite slope contact angle, and also with the lubrication theory linearisation of the curvature term, and for both these reasons, the model becomes suspect if the margins are allowed to move.

1.2.6 Falling films

In this section we consider a class of flows called falling films, for which there is a predominant background flow which plays an important role on the film dynamics. Examples of such flows include rain falling down a windshield, or industrial coating problems. As we will see, despite having a long-thin aspect ratio, inertia may still play an important role in such flows.

We consider a thin two-dimensional falling film on a tilted plane with angle α to the horizontal. We use rotated coordinates x, z , as illustrated in figure 1.5, such that the impermeable base is located at $z = 0$. The dimensional Navier-Stokes equations in the tilted coordinates are given by

$$\begin{aligned}\nabla \cdot \mathbf{u} &= 0, \\ \rho[\mathbf{u}_t + (\mathbf{u} \cdot \nabla)\mathbf{u}] &= -\nabla p + \mu \nabla^2 \mathbf{u} - \rho \mathbf{g},\end{aligned}\tag{1.69}$$

where $\mathbf{g} = (-\sin \alpha, \cos \alpha)$. We impose no slip conditions $u = w = 0$ on $z = 0$. In the case where the upper surface is at constant level $z = h_0$, the stress conditions become $p = p_a$ and $u_z = 0$ at $z = h_0$. There is an exact solution for this scenario, which is given by

$$\begin{aligned}\bar{u} &= \frac{\rho g \sin \alpha}{2\mu}(2h_0 z - z^2), \\ \bar{w} &= 0, \\ \bar{p} &= p_a - \rho g \cos \alpha(z - h_0),\end{aligned}\tag{1.70}$$

where we use bar notation to indicate that this is the base state.

We consider long-wave perturbations to this flow, with aspect ratio $\varepsilon = h_0/l \ll 1$. Dimensional scalings are chosen as

$$x \sim l, \quad z \sim \varepsilon l, \quad \bar{u} \sim U = \frac{\rho g \sin \alpha h_0^2}{2\mu}, \quad \bar{w} \sim \varepsilon U, \quad \bar{p} - p_a \sim \rho g h_0 \sin \alpha.\tag{1.71}$$

We consider perturbations to the base state of the form

$$\begin{aligned} u &= \bar{u} + \hat{u}, \\ w &= \hat{w}, \\ p &= \bar{p} + \hat{p}, \end{aligned} \tag{1.72}$$

and we consider a variable profile for the thin film $z = h(x, t)$. Hence, the governing equations become

$$\begin{aligned} \hat{u}_x + \hat{w}_z &= 0, \\ \text{Re } \varepsilon [\hat{u}_t + (\bar{u} + \hat{u})\hat{u}_x + \hat{w}(\bar{u}_z + \hat{u}_z)] &= -2\varepsilon\hat{p}_x + \hat{u}_{zz} + \varepsilon^2\hat{u}_{xx}, \\ \text{Re } \varepsilon^2 [\hat{w}_t + (\bar{u} + \hat{u})\hat{w}_x + \hat{w}\hat{w}_z] &= -2\hat{p}_z + \varepsilon(\hat{w}_{zz} + \varepsilon^2\hat{w}_{xx}), \end{aligned} \tag{1.73}$$

where $\text{Re} = \rho U h_0 / \mu$. The no-slip boundary conditions at $z = 0$ become

$$\hat{u} = \hat{w} = 0, \tag{1.74}$$

whereas the kinematic and stress conditions at $z = h(x, t)$ become

$$\begin{aligned} \hat{w} &= h_t + (\bar{u} + \hat{u})h_x, \\ \bar{p} + \hat{p} &= -\frac{\gamma}{\rho g l^2 \sin \alpha} h_{xx} + \mathcal{O}(\varepsilon^2), \\ \bar{u}_z + \hat{u}_z &= \mathcal{O}(\varepsilon^2). \end{aligned} \tag{1.75}$$

It is assumed that $S = \gamma / (\rho g l^2 \sin \alpha)$ is an order $\mathcal{O}(1)$ constant. Conservation of mass can be written as

$$h_t + \frac{\partial}{\partial x} \left[\int_0^h (\bar{u} + \hat{u}) dz \right] = 0, \tag{1.76}$$

which holds true at all orders. In the limit of $\varepsilon \rightarrow 0$, the above system has solution

$$\begin{aligned} \hat{u}_0 &= 2z(h - 1), \\ \hat{w}_0 &= -z^2 h_x, \\ \hat{p}_0 &= (h - 1) \cot \alpha - S h_{xx}. \end{aligned} \tag{1.77}$$

Likewise, (1.76) indicates that

$$h_t + 2h^2 h_x = 0, \tag{1.78}$$

which is a nonlinear advection equation that has stable solutions. Next, we consider an asymptotic expansion solution of the form

$$\begin{aligned} \hat{u} &= \hat{u}_0 + \varepsilon \hat{u}_1 + \dots, \\ \hat{w} &= \hat{w}_0 + \varepsilon \hat{w}_1 + \dots, \\ \hat{p} &= \hat{p}_0 + \varepsilon \hat{p}_1 + \dots \end{aligned} \tag{1.79}$$

Inserting this into the x momentum equation (1.73) gives us

$$\operatorname{Re} [-4zh^2h_x + 2z^2hh_x] = -2\frac{\partial}{\partial x} [(h-1)\cot\alpha - Sh_{xx}] + \hat{u}_{1_{zz}}, \quad (1.80)$$

at first order. Likewise, the boundary conditions at first order indicate that

$$\begin{aligned} \hat{u}_{1_z} &= 0 : & z &= h, \\ \hat{u}_1 &= 0 : & z &= 0. \end{aligned} \quad (1.81)$$

Hence, the first order velocity correction is given by

$$\hat{u}_1 = [h_x \cot\alpha - Sh_{xxx}] (z^2 - 2zh) + \frac{1}{6} \operatorname{Re} hh_x (z^4 - 4z^3h + 8h^3z). \quad (1.82)$$

Inserting this into (1.76) gives the thin film equation

$$h_t + 2h^2h_x + \varepsilon \frac{\partial}{\partial x} \left[h^3 \left(-\frac{2}{3} h_x \cot\alpha + Sh_{xxx} \right) + \frac{8}{15} \operatorname{Re} h^6 h_x \right] = 0. \quad (1.83)$$

This is sometimes referred to as the ‘Benney equation’ after a paper published by D.J. Benney in 1966. The second term represents the base flow, the third term is gravity-driven diffusion, the fourth term is surface-tension-driven diffusion, and the fifth term is a non-linear inertial term.

This example of lubrication theory is different to the previous examples because inertia plays an important role despite the fact that the flow is long and thin. The inertial term can cause waves to bunch up and grow. This can be seen by considering a small perturbation

$$h = 1 + \eta, \quad (1.84)$$

where $\eta(x, t) \ll 1$. Inserting this into the Benney equation and linearising yields

$$\eta_t + 2\eta_x + \varepsilon \left[-\frac{2}{3} \eta_{xx} \cot\alpha + S\eta_{xxx} + \frac{8}{15} \operatorname{Re} \eta_{xx} \right] = 0. \quad (1.85)$$

Switching to the moving frame $\xi = x + 2t$ and imposing a wave-like perturbation of the form $\eta = \exp(\sigma t + ik\xi)$ results in the dispersion relation

$$\sigma = \varepsilon k^2 \left[-\frac{2}{3} \cot\alpha + \frac{8}{15} \operatorname{Re} - Sk^2 \right]. \quad (1.86)$$

Hence, we can see that we require a base flow which is faster than $\operatorname{Re} > (5/4) \cot\alpha$ for an instability to form.

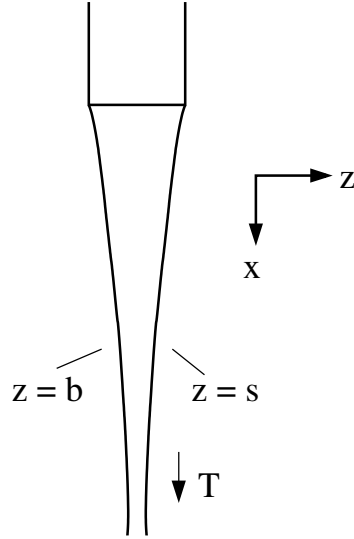


Figure 1.6: An elongational film flow.

1.3 Elongational flows

A different application of lubrication theory occurs in a falling sheet of fluid, such as occurs when a tap is switched on. At low velocities, the flow is continuous and laminar (though at very low flow rates it breaks up into droplets), and is also thin, but is distinguished from surface droplets or bearing flows by the fact that *both* surfaces of the fluid have zero stress acting on them.

To be specific, we consider the situation shown in figure 1.6. We consider flow from an orifice, and we take the flow to be two-dimensional, with the x direction in the direction of flow and z transverse to it. To begin with we ignore gravity and suppose that the flow is driven by an applied tension T (force per unit width in the y direction out of the page) at ∞ ; this is like drawing honey out of a jar with a spoon.

The basic equations are those as scaled in (1.3), and can be written in the form

$$\begin{aligned}
 u_x + w_z &= 0, \\
 Re \dot{u} &= -p_x + \tau_{1x} + \tau_{3z}, \\
 Re \dot{w} &= -p_z + \tau_{3x} - \tau_{1z},
 \end{aligned} \tag{1.87}$$

where

$$\tau_1 = 2u_x, \quad \tau_3 = u_z + w_x. \tag{1.88}$$

If the two free surfaces are $z = s$ and $z = b$, then the boundary conditions on both surfaces are $\sigma_{nn} = \sigma_{nt} = 0$ (we subtract off the ambient pressure), or in other words $\sigma_{ni} = \sigma_{ij}n_j = 0$, and for $z = s$, this gives

$$\begin{aligned}
 (p - \tau_1)s_x + \tau_3 &= 0, \\
 -\tau_3 s_x - p - \tau_1 &= 0.
 \end{aligned} \tag{1.89}$$

(These are actually equivalent to (1.19).)

Now we rescale the variables to account for the large aspect ratio. The difference with the earlier approach is that shear stresses are uniformly small, and so we also rescale τ_3 to be small. Thus we rescale the variables as

$$z \sim \varepsilon, \quad w \sim \varepsilon, \quad \tau_3 \sim \varepsilon, \quad (1.90)$$

and this leads to the rescaled equations

$$\begin{aligned} u_x + w_z &= 0, \\ Re \dot{u} &= -p_x + \tau_{1x} + \tau_{3z}, \\ \varepsilon^2 Re \dot{w} &= -p_z + \varepsilon^2 \tau_{3x} - \tau_{1z}, \end{aligned} \quad (1.91)$$

where

$$\tau_1 = 2u_x, \quad \varepsilon^2 \tau_3 = u_z + \varepsilon^2 w_x, \quad (1.92)$$

and on the free surfaces (e. g., $z = s$)

$$\begin{aligned} (p - \tau_1)s_x + \tau_3 &= 0, \\ -\varepsilon^2 \tau_3 s_x - p - \tau_1 &= 0. \end{aligned} \quad (1.93)$$

At leading order, we have $u = u(x, t)$, $p + \tau_1 = 0$, $p = -2u_x$, whence we find

$$\tau_{3z} = Re \dot{u} - 4u_{xx}, \quad (1.94)$$

with

$$\tau_3 = 4u_x s_x \quad \text{on} \quad z = s, \quad \tau_3 = 4u_x b_x \quad \text{on} \quad z = b,$$

and from these we deduce

$$\begin{aligned} Re h(u_t + uu_x) &= 4(hu_x)_x, \\ h_t + (hu)_x &= 0, \end{aligned} \quad (1.95)$$

where the second equation is derived as usual to represent conservation of mass. Note in this derivation that the inertial terms are not necessarily small; nevertheless the asymptotic procedure works in the usual way.

1.3.1 Steady flow

For a long filament such as that shown in figure 1.6, it is appropriate to prescribe inlet conditions, and these can be taken to be

$$h = u = 1 \quad \text{at} \quad x = 0, \quad (1.96)$$

by appropriate choice of U and d . In addition, we prescribe the force (per unit width in the third dimension) to be T , and this leads to

$$hu_x \rightarrow 1 \quad \text{as} \quad x \rightarrow \infty, \quad (1.97)$$

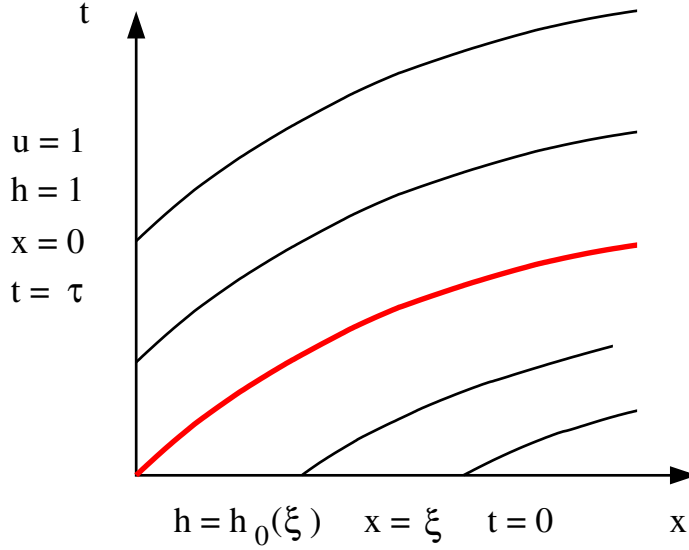


Figure 1.7: Characteristics for (1.95). The dividing characteristic from the origin is shown in red.

where the constant is set to one by choice of the length scale as

$$l = \frac{2\mu dU}{T}; \quad (1.98)$$

thus the aspect ratio is small ($d \ll l$) if $T \ll \mu U$.

If we consider a slow, steady flow in which the inertial terms can be ignored ($Re \rightarrow 0$), it is easy to solve the equations. We have $hu = 1$ and $hu_x = 1$, and thus

$$u = e^x, \quad h = e^{-x}. \quad (1.99)$$

As a matter of curiosity, one can actually solve the time-dependent problem (1.95), at least when $Re = 0$. We write the equations in the form

$$\begin{aligned} h_t + uh_x &= -1, \\ hu_x &= 1, \end{aligned} \quad (1.100)$$

with the boundary and initial conditions as shown in figure 1.7. The characteristic form of the first equation is

$$x_t = u[x(\xi, t), t], \quad h_t = -1, \quad (1.101)$$

where the partial derivatives are holding ξ fixed, i.e., we consider $x = x(\xi, t)$, $h = h(\xi, t)$. The dividing characteristic from the origin (which we define to be $t = t_d(x)$) divides the quadrant into two regions, in which the initial data is parameterised differently. For the lower region $t < t_d(x)$, we have

$$h = h_0(\xi) - t. \quad (1.102)$$

We take the first equation in (1.101), and differentiate with respect to ξ . Using the definition of u_x from (1.100), we find

$$x_{\xi t} = \frac{x_\xi}{h_0(\xi) - t}. \quad (1.103)$$

We can integrate this with respect to t , *holding ξ constant*, that is, the integral with respect to t is along a characteristic. It follows that

$$x_\xi = \frac{h_0(\xi)}{h_0(\xi) - t}, \quad (1.104)$$

in which we have applied the initial condition $x_\xi = 1$ at $t = 0$.

Next we integrate with respect to ξ *holding t constant*; since (1.104) only holds for $t < t_d(x)$, we integrate back to this, but note that this corresponds to the value $\xi = 0$; we then have

$$x = x_d(t) + \int_0^\xi \frac{h_0(s) ds}{h_0(s) - t}, \quad (1.105)$$

where x_d is the inverse of $t_d(x)$: to calculate this we need to solve for the upper region $t > t_d$.

To do this, we can proceed as above, but it is quicker to note that since the boundary conditions on $x = 0$ are constant, the solution is just the steady state solution (1.99). In particular, the characteristics are $e^{-x} = 1 - (t - \tau)$, and the dividing characteristic is that with $\tau = 0$, thus

$$t_d = 1 - e^{-x}, \quad x_d = -\ln(1 - t). \quad (1.106)$$

The solution in $t < t_d$ is thus

$$x = -\ln(1 - t) + \int_0^\xi \frac{h_0(s) ds}{h_0(s) - t}, \quad (1.107)$$

but the transient is of little interest since it disappears after finite time, $t = 1$. As a check, notice that if $h_0 = e^{-\xi}$, the steady state solution is regained everywhere.

The steady solution can be extended to positive Reynolds number. In steady flow we then find

$$u_x = Ku + \frac{1}{4}Re u^2 \quad (1.108)$$

for some constant K , and we see that there is no solution in which the filament can be drawn to ∞ , as pinch-off always occurs. This is in keeping with experience.

1.3.2 Capillary effects

As for the shear-driven droplet flows, one can add gravity to the model, and this is done in question 1.4. In this section we consider the modification to the equations

which occurs when capillary effects are included. The normal stress conditions are modified to

$$\begin{aligned} -\sigma_{nn} &= -\frac{\gamma s_{xx}}{(1+s_x^2)^{3/2}} \quad \text{on } z = s, \\ \sigma_{nn} &= -\frac{\gamma b_{xx}}{(1+b_x^2)^{3/2}} \quad \text{on } z = b. \end{aligned} \quad (1.109)$$

The definition of σ_{nn} is in (1.19), and with the basic scaling (all lengths scaled with l , etc.) this leads to

$$-p - \frac{2\tau_3 s_x}{1+s_x^2} - \frac{\tau_1(1-s_x^2)}{1+s_x^2} = \frac{1}{Ca} \frac{\gamma s_{xx}}{(1+s_x^2)^{3/2}} \quad \text{on } z = s, \quad (1.110)$$

where

$$Ca = \frac{\mu U}{\gamma} \quad (1.111)$$

is the capillary number; a similar expression applies on $z = b$, with the opposite sign on the right hand side. When the equations are re-scaled ($z \sim \varepsilon$, etc.), then these take the approximate form

$$\begin{aligned} p + \tau_1 &\approx -\frac{1}{C} s_{xx} \quad \text{on } z = s, \\ p + \tau_1 &\approx \frac{1}{C} b_{xx} \quad \text{on } z = b, \end{aligned} \quad (1.112)$$

where we write

$$Ca = \varepsilon C. \quad (1.113)$$

Now the normal stress is constant across the filament, thus

$$p + \tau_1 \approx -\frac{1}{C} s_{xx} \quad (1.114)$$

everywhere, and this forces symmetry of the filament, $s_{xx} = -b_{xx}$. The rest of the derivation proceeds as before, except that (1.94) gains an extra term $-s_{xxx}/C$ on the right hand side; integrating this and applying the boundary conditions leads to the modification of (1.95) as (bearing in mind that $h = s - b$ and thus $h_{xx} = 2s_{xx}$)

$$\begin{aligned} h_t + (hu)_x &= 0, \\ Re h(u_t + uu_x) &= \frac{1}{2C} h h_{xxx} + 4(hu_x)_x. \end{aligned} \quad (1.115)$$

Steady flow

The extra derivatives for h require, apparently, two extra boundary conditions. If we suppose the pressure becomes atmospheric at ∞ , then we might apply

$$h_{xx} \rightarrow 0 \quad \text{as } x \rightarrow \infty. \quad (1.116)$$

Since this also implies $h_x \rightarrow 0$, it may be sufficient. On the other hand, if $h \rightarrow 0$ at ∞ , the multiplication of the third derivative term by h may render an extra boundary condition unnecessary.

Again we can consider the steady state. Then $hu = 1$, and (1.115) has a first integral

$$K + \frac{Re}{h} = \frac{1}{2C} [hh_{xx} - \frac{1}{2}h_x^2] - \frac{4h_x}{h}, \quad (1.117)$$

where K is constant. Evidently there is no solution if $Re > 0$, as pinch-off must again occur. For the case of slow flow, taking $Re = 0$, we have $K = 4$ due to the far field stress condition, and

$$h^2 h_{xx} - \frac{1}{2} h h_x^2 - 8C(h_x + h) = 0. \quad (1.118)$$

We seek a solution of this with $h(0) = 1$ and $h(\infty) = 0$. Phase plane analysis shows that there is a unique such solution: see question 1.8.

Gravity

While we chose to model a thin filament pulled downwards by a tension, equally we might consider a filament descending under its own weight. In this case, the model can be derived much as before, but now the tension at infinity can be taken to be zero, and the length scale is then chosen to normalise the gravity term to equal one. The modification of (1.95) is then

$$\begin{aligned} h_t + (hu)_x &= 0, \\ h[Re(u_t + uu_x) - 1] &= 4(hu_x)_x. \end{aligned} \quad (1.119)$$

In this case, steady solutions extending to infinity exist, even if $Re > 0$, but if any non-zero tension is applied at infinity, the solution breaks down as before and pinch-out occurs. See also question 1.4.

Exercises

- 1.1 A thin incompressible liquid film flows in two dimensions (x, z) between a solid base $z = 0$ where the horizontal (x) component of the velocity is $U(t)$, and may depend on time, and a stationary upper solid surface $z = h(x)$, where a no slip condition applies. The upper surface is of horizontal length l , and is open to the atmosphere at the ends. Write down the equations and boundary conditions describing the flow, and non-dimensionalise them assuming that $U(t) \sim U_0$. (You may neglect gravity.)

Assuming $\varepsilon = d/l$ is sufficiently small, where d is a measure of the gap width, rescale the variables suitably, and derive an approximate equation for the pressure p . Hence derive a formal solution if the block is of finite length l , and the pressure is atmospheric at each end, and obtain an expression involving integrals of powers of h for the horizontal fluid flux, $q(t) = \int_0^h u dz$.

- 1.2 A two-dimensional incompressible fluid flow is contained between two surfaces $z = b(x, t)$ and $z = s(x, t)$, on which kinematic conditions hold:

$$w = s_t + us_x \quad \text{at} \quad z = s,$$

$$w = b_t + ub_x \quad \text{at} \quad z = b.$$

By integrating the equation of conservation of mass, show that the fluid thickness $h = s - b$ satisfies the conservation law

$$\frac{\partial h}{\partial t} + \frac{\partial}{\partial x} \int_b^s u \, dx = 0.$$

Extend the result to three dimensions to show that

$$h_t + \nabla_H \cdot \left[\int_b^s \mathbf{u}_H \, dz \right] = 0,$$

where $\mathbf{u}_H = (u, v)$ is the horizontal velocity, and $\nabla_H = \left(\frac{\partial}{\partial x}, \frac{\partial}{\partial y} \right)$ is the horizontal gradient operator.

- 1.3 A two-dimensional droplet has thickness $h(x, t)$ and satisfies the dimensionless equation

$$h_t = \left[\frac{1}{3} h^3 (h_x - h_{xxx}) \right]_x,$$

with conditions that $|h_x| = S$ when $h = 0$. Show that for a steady solution $h_0(x)$,

$$h_0 = \frac{S(\cosh \lambda - \cosh x)}{\sinh \lambda},$$

where λ is an arbitrary (positive) parameter. If the (dimensionless) ‘volume’ of the drop V is prescribed, show that λ is uniquely determined, and that it increases monotonically with V . Find approximate expressions for λ as $V \rightarrow 0$ and $V \rightarrow \infty$.

By writing $h = h_0 + h_1$, linearising, and then putting $h_1 = H(x)e^{\sigma t}$, derive a linear equation for H , and give the boundary conditions for H , assuming the margins of the drop do not move. By writing σ as a functional $[H]$ in terms of integrals of H and its derivatives, show that $\sigma < 0$ for any solution of this, and thus that the drop is stable.

Suppose that H is a solution of its governing differential equation with corresponding eigenvalue $\sigma[H]$. By considering variations δH to H such that $\int_{-\lambda}^{\lambda} (H^2 + H_x^2) \, dx$ remains constant, show that the first variation $\sigma[H + \delta H] - \sigma[H]$ is zero.

Now let $X = x + \lambda$ so that $h_0 \approx SX$. By considering limiting forms of the resulting approximate equation for H , show that either $H \propto X^2 + cX^3 + \dots$ or $H \propto 1 + bX \ln X + \dots$, and find the values of b and c .

- 1.4 An incompressible two-dimensional flow from a slit of width d falls vertically under gravity. Define *vertical* and *horizontal* coordinates x and z , with corresponding velocity components u and w . The stream is symmetric with free interfaces at $z = \pm s$, on which no stress conditions apply. Write down the equations and boundary conditions in terms of the deviatoric stress components $\tau_1 = \tau_{11} = -\tau_{33}$ and $\tau_3 = \tau_{13} = \tau_{31}$, and by scaling lengths with l , velocities with the inlet velocity U , and choosing suitable scales for time t and the pressure and stresses, show that the equations take the form

$$u_x + w_z = 0,$$

$$Re \dot{u} = -p_x + \tau_{1x} + \tau_{3z} + 1,$$

$$Re \dot{w} = -p_z + \tau_{3x} - \tau_{1z},$$

where you should define \dot{u} , the Reynolds number Re , and write down expressions for τ_1 and τ_3 .

Now define $\varepsilon = \frac{d}{l}$, and assume it is small. Find a suitable rescaling of the equations, and show that the vertical momentum equation takes the approximate form

$$h[Re \dot{u} - 1] = 4(hu_x)_x,$$

where $u = u(x, t)$ and h is the stream width.

Show also that

$$h_t + (hu)_x = 0.$$

Explain why suitable boundary conditions are

$$h = u = 1 \quad \text{at} \quad x = 0, \quad hu_x \rightarrow 0 \quad \text{as} \quad x \rightarrow \infty.$$

Write down a single second order equation for u in steady flow. If $Re = 0$, find the solution.

If $Re > 0$, find a pair of first order equations for $v = \ln u$ and $w = v_x$. (*Note: w here is no longer the horizontal velocity.*) Show that $(\infty, 0)$ is a saddle point, and that a unique solution satisfying the boundary conditions exists. If $Re \gg 1$ (but still $\varepsilon^2 Re \ll 1$), show (by rescaling $w = W/Re$ and $x = Re X$) that the required trajectory hugs the W -nullcline, and thus show that in this case

$$u \approx \left(1 + \frac{2x}{Re}\right)^{1/2}.$$

- 1.5 A (two-dimensional) droplet rests on a rough surface $z = b$ and is subject to gravity g and surface tension γ . Write down the equations and boundary conditions which govern its motion, non-dimensionalise them, and assuming the depth at the summit d is much less than the half-width l , derive an approximate

equation for the evolution in time of the depth h . Show that the horizontal velocity scale is

$$U = \frac{\rho g d^3}{\mu l},$$

and derive an approximate set of equations assuming

$$\varepsilon = \frac{d}{l} \ll 1, \quad F = \frac{U}{\sqrt{gd}} \ll 1.$$

Hence show that

$$h_t = \frac{\partial}{\partial x} \left[\frac{1}{3} h^3 \left(s_x - \frac{1}{B} s_{xxx} \right) \right],$$

where you should define the Bond number B .

Find a steady state solution of this equation for the case of a flat base, assuming that the droplet area A and a contact angle $\theta = \varepsilon\phi$ are prescribed, with $\phi \sim O(1)$, and show that it is unique. Explain how the solution chooses the unknowns d and l .

1.6 A droplet of thickness h satisfies the equation

$$h_t = \frac{\partial}{\partial x} \left[\frac{1}{3} h^3 h_x \right].$$

Find a similarity solution of this equation which describes the spread of a drop of area one which is initially concentrated at the origin (i. e., $h(x, 0) = \delta(x)$).

1.7 A three-dimensional droplet, subject to gravity and resting on a flat horizontal surface $z = 0$, has surface $z = h(x, y, t)$, on which the pressure is given by $p = \gamma \nabla \cdot \mathbf{n}$, where \mathbf{n} is the unit upward normal to the surface. Show that this condition can be written in the form

$$p = -\gamma \nabla \cdot \left[\frac{\nabla h}{\{1 + |\nabla h|^2\}^{1/2}} \right],$$

where now (and below) ∇ is the horizontal gradient $\left(\frac{\partial}{\partial x}, \frac{\partial}{\partial y} \right)$.

Use the assumptions of lubrication theory to derive the dimensionless droplet equation

$$h_t = \frac{1}{3} \nabla \cdot \left[h^3 \nabla \left\{ h - \frac{1}{Bo} \nabla^2 h \right\} \right],$$

and define the Bond number Bo .

Suppose that $Bo = \infty$ (what does this mean in terms of the surface tension?), and that a concentrated dollop of fluid of dimensionless volume 2π is released at $r = 0$ at $t = 0$. By seeking a similarity solution of the form

$$h = \frac{1}{t^\alpha} f(\eta), \quad \eta = \frac{r}{t^\beta},$$

derive and solve an equation for f , and hence show that the droplet is bounded by a moving front at

$$r \approx 1.55 t^{1/8}.$$

[Hint: $\left(\frac{8192}{343}\right)^{1/8} \approx 1.55$.]

Now suppose that $Bo < \infty$. Explain why we may take $Bo = 1$. Assuming this, and a boundary condition that $h_r = -S$ where $h = 0$, show that the steady solution satisfies

$$h_{rr} + \frac{1}{r}h_r - h = -K,$$

where K is constant, and deduce that

$$h = \frac{S[I_0(\lambda) - I_0(r)]}{I_0'(\lambda)},$$

where $I_0(r)$ is the modified Bessel function of the first kind, and $r = \lambda$ is the drop margin.

Suppose that the dimensionless volume V of the drop is prescribed, so that

$$\int_0^\lambda rh(r) dr = \frac{V}{2\pi}.$$

We want to show that this determines λ uniquely. By consideration of the equation for h , show that

$$L(\lambda) \equiv \lambda \left[\frac{\lambda I_0(\lambda)}{2I_0'(\lambda)} - 1 \right] = \frac{V}{2\pi S};$$

λ will thus be unique if $L(\lambda)$ is monotonically increasing.

Define

$$\eta(\lambda) = \frac{I_0'(\lambda)}{I_0(\lambda)},$$

and show that

$$\eta' = 1 - \frac{\eta}{\lambda} - \eta^2.$$

Assuming that $I_0(\lambda) \sim 1 + \frac{1}{4}\lambda^2 + \frac{1}{64}\lambda^4 + \dots$ as $\lambda \rightarrow 0$, find the limiting behaviour of η as $\lambda \rightarrow 0$, and by consideration of trajectory directions in the semi-phase plane (λ, η) , show that $\eta(\lambda)$ is a monotonically increasing function of λ , with $\eta(\infty) = 1$. Derive a differential equation for $g(\lambda) = 2\eta/\lambda$, and by the same device (but now using the (λ, g) semi-phase plane), show that g is a monotonically decreasing function of λ . Hence show that $L(\lambda)$ is a strictly increasing function, as required.

Denoting this steady state as $h_0(r)$, perturb h as $h = h_0 + h_1$, and linearise the equation. Now put $h_1 = H(x, y)e^{\sigma t}$ (do not assume that H is cylindrically symmetric) and write down the resulting eigenvalue problem for σ . Assuming that the drop margin is not perturbed, show that σ is real and negative for any solution of this eigenvalue problem, and hence that the drop is stable.

- 1.8 A film of fluid is drawn downwards under the action of a tensile force. A model for the dimensionless thickness h and dimensionless downwards velocity u of the film is

$$h_t + (hu)_x = 0,$$
$$Re h(u_t + uu_x) = \frac{1}{2C} h h_{xxx} + 4(hu_x)_x,$$

with

$$h = u = 1 \quad \text{on} \quad x = 0, \quad hu_x \rightarrow 1 \quad \text{as} \quad x \rightarrow \infty.$$

Show that a steady state solution in which $h \rightarrow 0$ as $x \rightarrow \infty$ can only occur if $Re = 0$. In that case, determine a second order differential equation satisfied by h , and by writing $h = \frac{1}{2}U^2$ and $V = U' = U_x$, write the equation as a pair of first order equations for U and V . Show that the origin is a (degenerate) saddle, and therefore show that a solution exists which satisfies the boundary conditions.

Chapter 2

Porous media

Groundwater is water which is stored in the soil and rock beneath the surface of the Earth. It forms a fundamental constituent reservoir of the hydrological system, and it is important because of its massive and long lived storage capacity. It is the resource which provides drinking and irrigation water for crops, and increasingly in recent decades it has become an unwilling recipient of toxic industrial and agricultural waste. For all these reasons, the movement of groundwater is an important subject of study.

Soil consists of very small grains of organic and inorganic matter, ranging in size from millimetres to microns. Differently sized (inorganic) particles have different names. Particularly, we distinguish clay particles (size < 2 microns) from silt particles (2–60 microns) and sand (60 microns to 1 mm). Coarser particles still are termed gravel.

Viewed at the large scale, soil thus forms a continuum which is granular at the small scale, and which contains a certain fraction of pore space, as shown in figure 2.1. The volume fraction of the soil (or sediment, or rock) which is occupied by the pore space (or void space, or voidage) is called the *porosity*, and is commonly denoted by the symbol ϕ ; sometimes other symbols are used, for example n .

Soils are formed by the weathering of rocks, and are specifically referred to as soils when they contain organic matter formed by the rotting of plants and animals. There are two main types of rock: igneous, formed by the crystallisation of molten lava, and sedimentary, formed by the cementation of sediments under conditions of great temperature and pressure as they are buried at depth.¹ Sedimentary rocks, such as sandstone, chalk, shale, thus have their porosity built in, because of the pre-existing granular structure. With increasing pressure, the grains are compacted, thus reducing their porosity, and eventually intergranular cements bond the grains into a rock.

Igneous rock tends to be porous also, for a different reason. It is typically the case for any rock that it is fractured. Most simply, rock at the surface of the Earth

¹There are also *metamorphic* rocks, which form from pre-existing rocks through chemical changes induced by burial at high temperatures and pressures; for example, marble is a metamorphic form of limestone.

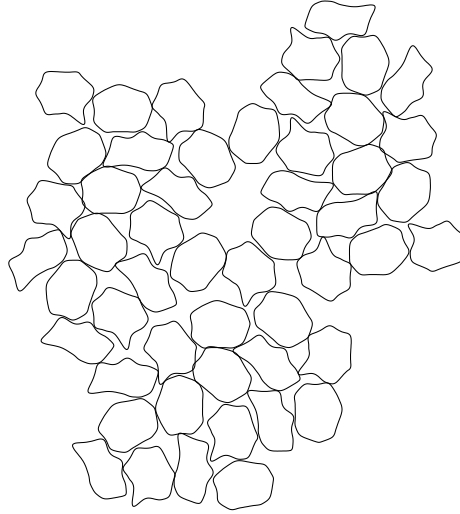


Figure 2.1: A granular porous medium.

is subjected to enormous tectonic stresses, which cause it to fold and fracture. Thus, even if the rock *matrix* itself is not porous, there are commonly faults and fractures within the rock which act as channels through which fluids may flow, and which act on the large scale as an effective porosity. If the matrix is porous at the grain scale also, then one refers to the rock as having a dual porosity, and the corresponding flow models are called double porosity models.

In the subsurface, whether it be soil, underlying regolith, a sedimentary basin, or oceanic lithosphere, the pore space contains liquid. At sufficient depth, the pore space will be saturated with fluid, normally water. At greater depths, other fluids may be present. For example, oil may be found in the pore space of the rocks of sedimentary basins. In the near surface, both air and water will be present in the pore space, and this (unsaturated) region is called the unsaturated zone, or the vadose zone. The surface separating the two is called the piezometric surface, the phreatic surface, or more simply the water table. Commonly it lies several metres below the ground surface, and more in arid regions.

2.1 Darcy's law

Groundwater is fed by surface rainfall, and as with surface water it moves under a pressure gradient driven by the slope of the piezometric surface. In order to characterise the flow of a liquid in a porous medium, we must therefore relate the flow rate to the pressure gradient. An idealised case is to consider that the pores consist of uniform cylindrical tubes of radius a ; initially we will suppose that these are all aligned in one direction. If a is small enough that the flow in the tubes is laminar (this will be the case if the associated Reynolds number is $\lesssim 1000$), then Poiseuille

flow in each tube leads to a volume flux in each tube of $q = \frac{\pi a^4}{8\mu} |\nabla p|$, where μ is the liquid viscosity, and ∇p is the pressure gradient along the tube. A more realistic porous medium is *isotropic*, which is to say that if the pores have this tubular shape, the tubules will be arranged randomly, and form an interconnected network. However, between nodes of this network, Poiseuille flow will still be appropriate, and an appropriate generalisation is to suppose that the volume flux vector is given by

$$\mathbf{q} \approx -\frac{a^4}{\mu X} \nabla p, \quad (2.1)$$

where the approximation takes account of small interactions at the nodes; the numerical tortuosity factor $X \gtrsim 1$ takes some account of the arrangement of the pipes.

To relate this to macroscopic variables, and in particular the porosity ϕ , we observe that $\phi \sim a^2/d_p^2$, where d_p is a representative particle or grain size so that $\mathbf{q}/d_p^2 \sim -\left(\frac{\phi^2 d_p^2}{\mu X}\right) \nabla p$. We define the volume flux per unit area (having units of velocity) as the discharge \mathbf{u} . Darcy's law then relates this to an applied pressure gradient by the relation

$$\mathbf{u} = -\frac{k}{\mu} [\nabla p + \rho g \hat{\mathbf{k}}], \quad (2.2)$$

where ρ is fluid density, g is the acceleration due to gravity, $\hat{\mathbf{k}}$ is a unit vector in the vertical (upwards) direction, and k is an empirically determined parameter called the *permeability*, having units of length squared. The discussion above suggests that we can write

$$k = \frac{d_p^2 \phi^2}{X}; \quad (2.3)$$

the numerical factor X may typically be of the order of 10^3 , but other assumptions can be made instead.

To check whether the pore flow is indeed laminar, we calculate the (particle) Reynolds number for the porous flow. If \mathbf{v} is the (average) fluid velocity in the pore space (what we will call the *phase-averaged* velocity), then

$$\mathbf{v} = \frac{\mathbf{u}}{\phi}; \quad (2.4)$$

If a is the pore radius, then we define a particle Reynolds number based on grain size as

$$Re_p = \frac{2\rho v a}{\mu} \sim \frac{\rho |\mathbf{u}| d_p}{\mu \sqrt{\phi}}, \quad (2.5)$$

since $\phi \sim a/d_p$. Suppose (2.3) gives the permeability, and we use the gravitational pressure gradient ρg to define (via Darcy's law) a velocity scale²; then

$$Re_p \sim \frac{\phi^{3/2}}{X} \left(\frac{\rho \sqrt{g d_p} d_p}{\mu} \right)^2 \sim 10 [d_p]^3, \quad (2.6)$$

²This scale is thus the hydraulic conductivity, defined below in (2.9).

where $d_p = [d_p]$ mm, and we have used $\phi^{3/2}/X = 10^{-3}$, $g = 10 \text{ m s}^{-2}$, $\mu/\rho = 10^{-6} \text{ m}^2 \text{ s}^{-2}$. Thus the flow is laminar for $d < 5 \text{ mm}$, corresponding to a gravel. Only for free flow through very coarse gravel could the flow become turbulent, but for water percolation in rocks and soils, we invariably have slow, laminar flow.

In other situations, and notably for forced gas stream flow in fluidised beds or in packed catalyst reactor beds, the flow can be rapid and turbulent. In this case, the Poiseuille flow balance $-\nabla p = \mu \mathbf{u}/k$ can be replaced by the *Ergun equation*

$$-\nabla p = \frac{\rho |\mathbf{u}| \mathbf{u}}{k'}; \quad (2.7)$$

more generally, the right hand side will be a sum of the two (laminar and turbulent) interfacial resistances. The Ergun equation reflects the fact that turbulent flow in a pipe is resisted by *Reynolds stresses*, which are generated by the fluctuation of the inertial terms in the momentum equation. Just as for the laminar case, the parameter k' , having units of length, depends both on the grain size d_p and on ϕ . Evidently, we will have

$$k' = d_p E(\phi), \quad (2.8)$$

with the numerical factor $E \rightarrow 0$ as $\phi \rightarrow 0$.

Hydraulic conductivity

Another measure of flow rate in porous soil or rock relates specifically to the passage of water through a porous medium under gravity. For free flow, the pressure gradient downwards due to gravity is just ρg , where ρ is the density of water and g is the gravitational acceleration; thus the water flux per unit area in this case is just

$$K = \frac{k \rho g}{\mu}, \quad (2.9)$$

and this quantity is called the *hydraulic conductivity*. It has units of velocity. A hydraulic conductivity of $K = 10^{-5} \text{ m s}^{-1}$ (about 300 m y^{-1}) corresponds to a permeability of $k = 10^{-12} \text{ m}^2$, this latter unit also being called the *darcy*.

2.1.1 Homogenisation

The ‘derivation’ of Darcy’s law can be carried out in a more formal way using the method of homogenisation. This is essentially an application of the method of multiple (space) scales to problems with microstructure. Usually (for analytic reasons) one assumes that the microstructure is periodic, although this is probably not strictly necessary (so long as local averages can be defined).

Consider the Stokes flow equations for a viscous fluid in a medium of macroscopic length l , subject to a pressure gradient of order $\Delta p/l$. For simplicity we will ignore gravity. If the microscopic (e. g., grain size) length scale is d_p , and $\varepsilon = d_p/l$, then if we scale velocity with $d_p^2 \Delta p / l \mu$ (appropriate for local Poiseuille-type flow), length

with l , and pressure with Δp , the Navier-Stokes equations can be written in the dimensionless form

$$\begin{aligned}\nabla \cdot \mathbf{u} &= 0, \\ 0 &= -\nabla p + \varepsilon^2 \nabla^2 \mathbf{u},\end{aligned}\tag{2.10}$$

together with the no-slip boundary condition,

$$\mathbf{u} = 0 \text{ on } S : f(\mathbf{x}/\varepsilon) = 0,\tag{2.11}$$

where S is the interfacial surface. We put $\mathbf{x} = \varepsilon \boldsymbol{\xi}$ and seek solutions in the form

$$\begin{aligned}\mathbf{u} &= \mathbf{u}^{(0)}(\mathbf{x}, \boldsymbol{\xi}) + \varepsilon \mathbf{u}^{(1)}(\mathbf{x}, \boldsymbol{\xi}) \dots \\ p &= p^{(0)}(\mathbf{x}, \boldsymbol{\xi}) + \varepsilon p^{(1)}(\mathbf{x}, \boldsymbol{\xi}) \dots\end{aligned}\tag{2.12}$$

Expanding the equations in powers of ε and equating terms leads to $p^{(0)} = p^{(0)}(\mathbf{x})$, and $\mathbf{u}^{(0)}$ satisfies

$$\begin{aligned}\nabla_{\boldsymbol{\xi}} \cdot \mathbf{u}^{(0)} &= 0, \\ 0 &= -\nabla_{\boldsymbol{\xi}} p^{(1)} + \nabla_{\boldsymbol{\xi}}^2 \mathbf{u}^{(0)} - \nabla_x p^{(0)},\end{aligned}\tag{2.13}$$

equivalent to Stokes' equations for $\mathbf{u}^{(0)}$ with a forcing term $-\nabla_x p^{(0)}$. If \mathbf{w}^j is the velocity field which (uniquely) solves

$$\begin{aligned}\nabla_{\boldsymbol{\xi}} \cdot \mathbf{w}^j &= 0, \\ 0 &= -\nabla_{\boldsymbol{\xi}} P + \nabla_{\boldsymbol{\xi}}^2 \mathbf{w}^j + \mathbf{e}_j,\end{aligned}\tag{2.14}$$

with periodic (in $\boldsymbol{\xi}$) boundary conditions and $\mathbf{u} = 0$ on $f(\boldsymbol{\xi}) = 0$, where \mathbf{e}_j is the unit-vector in the ξ_j direction, then (since the equation is linear) we have (summing over j)³

$$\mathbf{u}^{(0)} = -\frac{\partial p^{(0)}}{\partial x_j} \mathbf{w}^j.\tag{2.15}$$

We define the average flux

$$\langle \mathbf{u} \rangle = \frac{1}{V} \int_V \mathbf{u}^{(0)} dV,\tag{2.16}$$

where V is the volume over which S is periodic.⁴ Averaging (2.15) then gives

$$\langle \mathbf{u} \rangle = -\mathbf{k}^* \cdot \nabla p,\tag{2.17}$$

³In other words, we employ the summation convention which states that summation is implied over repeated suffixes, see for example Jeffreys and Jeffreys (1953).

⁴Specifically, we take V to be the soil volume, but the integral is only over the pore space volume, where \mathbf{u} is defined. In that case, the average $\langle \mathbf{u} \rangle$ is in fact the Darcy flux (i. e., volume fluid flux per unit area).

where the (dimensionless) permeability tensor is defined by

$$k_{ij}^* = \langle w_i^j \rangle. \quad (2.18)$$

Recollecting the scales for velocity, length and pressure, we find that the dimensional version of (2.17) is

$$\langle \mathbf{u} \rangle = -\frac{\mathbf{k}}{\mu} \cdot \nabla p, \quad (2.19)$$

where

$$\mathbf{k} = \mathbf{k}^* d_p^2, \quad (2.20)$$

so that \mathbf{k}^* is the equivalent in homogenisation theory of the quantity ϕ^2/X in (2.3).

2.1.2 Empirical measures

While the validity of Darcy's law can be motivated theoretically, it ultimately relies on experimental measurements for its accuracy. The permeability k has dimensions of (length)², which as we have seen is related to the mean 'grain size'. If we write $k = d_p^2 C$, then the number C depends on the pore configuration. For a tubular network (in three dimensions), one finds $C \approx \phi^2/72\pi$ (as long as ϕ is relatively small). A different and often used relation is that of Carman and Kozeny, which applies to pseudo-spherical grains (for example sand grains); this is

$$C \approx \frac{\phi^3}{180(1-\phi)^2}. \quad (2.21)$$

The factor $(1-\phi)^2$ takes some account of the fact that as ϕ increases towards one, the resistance to motion becomes negligible. In fact, for media consisting of uncemented (i. e., separate) grains, there is a critical value of ϕ beyond which the medium as a whole will deform like a fluid. Depending on the grain size distribution, this value is about 0.5 to 0.6. When the medium deforms in this way, the description of the intergranular fluid flow can still be taken to be given by Darcy's law, but this now constitutes a particular choice of the interactive drag term in a two-phase flow model. At lower porosities, deformation can still occur, but it is elastic not viscous (on short time scales), and given by the theory of consolidation or compaction, which we discuss later.

In the case of soils or sediments, empirical power laws of the form

$$C \sim \phi^m \quad (2.22)$$

are often used, with much higher values of the exponent (e.g. $m = 8$). Such behaviour reflects the (chemically-derived) ability of clay-rich soils to retain a high fraction of water, thus making flow difficult. Table 2.1 gives typical values of the permeability of several common rock and soil types, ranging from coarse gravel and sand to finer silt and clay.

k (m ²)	material
10 ⁻⁸	gravel
10 ⁻¹⁰	sand
10 ⁻¹²	fractured igneous rock
10 ⁻¹³	sandstone
10 ⁻¹⁴	silt
10 ⁻¹⁸	clay
10 ⁻²⁰	granite

Table 2.1: Different grain size materials and their typical permeabilities.

An explicit formula of Carman-Kozeny type for the turbulent Ergun equation expresses the ‘turbulent’ permeability k' , defined in (2.7), as

$$k' = \frac{\phi^3 d_p}{175(1 - \phi)}. \quad (2.23)$$

2.2 Basic groundwater flow

Darcy’s equation is supplemented by an equation for the conservation of the fluid phase (or phases, for example in oil recovery, where these may be oil and water). For a single phase, this equation is of the simple conservation form

$$\frac{\partial}{\partial t}(\rho\phi) + \nabla \cdot (\rho\mathbf{u}) = 0, \quad (2.24)$$

supposing there are no sources or sinks within the medium. In this equation, ρ is the material density, that is, mass per unit volume *of the fluid*. A term ϕ is not present in the divergence term, since \mathbf{u} has already been written as a volume flux (i.e., the ϕ has already been included in it: *cf.* (2.4)).

Eliminating \mathbf{u} , we have the parabolic equation

$$\frac{\partial}{\partial t}(\rho\phi) = \nabla \cdot \left[\frac{k}{\mu} \rho \{ \nabla p + \rho g \hat{\mathbf{k}} \} \right], \quad (2.25)$$

and we need a further equation of state (or two) to complete the model. The simplest assumption corresponds to incompressible groundwater flowing through a rigid porous medium. In this case, ρ and ϕ are constant, and the governing equation reduces (if also k is constant) to Laplace’s equation

$$\nabla^2 p = 0. \quad (2.26)$$

This simple equation forms the basis for the following development. Before pursuing this, we briefly mention one variant, and that is when there is a compressible

pore fluid (e. g., a gas) in a non-deformable medium. Then ϕ is constant (so k is constant), but ρ is determined by pressure and temperature. If we can ignore the effects of temperature, then we can assume $p = p(\rho)$ with $p'(\rho) > 0$, and (also neglecting gravity whose effect for gases is commonly small)

$$\rho_t = \frac{k}{\mu\phi} \nabla \cdot [\rho p'(\rho) \nabla \rho], \quad (2.27)$$

which is a nonlinear diffusion equation for ρ , sometimes called the *porous medium equation*. If $p \propto \rho^\gamma$, $\gamma > 0$, this is degenerate when $\rho = 0$, and the solutions display the typical feature of finite spreading rate of compactly supported initial data.

2.2.1 Boundary conditions

The Laplace equation (2.26) in a domain D requires boundary data to be prescribed on the boundary ∂D of the spatial domain. Typical conditions which apply are a no flow through condition at an impermeable boundary, $\mathbf{u} \cdot \mathbf{n} = 0$, whence

$$\frac{\partial p}{\partial n} + \rho g \mathbf{n} \cdot \hat{\mathbf{k}} = 0 \quad \text{on} \quad \partial D, \quad (2.28)$$

or a permeable surface condition

$$p = p_a \quad \text{on} \quad \partial D, \quad (2.29)$$

where for example p_a would be atmospheric pressure at the ground surface. Another example of such a condition would be the prescription of oceanic pressure at the interface with the oceanic crust.

A more common application of the condition (2.29) is in the consideration of flow in the saturated zone below the water table (which demarcates the upper limit of the saturated zone). At the water table, the pressure is in equilibrium with the air in the unsaturated zone, and (2.29) applies. The water table is a free surface, and an extra kinematic condition is prescribed to locate it. This condition says that the phreatic surface is also a material surface for the underlying groundwater flow, so that its velocity is equal to the average fluid velocity (*not* the flux): bearing in mind (2.4), we have

$$\frac{\partial F}{\partial t} + \frac{\mathbf{u}}{\phi} \cdot \nabla F = 0 \quad \text{on} \quad \partial D, \quad (2.30)$$

if the free surface ∂D is defined by $F(\mathbf{x}, t) = 0$.

2.2.2 Dupuit approximation

One of the principally obvious features of mature topography is that it is relatively flat. A slope of 0.1 is very steep, for example. As a consequence of this, it is typically also the case that gradients of the free groundwater (phreatic) surface are also small, and a consequence of this is that we can make an approximation to the equations of

groundwater flow which is analogous to that used in shallow water theory or the lubrication approximation, i. e., we can take advantage of the large aspect ratio of the flow. This approximation is called the Dupuit, or Dupuit–Forchheimer, approximation.

To be specific, suppose that we have to solve

$$\nabla^2 p = 0 \quad \text{in} \quad 0 < z < h(x, y, t), \quad (2.31)$$

where z is the vertical coordinate, $z = h$ is the phreatic surface, and $z = 0$ is an impermeable basement. We let \mathbf{u} denote the horizontal (vector) component of the Darcy flux, and w the vertical component. In addition, we now denote by $\nabla = \left(\frac{\partial}{\partial x}, \frac{\partial}{\partial y} \right)$ the horizontal component of the gradient vector. The boundary conditions are then

$$\begin{aligned} p = 0, \quad \phi h_t + \mathbf{u} \cdot \nabla h = w \quad \text{on} \quad z = h, \\ \frac{\partial p}{\partial z} + \rho g = 0 \quad \text{on} \quad z = 0; \end{aligned} \quad (2.32)$$

here we take (gauge) pressure measured relative to atmospheric pressure. The condition at $z = 0$ is that of no normal flux, allowing for gravity.

Let us suppose that a horizontal length scale of relevance is l , and that the corresponding variation in h is of order d , thus

$$\varepsilon = \frac{d}{l} \quad (2.33)$$

is the size of the phreatic gradient, and is small. We non-dimensionalise the variables by scaling as follows:

$$\begin{aligned} x, y \sim l, \quad z \sim d, \quad p \sim \rho g d, \\ \mathbf{u} \sim \frac{k \rho g d}{\mu l}, \quad w \sim \frac{k \rho g d^2}{\mu l^2}, \quad t \sim \frac{\phi \mu l^2}{k \rho g d}. \end{aligned} \quad (2.34)$$

The choice of scales is motivated by the same ideas as lubrication theory. The pressure is nearly hydrostatic, and the flow is nearly horizontal.

The dimensionless equations are

$$\begin{aligned} \mathbf{u} = -\nabla p, \quad \varepsilon^2 w = -(p_z + 1), \\ \nabla \cdot \mathbf{u} + w_z = 0, \end{aligned} \quad (2.35)$$

with

$$\begin{aligned} p_z = -1 \quad \text{on} \quad z = 0, \\ p = 0, \quad h_t = w + \nabla p \cdot \nabla h \quad \text{on} \quad z = h. \end{aligned} \quad (2.36)$$

At leading order as $\varepsilon \rightarrow 0$, the pressure is hydrostatic:

$$p = h - z + O(\varepsilon^2). \quad (2.37)$$

More precisely, if we put

$$p = h - z + \varepsilon^2 p_1 + \dots, \quad (2.38)$$

then (2.35) implies

$$p_{1zz} = -\nabla^2 h, \quad (2.39)$$

with boundary conditions, from (2.36),

$$p_{1z} = 0 \quad \text{on} \quad z = 0,$$

$$p_{1z} = -h_t + |\nabla h|^2 \quad \text{on} \quad z = h. \quad (2.40)$$

Integrating (2.39) from $z = 0$ to $z = h$ thus yields the evolution equation for h in the form

$$h_t = \nabla \cdot [h \nabla h], \quad (2.41)$$

which is a nonlinear diffusion equation of degenerate type when $h = 0$.

This is easily solved numerically, and there are various exact solutions which are indicated in the exercises. In particular, steady solutions are found by solving Laplace's equation for $\frac{1}{2}h^2$, and there are various kinds of similarity solution. (2.41) is a second order equation requiring two boundary conditions. A typical situation in a river catchment is where there is drainage from a watershed to a river. A suitable problem in two dimensions is

$$h_t = (hh_x)_x + r, \quad (2.42)$$

where the source term r represents recharge due to rainfall. It is given by

$$r = \frac{r_D}{\varepsilon^2 K}, \quad (2.43)$$

where r_D is the rainfall rate and $K = k\rho g/\mu$ is the hydraulic conductivity. At the divide (say, $x = 0$), we have $h_x = 0$, whereas at the river (say, $x = 1$), the elevation is prescribed, $h = 1$ for example. The steady solution is

$$h = [1 + r - rx^2]^{1/2}, \quad (2.44)$$

and perturbations to this decay exponentially. If this value of the elevation of the water table exceeds that of the land surface, then a seepage face occurs, where water seeps from below and flows over the surface. This can sometimes be seen in steep mountainous terrain, or on beaches, when the tide is going out.

The Dupuit approximation is not uniformly valid at $x = 1$, where conditions of symmetry at the base of a valley would imply that $u = 0$ (below the river), and thus $p_x = 0$. There is therefore a boundary layer near $x = 1$, where we rescale the variables by writing

$$x = 1 - \varepsilon X, \quad w = \frac{W}{\varepsilon}, \quad h = 1 + \varepsilon H, \quad p = 1 - z + \varepsilon P. \quad (2.45)$$

Substituting these into the two-dimensional version of (2.35) and (2.36), we find

$$u = P_X, \quad W = -P_z, \quad \nabla^2 P = 0 \quad \text{in} \quad 0 < z < 1 + \varepsilon H, \quad 0 < X < \infty, \quad (2.46)$$

with boundary conditions

$$\begin{aligned}
P &= H, \quad \varepsilon H_t + P_X H_X = \frac{W}{\varepsilon} + r \quad \text{on} \quad z = 1 + \varepsilon H, \\
P_X &= 0 \quad \text{on} \quad X = 0, \\
P_z &= 0 \quad \text{on} \quad z = 0, \\
P &\sim H \sim rX \quad \text{as} \quad X \rightarrow \infty.
\end{aligned} \tag{2.47}$$

At leading order in ε , this is simply

$$\begin{aligned}
\nabla^2 P &= 0 \quad \text{in} \quad 0 < z < 1, \quad 0 < X < \infty, \\
P_z &= 0 \quad \text{on} \quad z = 0, 1, \\
P_X &= 0 \quad \text{on} \quad X = 0, \\
P &\sim rX \quad \text{as} \quad X \rightarrow \infty.
\end{aligned} \tag{2.48}$$

Evidently, this has no solution unless we allow the incoming groundwater flux r from infinity to drain to the river at $X = 0, z = 1$. We do this by having a singularity in the form of a sink at the river,

$$P \sim \frac{r}{\pi} \ln \{X^2 + (1 - z)^2\} \quad \text{near} \quad X = 0, \quad z = 1. \tag{2.49}$$

The solution to (2.48) can be obtained by using complex variables and the method of images, by placing sinks at $z = \pm(2n + 1)$, for integral values of n . Making use of the infinite product formula (Jeffrey 2004, p. 72)

$$\prod_1^{\infty} \left(1 + \frac{\zeta^2}{(2n + 1)^2}\right) = \cosh \frac{\pi\zeta}{2}, \tag{2.50}$$

where $\zeta = X + iz$, we find the solution to be

$$P = \frac{r}{\pi} \ln \left[\cosh^2 \frac{\pi X}{2} \cos^2 \frac{\pi z}{2} + \sinh^2 \frac{\pi X}{2} \sin^2 \frac{\pi z}{2} \right]. \tag{2.51}$$

The complex variable form of the solution is

$$\phi = P + i\psi = \frac{2r}{\pi} \ln \cosh \frac{\pi\zeta}{2}, \tag{2.52}$$

which is convenient for plotting. The streamlines of the flow are the lines $\psi = \text{constant}$, and these are shown in figure 2.2.

This figure illustrates an important point, which is that although the flow towards a drainage point may be more or less horizontal, near the river the groundwater seeps upwards from depth. Drainage is not simply a matter of near surface recharge and drainage. This means that contaminants which enter the deep groundwater may reside there for a very long time.

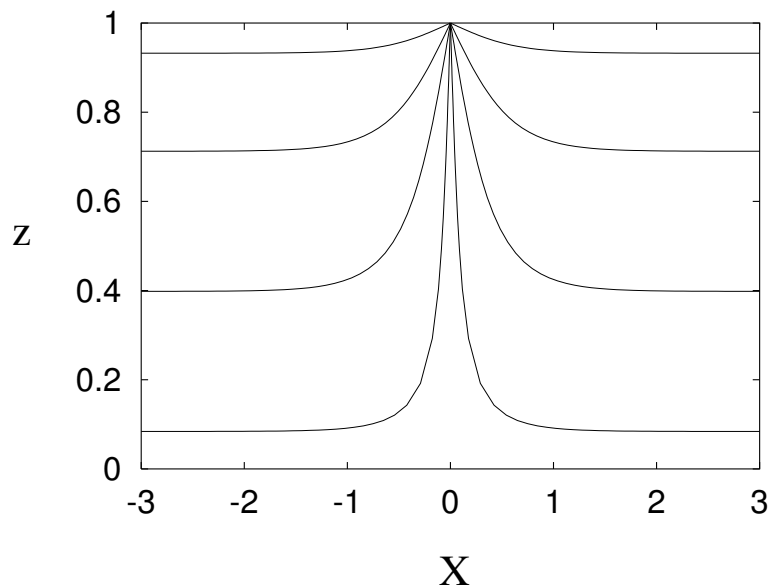


Figure 2.2: Groundwater flow lines towards a river at $X = 0$, $z = 1$.

A related point concerns the recharge parameter r defined in (2.43). According to table 2.1, a typical permeability for sand is 10^{-10} m^2 , corresponding to a hydraulic conductivity of $K = 10^{-3} \text{ m s}^{-1}$, or $3 \times 10^4 \text{ m y}^{-1}$. Even for phreatic slopes as low as $\varepsilon = 10^{-2}$, the recharge parameter $r \lesssim O(1)$, and shallow aquifer drainage is feasible.

However, finer-grained sediments are less permeable, and the calculation of r for a silt with permeability of 10^{-14} m^2 ($K = 10^{-7} \text{ m s}^{-1} = 3 \text{ m y}^{-1}$) suggests that $r \sim 1/\varepsilon^2 \gg 1$, so that if the Dupuit approximation applied, the groundwater surface would lie above the Earth's surface everywhere. This simply points out the obvious fact that if the groundmass is insufficiently permeable, drainage cannot occur through it but water will accumulate at the surface and drain by overland flow. The fact that usually the water table is below but quite near the surface suggests that the long term response of landscape to recharge is to form topographic gradients and sufficiently deep sedimentary basins so that this *status quo* can be maintained.

2.2.3 Saltwater intrusion in a coastal aquifer

In many dry coastal areas around the world, such as Cyprus, Israel or Australia, porous aquifers are often used as a means of storing and filtering water for safe use (e.g. drinking water). Typically, aquifers are chosen above an impermeable bed rock and are often dammed upstream to control the flow of water. Water flows towards the sea, with fresh water meeting salty water below the coastline. It is important that the salt water does not invade the aquifer since this would render the water unsuitable for supply and put the aquifer out of use for a significant time. Hence, the groundwater level is frequently monitored at various locations, and controlled by recharging if

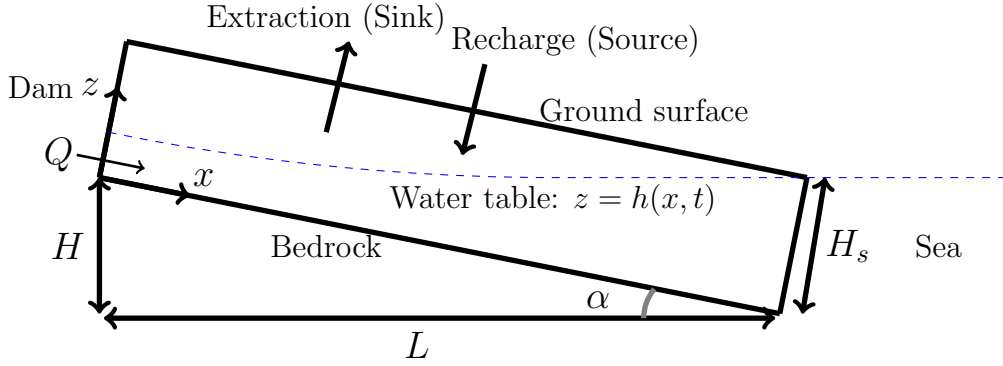


Figure 2.3: Schematic diagram of the long and thin sloping aquifer. The water table level is indicated with the blue dashed curve. The coordinate system x and z is taken respectively along and perpendicular to the bedrock, which is assumed to be flat and α is the angle to the horizontal level. (Taken from Mondal et al. (2019)).

necessary. Below the water table the aquifer is fully saturated and approximately dry above it. Here we will briefly describe and mathematically formulate such a scenario.

We choose a rotated coordinate system such that the x direction is parallel to the bedrock level, inclined at a constant angle α to the horizontal, and the z direction is perpendicular to the bedrock. L and H are the length and elevation of the aquifer, respectively, and $\tan \alpha = H/L$ (see Fig. 2.3). We denote by (u, w) the velocity components in the (x, z) directions, and by p the pressure. The flow is governed by the continuity equation and the Darcy equations as follows:

$$\begin{aligned}
 u_x + w_z &= 0, \\
 u &= -\frac{k}{\mu} (p_x - \rho g \sin \alpha), \\
 w &= -\frac{k}{\mu} (p_z + \rho g \cos \alpha).
 \end{aligned} \tag{2.53}$$

The rate of extraction (sinks) and recharge (sources) is modelled by a function $s(x, t)$ in the kinematic condition

$$w = h_t + u h_x - s(x, t) : \quad z = h(x, t). \tag{2.54}$$

We also impose the dynamic condition $p = p_a$ on $z = h$, as well as impermeability $w = 0$ on $z = 0$, constant flux (seepage from the dam) Q at $x = 0$ and that the groundwater meets the sea level $h = H_s$ at $x = L$.

After appropriate non-dimensionalisation and using the small angle approximation $\sin \alpha \approx \alpha \approx H/L$, the governing equations and boundary conditions become

$$\begin{aligned}
 h_t + (h(1 - h_x))_x &= s, \\
 h(1 - h_x) &= \hat{Q} : \quad x = 0, \\
 h &= \hat{H} : \quad x = 1,
 \end{aligned} \tag{2.55}$$

where $\hat{Q} = QL/\epsilon KH^2$ and $\hat{H} = H_s/H$. In the steady state we can integrate this system by defining

$$S = \int_0^x s \, dx, \quad (2.56)$$

which is the cumulative extraction/recharge. Hence, the dimensionless velocity of the flow is

$$1 - h_x = \frac{\hat{Q} + S(x)}{h}, \quad (2.57)$$

indicating that the outflow will be positive under the condition

$$u(x = 1) > 0 \quad \text{if} \quad \hat{Q} + S(1) > 0. \quad (2.58)$$

This imposes a constraint on the recharge rate S (given seepage rate \hat{Q}) such that seawater is not flowing into the aquifer (i.e. this allows water management teams to recharge sufficiently to avoid seawater intrusion). Note, in the simple case where $S = 0$ the solution is given implicitly as

$$h - \hat{H} + \hat{Q} \log \frac{h - \hat{Q}}{\hat{H} - \hat{Q}} = x - 1. \quad (2.59)$$

It is worth discussing the boundary between the fresh and salty water in more detail. In general, this boundary is modelled as being sharp (for the sake of simplicity) or diffuse, due to the transport of salt. In the case of a sharp interface model, there is a level beneath the water table, below which the water is salty (with uniform salt concentration) and above which it is completely fresh. In non-rotated coordinates (i.e. measuring z above sea level), the water table height is denoted h_w , whereas the saltwater table height is denoted h_s , such that an Archimedes balance indicates

$$h_s = \frac{\rho_w}{\rho_s - \rho_w} h_w \approx 40h_w, \quad (2.60)$$

where ρ_s is the density of salty water. Under the small angle approximation we have

$$h_w \approx h - \left(\hat{H} + x - 1 \right), \quad (2.61)$$

where the subtracted quantity is the zero-flow case ($u = 0$). Hence, we can rearrange to find the saltwater level

$$h_s = \frac{\rho_w}{\rho_s - \rho_w} \left[h - \left(\hat{H} + x - 1 \right) \right]. \quad (2.62)$$

Again, this serves as a useful tool for estimating the intrusion of saltwater into the aquifer, and to control recharge rates accordingly to avoid contamination. In practice, the interface between these two bodies of water is not sharp, because the salt undergoes both advection and diffusion. In this case, the Boussinesq approximation can be applied to the density, such that

$$\rho = \rho_w(1 + \beta c), \quad (2.63)$$

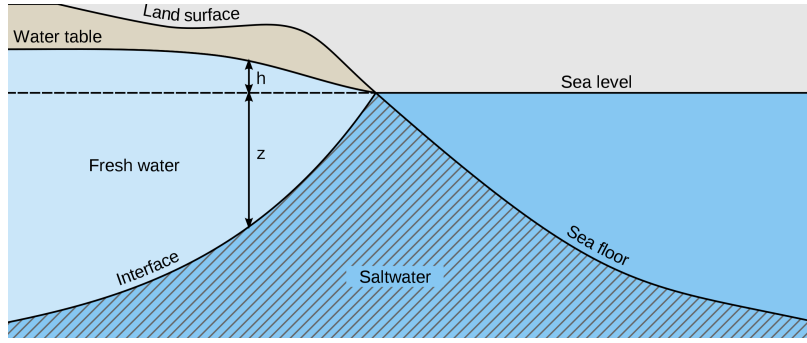


Figure 2.4: Schematic diagram of the Ghyben-Herzberg relationship for salt water intrusion in a coastal aquifer (Taken from Barlow (2003)). In (2.60) the variables h_s, h_w correspond to z, h in the image.

where β is an empirical parameter, and c is the concentration of salt which is subject to the advection-diffusion equation

$$c_t + \mathbf{u} \cdot \nabla c = D \nabla^2 c, \quad (2.64)$$

where D is the diffusion coefficient. This must be solved in conjunction with the Darcy equations, typically using a numerical scheme. In such cases, iso-levels for the concentration indicate the location of dangerous levels of saltwater intrusion.

2.2.4 Carbon capture and storage

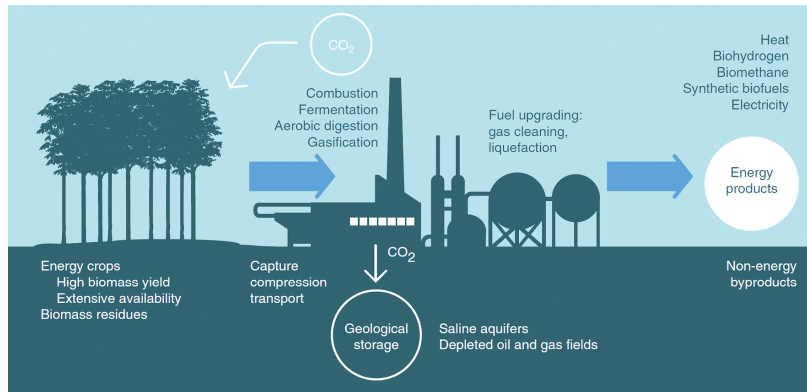


Figure 2.5: Illustration of the process of Carbon Capture and Storage (CCS). In this example, biomass (carbon sink) is combusted and CO_2 emissions captured and stored in a geological reservoir. (taken from Bui et al. (2018)).

The overproduction of carbon dioxide emissions is one of biggest challenges facing humankind over the next century. As outlined in the Paris Agreement (2015), it is

necessary to limit global warming to less than 2° C by the year 2100 to avoid the most dangerous consequences of climate change. To meet these temperature targets it is imperative to reduce our CO₂ emissions quickly, and by as much as possible.

One of the few proposed technological solutions to this problem is carbon capture and storage (CCS) - that is, capturing CO₂ at source (e.g. power plants and factories) and injecting it into porous geological reservoirs to be sequestered (stored) several kilometres beneath the ground. Trapping of the CO₂ occurs in a variety of different ways that take place over vastly different timescales, as illustrated in Fig. 2.5 (taken from Krevor et al (2015)). Initially (over the first few years of injection) the CO₂ is trapped by impermeable caprocks preventing it from rising upwards; then over longer timescales it is trapped by small scale capillary forces and by dissolution within the surrounding salty brine. Finally, over much longer time scales, the CO₂ is converted into various minerals and stored permanently in the rock.

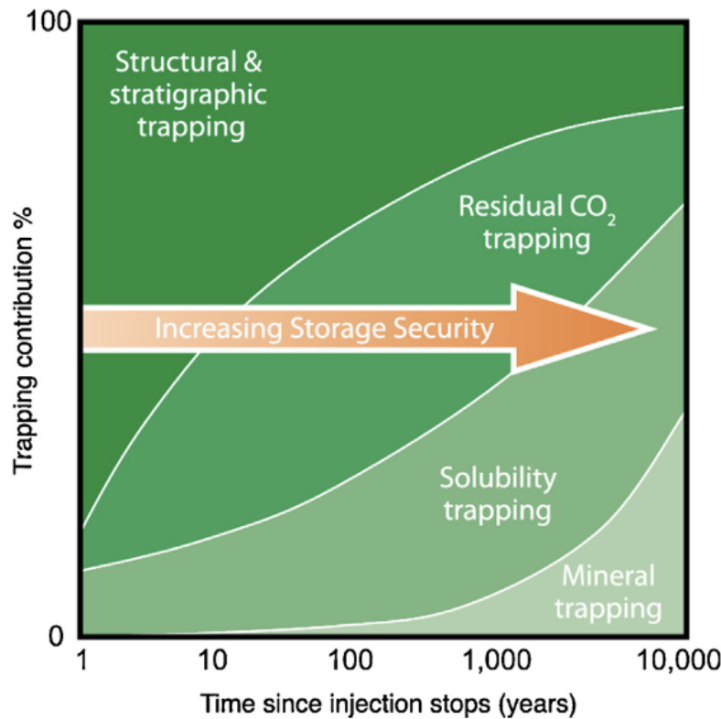


Figure 2.6: Diagram showing the different trapping mechanisms for CO₂ sequestration and the timescales over which they take place (taken from Krevor et al. (2015)).

CO₂ sequestration is currently being developed as a technology in different sites around the world. Many sites still remain in the research phase, whilst others are being designed and built to be used in conjunction with future power stations. The most famous case study of CCS is at Sleipner, a natural gas field in the Norwegian North Sea. Since 1996, after the Norwegian government introduced a significant tax on carbon emissions, the operators began capturing and sequestering CO₂ which is

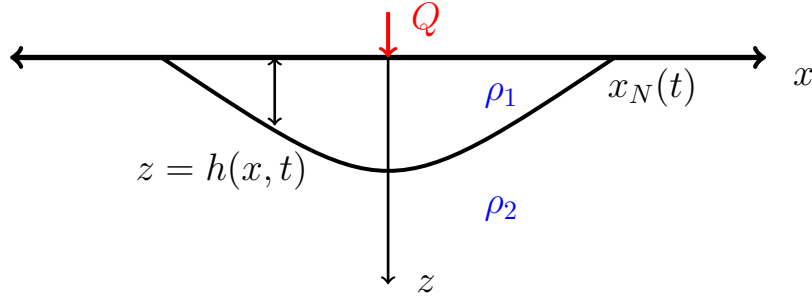


Figure 2.7: Schematic diagram of CO₂ injected at a rate Q beneath an impermeable cap rock located at $z = 0$.

extracted as a by-product of the natural gas (before this tax the CO₂ was simply released into the atmosphere). Between 1996 (when the project began) and 2018, approximately one million tonnes of CO₂ were stored at Sleipner, and it will continue to be used for many years to come.

The complex flow patterns involved during CO₂ sequestration, together with the multi-scale nature of the process (with rock variations from the millimetre to the kilometre), presents several modelling challenges. Here we discuss several useful mathematical tools, such as similarity and asymptotic analyses, to gain insights into the factors that affect CO₂ migration, and to help improve the overall safety and efficiency of CO₂ sequestration in porous geological reservoirs.

A simple illustration of CO₂ injected at a rate Q beneath an impermeable cap rock is illustrated in Fig. 2.7. For simplicity, we model this in two-dimensions (which is equivalent to CO₂ injected from a line source). The injected CO₂ has a lower density than the surrounding brine, such that $\rho_1 < \rho_2$. A coordinate system is chosen with z increasing downwards, such that the impermeable cap rock is located at $z = 0$, whereas the shape of the current is given by $z = h(x, t) \geq 0$. We consider a symmetric current and therefore restrict our attention to the half-width $x \in [0, x_N(t)]$, where $x_N(t)$ is the position of the leading edge. We denote the density difference between fluids as $\Delta\rho = \rho_2 - \rho_1$ and the conductivity as $K = k\Delta\rho g/\mu$.

By non-dimensionalising variables according to

$$x, h \sim Q/K, \quad t \sim \phi Q/K^2, \quad (2.65)$$

and applying the Dupuit approximation, the governing system of equations and boundary conditions become

$$\begin{aligned} h_t &= (hh_x)_x, \\ -hh_x &= 1, \quad x = 0, \\ -hh_x &= 0, \quad x = x_N(t), \\ h &= 0, \quad x = x_N(t). \end{aligned} \quad (2.66)$$

One of these boundary conditions can be replaced by the mass conservation condition

$$\int_0^{x_N} h \, dx = t. \quad (2.67)$$

As discussed previously, such systems often admit self-similar solutions. In this case, a self-similar solution exists of the form

$$h = t^{1/3} f(\eta), \quad \eta = x/t^{2/3}, \quad (2.68)$$

for which the system reduces to a BVP of the form

$$\begin{aligned} \frac{1}{3} [f - 2\eta f'] &= [f f']', \\ -f f' &= 1, \quad \eta = 0, \\ f &= 0, \quad \eta = \eta_N, \\ \int_0^{\eta_N} f \, d\eta &= 1, \end{aligned} \quad (2.69)$$

where η_N is an unknown constant which is found as part of the solution (i.e. a free boundary problem).

2.2.5 Numerical solutions to nonlinear differential equations

Whilst we have seen such problems before, we have not yet discussed how a solution could actually be calculated. In general such problems must be solved numerically, using a finite difference scheme for example. In such a numerical approach, it is inconvenient that the size of the numerical domain (η_N) is unknown, so instead we introduce a stretched coordinate system

$$y = \eta/\eta_N, \quad F(y) = f(\eta), \quad (2.70)$$

such that the system is written as

$$\begin{aligned} \frac{\eta_N^2}{3} [F - 2yF'] &= [FF']', \\ -\frac{1}{\eta_N} FF' &= 1, \quad y = 0, \\ F &= 0, \quad y = 1, \\ \eta_N \int_0^1 F \, dy &= 1. \end{aligned} \quad (2.71)$$

Using a finite difference approach, we discretise space into N steps, y_1, y_2, \dots, y_N , where $y_1 = 0$, $y_N = 1$ and $y_i - y_{i-1} = dy$ is a constant step size. We denote the corresponding function values as F_1, F_2, \dots, F_N , and we consider second order

accurate scheme (i.e. which solves the system up to an accuracy of $\mathcal{O}(dy^2)$). There are many different possible ways we can choose to approximate derivatives using finite difference. For example, we could use a forward, central, or backward scheme, which are each given by

$$F'(y_i) \approx \frac{1}{2dy} (-3F_i + 4F_{i+1} - F_{i+2}), \quad (2.72)$$

$$F'(y_i) \approx \frac{1}{2dy} (-F_{i-1} + F_{i+1}), \quad (2.73)$$

$$F'(y_i) \approx \frac{1}{2dy} (F_{i-2} - 4F_{i-1} + 3F_i), \quad (2.74)$$

respectively (note, these coefficients are calculated by considering a Taylor expansion about the function F evaluated at different locations). Hence, a consistent way of writing a derivative matrix $\underline{\underline{\mathbf{D}}}$ (which operates on the vector $\underline{\mathbf{F}}$) is:

$$\underline{\underline{\mathbf{D}}}\underline{\mathbf{F}} = \frac{1}{dy} \begin{pmatrix} -3/2 & 2 & -1/2 & & & \\ -1 & 0 & 1 & & & \\ & & \ddots & & & \\ & & & -1 & 0 & 1 \\ & & & 1/2 & -2 & 3/2 \end{pmatrix} \begin{pmatrix} F_1 \\ F_2 \\ \vdots \\ F_{N-1} \\ F_N \end{pmatrix}. \quad (2.75)$$

In this way, the derivative can be approximated to second order accuracy across the whole domain without using any more or fewer points than necessary. Of course, we could have used a higher (or lower) order method, in which case the above matrix would contain more (or fewer) column entries corresponding to extra terms in the Taylor series for the derivative.

The vector form of our governing equation is therefore

$$\underline{\mathbf{G}} := \frac{\eta_N^2}{3} [\underline{\mathbf{F}} - 2\underline{\mathbf{y}} \circ \underline{\underline{\mathbf{D}}}\underline{\mathbf{F}}] - \underline{\underline{\mathbf{D}}} [\underline{\mathbf{F}} \circ \underline{\underline{\mathbf{D}}}\underline{\mathbf{F}}] = \underline{\mathbf{0}}, \quad (2.76)$$

where the notation \circ indicates the pointwise product ($\underline{\mathbf{a}} \circ \underline{\mathbf{b}} = (a_1b_1, a_2b_2, \dots, a_Nb_N)$). This vector equation applies to all points $i = 2, 3, \dots, N-1$, whereas the boundary conditions must be applied to the first and last points F_1 and F_N . These take the form:

$$\begin{aligned} G_1 : &= \frac{1}{\eta_N} [\underline{\mathbf{F}} \circ \underline{\underline{\mathbf{D}}}\underline{\mathbf{F}}]_1 + 1 = 0, \\ G_N : &= F_N = 0. \end{aligned} \quad (2.77)$$

This defines a square system of N equations ($\underline{\mathbf{G}}$) for N unknowns $\underline{\mathbf{F}}$. However, this neglects the fact that η_N is also an unknown. Hence, the mass conservation constraint provides a final equation, and we approximate this using the trapezoidal rule

$$G_{N+1} := \frac{\eta_N dy}{2} \left[F_1 + F_N + \sum_{i=2}^{N-1} 2F_i \right] - 1 = 0. \quad (2.78)$$

Hence, we now have a $(N + 1) \times (N + 1)$ square system that is well-defined. However, we note that the governing equations and hence the system is nonlinear, and therefore cannot be solved by simple matrix inversion.

One way of solving the above system is using Newton's method. If we write the combined vector $\underline{\mathbf{X}} = (F_1, F_2, \dots, F_N, \eta_N)$, then Newton's method provides iterations for converging to the root of the function $\underline{\mathbf{G}}(\underline{\mathbf{X}})$. Starting with an initial guess $\underline{\mathbf{X}}^0$, iterations are thereafter given by

$$\underline{\mathbf{X}}^{n+1} = \underline{\mathbf{X}}^n - \underline{\underline{\mathbf{J}}}^{-1}(\underline{\mathbf{X}}^n)\underline{\mathbf{G}}(\underline{\mathbf{X}}^n), \quad (2.79)$$

where $\underline{\underline{\mathbf{J}}}$ is the Jacobian matrix. The Jacobian is defined (using subscript notation) as

$$J_{ij} = \frac{\partial G_i}{\partial X_j}. \quad (2.80)$$

There are several ways we could calculate $\underline{\underline{\mathbf{J}}}$. In principle, none of the individual $\underline{\mathbf{G}}$ equations are very complicated, so it's feasible to calculate these analytically. However, this is extremely tedious and prone to error, considering the number of equations involved (i.e. for large N). Hence, one approach is to calculate $\underline{\underline{\mathbf{J}}}$ using finite differences, by evaluating $\underline{\mathbf{G}}$ at different values of $\underline{\mathbf{X}}$. However, since $\underline{\mathbf{G}}$ and $\underline{\mathbf{X}}$ are both of length $N + 1$, this requires $(N + 1)^2$ function evaluations per Newton iteration. In other words, this becomes intractable for large N . However, for smaller values of N (as we will see in Problem Sheet 2), this works fine.

Another approach is to use a computer to calculate the derivatives in $\underline{\underline{\mathbf{J}}}$ for us, which is known as *automatic differentiation*. This is an extremely powerful (but surprisingly seldom used) tool. The idea is that all variables written in computer code are defined in terms of operations like multiplication, addition, and so on, which can all be differentiated by the chain and product rules. Even more complicated functions such as $\sin(x)$, $\exp(x)$, etc... are usually defined in terms of a Taylor series on a computer, and therefore are simply defined in terms of addition and multiplication. In this way, a computer can compile the Jacobian matrix in terms of a very long list of chain rule operations given in terms of the variables $\underline{\mathbf{X}}$. This only needs to be compiled once (before running the code) and can thereafter be evaluated at every iteration. For example, the 1st row of $\underline{\mathbf{G}}$ is

$$G_1 = \frac{1}{2\eta_N dy} F_1 (-3F_1 + 4F_2 - F_3) + 1. \quad (2.81)$$

It is straightforward for a computer to calculate derivatives of G_1 using the product and chain rule. For example, the first entry of the Jacobian (as seen by an automatic differentiation algorithm) is

$$\frac{\partial G_1}{\partial F_1} = \frac{1}{2\eta_N dy} \frac{\partial F_1}{\partial F_1} (-3F_1 + 4F_2 - F_3) + \frac{1}{2\eta_N dy} F_1 \left(-3 \frac{\partial F_1}{\partial F_1} + 0 - 0 \right) + 0. \quad (2.82)$$

Automatic differentiation is a feature of the *Julia* programming language, for example (see Problem Sheet 2).

Another approach to solve such problems is known as the *shooting method*. This is where we convert the above BVP into an IVP and guess the value of $\eta_N = \eta_{N_0}$. First we note that we can write the problem as a system of first order ODE's,

$$\begin{aligned} F'(y) &= -\frac{L}{F}, \\ L'(y) &= -\frac{\eta_N^2}{3} \left(F + 2y \frac{L}{F} \right), \end{aligned} \quad (2.83)$$

where we have introduced the flux function $L = -FF'$. At the right hand boundary the variables satisfy

$$L(1) = 0, \quad F(1) = 0, \quad \lim_{y \rightarrow 1} \frac{L}{F} = \frac{2\eta_N^2}{3}, \quad (2.84)$$

where the last of these is found by analysing the governing ODE's near $y \approx 1$. One can then discretise the variables \mathbf{F} , \mathbf{L} , into N points, as before. Then, the solution is found by marching backwards from $y = 1$ down towards $y = 0$ using a suitable finite difference scheme. For example, a simple first order scheme gives us

$$\begin{aligned} F_{i-1} &= F_i - dy \left[-\frac{L}{F} \right]_i, \\ L_{i-1} &= L_i - dy \left[-\frac{\eta_N^2}{3} \left(F + 2y \frac{L}{F} \right) \right]_i, \end{aligned} \quad (2.85)$$

which can be evaluated for $i = N, N-1, \dots, 2$. Hence, the flux value at the origin, L_1 will not satisfy the correct condition $L_1 = \eta_N$ unless the correct value of η_{N_0} was used as an initial guess. Equivalently, the same applies to the mass conservation condition (2.67) (which is (2.78) in discretised form).

This is why the above approach is known as the shooting method. A guess is chosen for the parameter η_{N_0} , after which one shoots towards the origin (missing one's target), and η_N is updated accordingly to get closer and closer to the target iteratively. Essentially, we treat the above approach as a root-finding method for the function

$$\mathcal{F}(\eta_N) = \eta_N \int_0^1 F dy - 1, \quad (2.86)$$

where the integral is discretised (e.g. using the trapezoidal rule) and the vector \mathbf{F} , which is calculated numerically using the shooting method, is considered a function of the parameter η_N . Hence, η_N can be updated using any root-finding algorithm, such as Newton's method for example.

Whilst these examples give two possible approaches to solve nonlinear differential equations, there are plenty of other methods, such as *pseudo-time-stepping*, for example. Let's briefly discuss time-stepping methods in general, since these are essential in most fluid dynamics problems. Suppose that the boundary conditions of the above problem were modified in such a way that no self-similar solution exists. For example,

this can be achieved by setting the inflow condition to some function of time $Q = Q(t)$ which is not necessarily power law (e.g. set by the operator of the CO₂ sequestration site). In this case it is not possible to convert to a set of similarity equations, but instead we must solve the full PDE system (2.66) numerically. However, there is no need to fear since we already have nearly all the tools to do this.

First we discretise the shape of the current into a vector of N spatial points, $\underline{\mathbf{h}}$. Then, we discretise in time by considering a time step of size dt and marching forwards from $t = 0$ to the n^{th} time step value, $t = ndt$. Approximating the time derivative using a first order implicit Euler scheme, we get

$$\frac{1}{dt} (\underline{\mathbf{h}}^{n+1} - \underline{\mathbf{h}}^n) = (\underline{\mathbf{D}} \underline{\mathbf{h}}^{n+1}) \circ (\underline{\mathbf{D}} \underline{\mathbf{h}}^{n+1}) + \underline{\mathbf{h}}^{n+1} \circ (\underline{\mathbf{D}}^2 \underline{\mathbf{h}}^{n+1}). \quad (2.87)$$

This is known as an implicit scheme because the right hand side is evaluated at the $n+1$ time step, rather than the n time step, which is far more stable (see any standard textbook on numerical analysis). Hence, the above can be rearranged into a system of equations for the unknown vector $\underline{\mathbf{h}}^{n+1}$, which are

$$\underline{\mathbf{G}}(\underline{\mathbf{h}}^{n+1}) := \underline{\mathbf{h}}^{n+1} - \underline{\mathbf{h}}^n - dt [(\underline{\mathbf{D}} \underline{\mathbf{h}}^{n+1}) \circ (\underline{\mathbf{D}} \underline{\mathbf{h}}^{n+1}) + \underline{\mathbf{h}}^{n+1} \circ (\underline{\mathbf{D}}^2 \underline{\mathbf{h}}^{n+1})], \quad (2.88)$$

where $\underline{\mathbf{h}}^n$ is known. This approach is often called the *method of lines*.

As before, we need to ensure that the boundary conditions are satisfied at $x = 0$ and $x = x_N(t)$. The flux boundary condition at $x = 0$ is imposed by replacing the first equation in (2.88) with

$$G_1 := [\underline{\mathbf{h}}^{n+1} \circ (\underline{\mathbf{D}} \underline{\mathbf{h}}^{n+1})]_1 + Q^{n+1} = 0, \quad (2.89)$$

where Q^{n+1} is the function $Q(t)$ discretised and evaluated at the $n+1$ time step.

The boundary conditions at $x = x_N(t)$ can be dealt with using a special trick, making use of the fact that the shape function $h(x, t)$ has *compact support*. In other words, for $x \geq x_N(t)$ the shape satisfies $h = 0$, and $-hh_x = 0$ exactly. Therefore, if we define our numerical domain $x \in [0, L]$ and discretise into N points h_i , then we can set the initial conditions for the gravity current as

$$h_i^0 = \begin{cases} f(x_i) : & 0 < x_i < x_N(0), \\ 0 : & x_N(0) \leq x_i \leq L, \end{cases} \quad (2.90)$$

for some function f which is continuous at the initial nose position $x = x_N(0)$. Henceforth, for all time steps $n > 0$ we solve the nonlinear square system (2.88) (with first entry (2.89)) using Newton's method, and there is no need to impose any boundary conditions at $x = x_N$. This is because the flux $-hh_x$ naturally vanishes wherever the thickness h drops to zero, i.e. at the moving boundary $x_N(t)$. There is no need to impose the dynamic evolution of $x_N(t)$, since this will naturally follow from conservation of mass (i.e. since the PDE and BC's are satisfied). This method can be applied to many diffusion problems with compact support, and we will explore further in Problem Sheet 2.

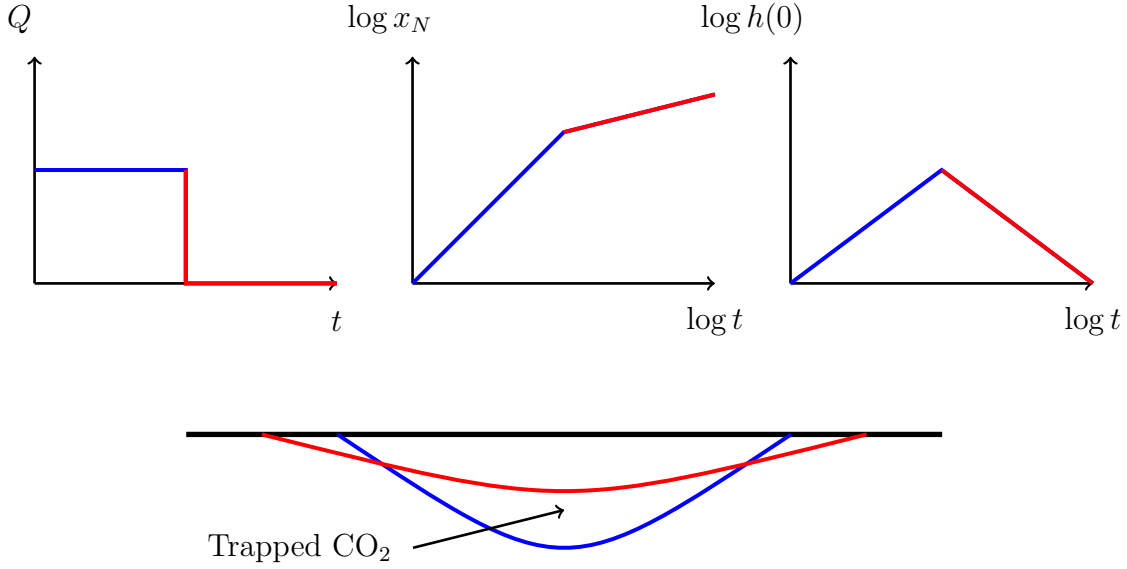


Figure 2.8: Illustration of gravity current dynamics when CO_2 is injected over an interval.

2.2.6 Injection intervals

Suppose that at some time after injection the flow rate is switched off $Q = 0$. In this case, conservation of mass indicates that the gravity current must satisfy

$$\int_0^{x_N(t)} h \, dx = V, \quad (2.91)$$

for all time thereafter, where V is some constant. It is straightforward to show that this setup admits a similarity solution of the form

$$h = t^a f(\eta), \quad \eta = x/t^b, \quad (2.92)$$

where $a = -1/3$ and $b = 1/3$. Attention must be paid when considering the non-dimensionalisation of this model, since Q no longer exists as a dimensional parameter. Instead, appropriate scalings are given in terms of the volume (per unit width) of the current

$$x, h \sim V^{1/2}, \quad t \sim \phi V^{1/2}/K. \quad (2.93)$$

We note that the vertical extent of the current h shrinks like $\sim t^{-1/3}$ when $Q = 0$, compared to growing like $\sim t^{1/3}$ when Q is a constant. Hence, if we consider an injection interval in which Q is switched off after some finite time t_c , then the motion of the current changes from a situation in which it is invading new vertical space to a situation in which it is withdrawing from that vertical space. As we will discuss later, due to contact line effects between the CO_2 , rock and water, the invading and retreating properties of CO_2 are different. In fact, as the CO_2 withdraws from pore

space, it typically leaves a fraction of its mass behind, trapped in the pore spaces due to small scale capillary forces. This scenario is illustrated in Fig. 2.8, indicating the region of trapped CO_2 as the injection switches off. Since the objective of CCS is to sequester as much CO_2 as possible within a reservoir, there is an important and active area of research in understanding ways to optimally store CO_2 by controlling injection rates in such ways.

2.2.7 Heterogeneities



Figure 2.9: Tullig point, Co. Clare, Ireland. (taken from Woods (2005)).

So far we have only considered spatially uniform rocks with constant permeability k and porosity ϕ . In practice, all real porous media in the environment have significantly non-uniform values of k and ϕ . For example, rocks are often composed of sedimentary layers, as can be seen on some coastal cliffs. Such rocks were formed by the deposition of different types of sediment over time, resulting in layers with potentially very different properties (such as permeability), as shown in Fig. 2.9. When considering flow of CO_2 , groundwater, or any such fluid through a heterogeneous rock, the resulting patterns can become extremely complex and difficult to resolve. Hence, it is often desirable to describe the averaged, or *upscaled*, properties of heterogeneous porous media, rather than modelling the precise details of these complex layer arrangements. Here we will briefly discuss some approaches for upscaling heterogeneous media, and how these heterogeneities can affect the macroscopic arrangement of the flow.

Consider the two flow scenarios depicted in Fig. 2.10. A constant pressure drop $p_b - p_a$ is imposed across a layered rock of width L . We consider separately the flow perpendicular to, and parallel to a two layer system with permeability values k_1 and

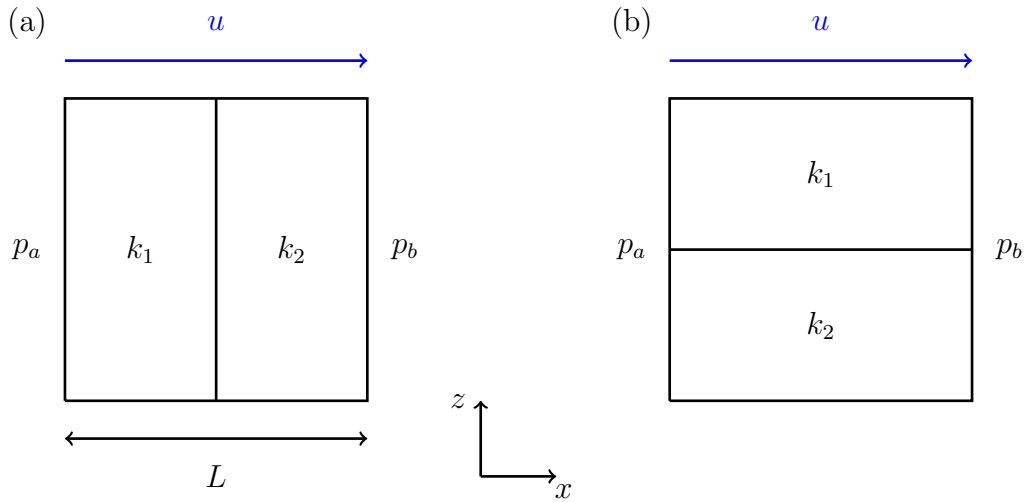


Figure 2.10: Schematic diagram of flow perpendicular (a) and parallel (b) to sedimentary layers in a porous rock.

k_2 . Starting with the first (perpendicular) case, Darcy's law states that the horizontal flow is given by

$$u = -\frac{k(x)}{\mu} p_x. \quad (2.94)$$

By integrating across the width of the flow region, we get

$$\Delta p = p_b - p_a = \int_0^L -\frac{\mu u}{k(x)} dx. \quad (2.95)$$

Meanwhile, the continuity equation $u_x + w_z = 0$ indicates that if there is no vertical flow then u must be a constant. By symmetry (or by considering an infinitely tall system) we see that $w = 0$, and hence the above integral simplifies and rearranges to

$$u = -\frac{k_{\perp} \Delta p}{\mu L}, \quad (2.96)$$

where the effective permeability in the perpendicular direction is given by

$$k_{\perp} = \frac{2}{1/k_1 + 1/k_2}, \quad (2.97)$$

which is incidentally the harmonic mean of the two permeability values. Since u is a constant in this system, it is also equivalent to the average velocity value, and hence we write $u = \bar{u}$.

In the case of flow parallel to the layers (as shown in Fig. 2.10b), the horizontal flow is different in each of the two layers

$$\begin{aligned} u_1 &= -\frac{k_1 \Delta p}{\mu L}, \\ u_2 &= -\frac{k_2 \Delta p}{\mu L}. \end{aligned} \quad (2.98)$$

Hence, the average flow across the system is given by

$$\bar{u} = -\frac{k_{\parallel}\Delta p}{\mu L}, \quad (2.99)$$

where

$$k_{\parallel} = \frac{1}{2}(k_1 + k_2). \quad (2.100)$$

We now have two effective permeability values for flow perpendicular and parallel to the layers. In this way, we can define the ratio between the two as

$$\alpha = \frac{k_{\perp}}{k_{\parallel}} = \frac{4\kappa}{(1 + \kappa)^2}, \quad (2.101)$$

where $\kappa = k_1/k_2$. Clearly, $\alpha(\kappa)$ has a unique maximum at $\kappa = 1$. This indicates that perpendicular flow is always less than parallel flow for a fixed pressure gradient and viscosity.

In general, these upscaled permeability values are a good approximation for flow across or along many-layered systems, so long as the flow length scale h is much larger than the layer width scale d , such that $h/d \gg 1$. In other words, a unidirectional flow across a system of many layers can be well approximated as a flow through a homogeneous medium with uniform permeability given by k_{\perp} .

In the case where the flow has more complex layer structures (i.e. with more than two permeability values, or with differing layer widths), the above upscaling analysis can be extended easily. In this case, we have

$$\begin{aligned} k_{\perp} &= \left[\frac{1}{L} \int_0^L \frac{1}{k} dx \right]^{-1}, \\ k_{\parallel} &= \frac{1}{H} \int_0^H k dz, \end{aligned} \quad (2.102)$$

where H is the vertical extent of the flow region.

For real sedimentary systems the ratio $\alpha(\kappa)$ has been measured in the range $10^{-4} - 10^{-1}$. Next we will investigate the possible consequences of such a large permeability ratio. To do so, we consider a porous medium with upscaled properties k_{\parallel} and k_{\perp} in the x and z directions. This is known as an *anisotropic* permeability field, for which Darcy's law is written

$$\mathbf{u} = -\frac{1}{\mu} \underline{\mathbf{k}} \cdot \nabla [p + \rho gz], \quad (2.103)$$

where $\underline{\mathbf{k}} = \text{diag}(k_{\parallel}, k_{\perp})$. In doing so, we have approximated a heterogeneous system of layers as a single medium with anisotropic properties. As discussed previously, this is only valid when the flow extends across many layers. Alternatively, (2.103) is also a valid model for rocks which are genuinely anisotropic, as can happen when sedimentary layers undergo compaction due to high lithostatic pressures (i.e. the weight of overlying rock) over very long time scales. In either case, such a model is relevant to many real flow scenarios in porous media.

2.2.8 Injection into anisotropic media

Consider the injection Q of CO_2 into a two-dimensional anisotropic porous medium with permeability field $\underline{k} = \text{diag}(k_{\parallel}, k_{\perp})$ in the x, z directions. As before, we consider that the flow is bounded above by a horizontal impermeable cap rock located at $z = 0$. Due to the continuity equation, the pressure satisfies

$$k_{\parallel} p_{xx} + k_{\perp} p_{zz} = 0, \quad (2.104)$$

within the injected fluid. By switching to a stretched coordinate system

$$\xi = \alpha^{1/4} x, \quad \zeta = \alpha^{-1/4} z, \quad (2.105)$$

the pressure then satisfies the standard Laplace equation,

$$p_{\xi\xi} + p_{\zeta\zeta} = 0. \quad (2.106)$$

The pressure solution (which satisfies suitable flux conditions at the origin) is simply the Green's function in two dimensions

$$p = -\frac{Q\mu}{\pi k_e} \log r + f(t), \quad (2.107)$$

where $r = (\xi^2 + \zeta^2)^{1/2}$, $f(t)$ is some function of time, and $k_e = k_{\parallel}\alpha^{1/2} = k_{\perp}\alpha^{-1/2}$ is the effective permeability. This solution does not include the effects of gravity and is therefore only valid very close to the injection point. Hence, this is the appropriate form of the pressure at very early times, when the injected region is very small. This can be seen by comparing the dimensional pressure scaling associated with (2.107) ($Q\mu/k_e$) and the pressure scale associated with the weight of a current of depth H ($\Delta\rho g H$). Hence, (2.107) is valid for currents which satisfy

$$\frac{Q\mu}{k_e} \gg \Delta\rho g H. \quad (2.108)$$

In this case, gravity can be ignored and the appropriate boundary condition for the pressure at the edge of the current is $p = p_a$. By symmetry (since gravity is negligible) the current must grow radially outwards like a circle of radius $R(t)$. Hence, we have

$$p - p_a = -\frac{Q\mu}{\pi k_e} \log \frac{r}{R(t)}. \quad (2.109)$$

The dynamics of the radius are determined by the kinematic condition, which states that

$$\dot{R} = \frac{u_r}{\phi}, \quad (2.110)$$

where u_r is the radial velocity outwards, given by

$$u_r = -\frac{k_e}{\mu} \frac{\partial p}{\partial r} \Big|_{r=R(t)} = \frac{Q}{\pi R}. \quad (2.111)$$

Hence, integrating the above two equations gives

$$\frac{1}{2}R^2 = \frac{Qt}{\pi\phi}. \quad (2.112)$$

Note that this equation could also be derived by considering that an injected volume Qt (per unit depth) must occupy a semicircle of area $\phi\pi R^2/2$.

In the original coordinate system the radius satisfies

$$R^2 = \xi^2 + \zeta^2 = x^2\alpha^{1/2} + z^2\alpha^{-1/2}. \quad (2.113)$$

Hence, the shape of the injected flow is actually an ellipse with semi-major and semi-minor axes

$$R_H = R\alpha^{-1/4}, \quad R_V = R\alpha^{1/4}. \quad (2.114)$$

Since $\alpha \leq 1$, the ellipse is always elongated in the horizontal direction (H) and squashed in the vertical direction (V). Hence, the effect of anisotropy is to create a long-thin elliptical flow (but not hydrostatic, as is typically assumed for long-thin flows!).

Next, we consider the effects of gravity. From the earlier analysis (2.108) it is clear that the effects of gravity are appreciable when

$$R_V \approx \frac{Q\mu}{k_e\Delta\rho g} = \frac{Q}{K_e}, \quad (2.115)$$

where $K_e = k_e\Delta\rho g/\mu$ is the effective conductivity. From (2.112),(2.114), this happens at a time

$$t = \frac{\pi\phi Q}{2K_e^2\alpha^{1/2}}. \quad (2.116)$$

Hence, writing everything in terms of the conductivity in the parallel direction $K = k_{\parallel}\Delta\rho g/\mu$ (which is the most commonly used), we see that the solution regime is determined by two critical parameter values for R_V and t , which are

$$R_V^* = H^* := \frac{Q}{\alpha^{1/2}K}, \quad t^* := \frac{\pi\phi Q}{2\alpha^{3/2}K^2}. \quad (2.117)$$

The regimes are summarised as follows: At early times $t \ll t^*$ (or when $R_V \ll H^*$) the flow is dominated by injection and gravity is negligible; at late times $t \gg t^*$ (or when $R_V \gg H^*$) the flow is dominated by gravity. In the latter case, the earlier gravity current analysis (i.e. (2.66)) is applicable, for which self-similar solutions exist in which $x \sim t^{2/3}$ and $z \sim t^{1/3}$.

This analysis illustrates that the effect of anisotropy is to delay the time at which gravity dominates the flow. Indeed for very heterogeneous/anisotropic geological reservoirs, for which $\alpha = \mathcal{O}(10^{-4})$, the CO₂ current may not feel the effects of gravity until several years after injection begins. This is very important to know, both from the perspective of efficiency as well as safety, before selecting a geological reservoir for carbon storage. Hence, detailed measurements are taken in as many locations as possible, in conjunction with seismic surveys, to assess the landscape of heterogeneities.

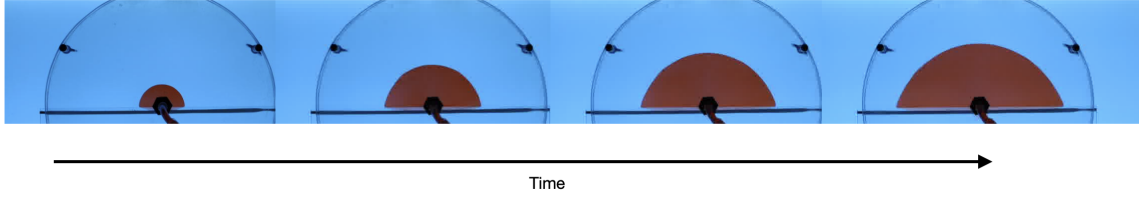


Figure 2.11: Experiments of glycerol (dyed red) injected into a Hele-Shaw cell, aligned vertically so gravity acts downwards. The flow is bounded below by an impermeable substrate.

Despite the simplicity of this problem, we have shown that there exist two separate self-similar regimes. These are summarised by the horizontal and vertical extents of the current R_H and R_V . Hence we have

$$\begin{aligned}
 R_H/H^* &\propto \begin{cases} (t/t^*)^{1/2} : & t \ll t^*, \\ (t/t^*)^{2/3} : & t \gg t^*, \end{cases} \\
 R_V/H^* &\propto \begin{cases} (t/t^*)^{1/2} : & t \ll t^*, \\ (t/t^*)^{1/3} : & t \gg t^*. \end{cases}
 \end{aligned} \tag{2.118}$$

Snapshots taken from an experiment of glycerol injected between two glass plates (known as a Hele-Shaw cell) are shown in Fig. 2.11. This is the inverted version of a CO_2 current since glycerol is heavy compared with the surrounding air, so gravity causes it to slump downwards. At early times (towards the left of the figure) the current grows like a semi-circle, whereas at late times (towards the right of the figure) the current collapses into a classical gravity current, exactly as we have predicted here.

A similar analysis can be performed in three dimensions, assuming an axisymmetric injection. In this case, different scalings are derived. For example, at early times we have an ellipsoid with

$$R_H = \alpha^{-1/6} R, \quad R_V = \alpha^{1/3} R, \tag{2.119}$$

where $R = (3Qt/4\pi\phi)^{1/3}$ and the transition scalings

$$H^* = \left(\frac{Q}{K}\right)^{1/2}, \quad t^* = \frac{2\pi\phi}{3\alpha} \left(\frac{Q}{K^3}\right)^{1/2}. \tag{2.120}$$

2.3 Unsaturated soils

Let us now consider flow in the unsaturated zone. Above the water table, water and air occupy the pore space. If the porosity is ϕ and the water volume fraction per unit volume of soil is W , then the ratio $S = W/\phi$ is called the *relative saturation*. If $S = 1$, the soil is saturated, and if $S < 1$ it is unsaturated. The pore space of an unsaturated soil is configured as shown in figure 2.12. In particular, the air/water

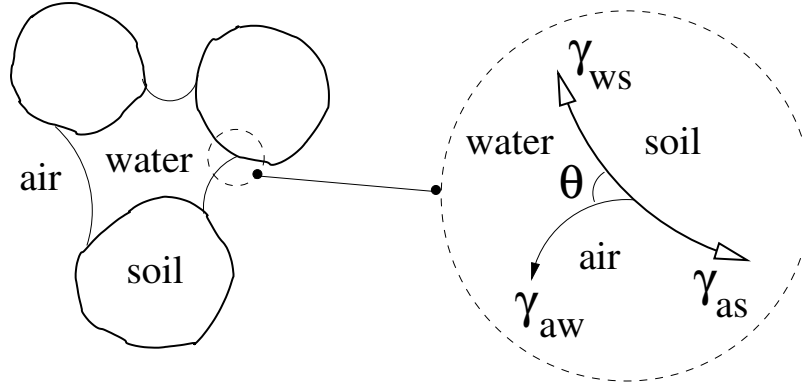


Figure 2.12: Configuration of air and water in pore space. The contact angle θ measured through the water is acute, so that water is the *wetting* phase. γ_{ws} , γ_{as} and γ_{aw} are the surface energies of the three interfaces.

interface is curved, and in an equilibrium configuration the curvature of this interface will be constant throughout the pore space. The value of the curvature depends on the amount of liquid present. The less liquid there is (i. e., the smaller the value of S), then the smaller the pores where the liquid is found, and thus the higher the curvature. Associated with the curvature is a suction effect due to surface tension across the air/water interface. The upshot of all this is that the air and water pressures are related by a *capillary suction characteristic* or *capillary pressure* function which expresses the difference between the pressures as a function of mean curvature, and hence, directly, S . Elementary geometry in a cylindrical pore of diameter d_p implies

$$p_a - p = \frac{2\gamma \cos \theta}{d_p}, \quad (2.121)$$

where θ is the contact angle. More generally, we can take

$$p_a - p = f(S). \quad (2.122)$$

The suction characteristic $f(S)$ is equal to $2\gamma\kappa$, where κ is the mean interfacial curvature: γ is the surface tension. For air and water in soil, f is positive as water is the *wetting phase*, that is, the *contact angle* at the contact line between air, water and soil grain is acute, measured through the water (see figure 2.12). The resulting form of $f(S)$ displays hysteresis as indicated in figure 2.13, with different curves depending on whether drying or wetting is taking place.

2.3.1 The Richards equation

To model the flow, we have the conservation of mass equation in the form

$$\frac{\partial(\phi S)}{\partial t} + \nabla \cdot \mathbf{u} = 0, \quad (2.123)$$

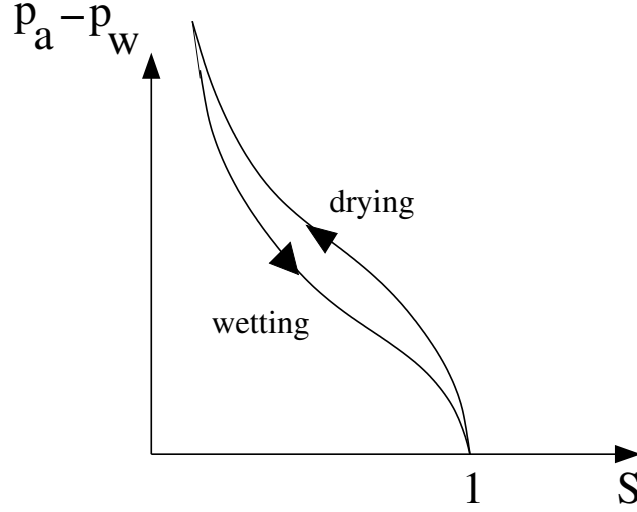


Figure 2.13: Capillary suction characteristic (A.K.A. capillary pressure). It displays hysteresis in wetting and drying.

where we take ϕ as constant. Darcy's law for an unsaturated flow has the form

$$\mathbf{u} = -\frac{k(S)}{\mu}[\nabla p + \rho g \hat{\mathbf{k}}], \quad (2.124)$$

where the permeability k depends on S . If $k(1) = k_0$ (the saturated permeability), then one commonly writes $k = k_0 k_r(S)$, where k_r is the *relative permeability*. The most obvious assumption would be $k_r = S$, but this is rarely appropriate, and a better representation is a convex function, such as $k_r = S^3$. An even better representation is a function such as $k_r = \left(\frac{S - S_0}{1 - S_0}\right)_+^3$, where S_0 is known as the residual saturation. It represents the fact that in fine-grained soils, there is usually some minimal water fraction which cannot be removed. It is naturally associated with a capillary suction characteristic function $p_a - p = f(S)$ which tends to infinity as $S \rightarrow S_0+$, also appropriate for fine-grained soils.

In one dimension, and if we take the vertical coordinate (upwards) to be z , we obtain the *Richards equation*

$$\phi \frac{\partial S}{\partial t} - \frac{\partial V(S)}{\partial z} = \frac{\partial}{\partial z} \left[D(S) \frac{\partial S}{\partial z} \right], \quad (2.125)$$

where

$$V(S) = K_0 k_r(S), \quad D(S) = -\frac{K_0}{\rho g} k_r(S) f'(S), \quad K_0 = \frac{k_0 \rho g}{\mu}; \quad (2.126)$$

K_0 is the saturated hydraulic conductivity. We are assuming $p_a = \text{constant}$ (and also that the soil matrix is incompressible).

2.3.2 Non-dimensionalisation

We choose scales for the variables as follows:

$$f = p_e \psi, \quad z \sim l, \quad t \sim \frac{\phi l}{K_0}, \quad (2.127)$$

where we have defined the capillary pressure scale to be

$$p_e = \frac{\gamma}{d_p}; \quad (2.128)$$

here d_p is the (mean) pore diameter and γ is the surface tension, assumed constant. The quantity p_e is often referred to as the pore entry pressure, and we will discuss this in more detail later.

The Richards equation then becomes, in dimensionless variables,

$$S_t - k'_r(S)S_z = \varepsilon [D^*(S)S_z]_z, \quad (2.129)$$

where

$$D^*(S) = -k_r(S)\psi'(S). \quad (2.130)$$

Note that ψ is a decreasing function, so that the diffusion coefficient $D^* > 0$, as is indeed necessary. The single dimensionless parameter is

$$\varepsilon = \frac{p_e}{\rho g l}, \quad (2.131)$$

and is small for coarse soils, and $O(1)$ for fine-grained soils. As a specific example, we take $l = 1$ m, so that $\rho g l \sim 10^4$ Pa. If we take $\gamma = 70$ mN m⁻¹ for water/air, and $d_p \sim 0.1$ mm, then $p_e \sim 700$ Pa, and $\varepsilon \sim 0.07$; this may be appropriate for sandy soils. For silty soils, we might have $d_p \sim 10$ μ m, and then $\varepsilon \sim 0.7$.

As a specific example, we consider the case of soil wetting due to surface infiltration: of rainfall, for example. Suppose that there is a constant downwards flux of (dimensional) rainfall q at the surface. It is convenient to define the depth $\zeta = -z$, and take the vadose zone to be in $0 < \zeta < 1$. The Richards equation is then

$$S_t + k'_r(S)S_\zeta = \varepsilon [D^*(S)S_\zeta]_\zeta, \quad (2.132)$$

and suitable boundary conditions for the saturation are

$$\begin{aligned} k_r(S) - \varepsilon D^*(S)S_\zeta &= q^* \quad \text{at} \quad \zeta = 0, & q^* &= \frac{q}{K_0}, \\ S &= 1 \quad \text{at} \quad \zeta = 1. \end{aligned} \quad (2.133)$$

In the steady state, the first condition in (2.133) applies everywhere, and the solution is a quadrature,

$$\int_S^1 \frac{\varepsilon D^*(S) dS}{k_r(S) - q^*} = 1 - \zeta. \quad (2.134)$$

Obviously S must be an increasing function of ζ , and this requires $q^* < k_r(1) = 1$, in other words $q < K_0$: the supplied rainfall must be less than the saturated hydraulic conductivity.

What if it is not? It is easy to see from the solution (2.134) that as $q^* \rightarrow 1-$, the saturation approaches one. If $q > K_0$, the supplied flux at the surface is greater than the soil's maximum drainage capacity (which is the saturated hydraulic conductivity). So in this case, water must pond at the surface, and the boundary condition is replaced by $S = 1$ at $\zeta = 0$; clearly in this case, the soil is waterlogged and the water table is pushed up to the soil surface. Such ponding is commonly observed during periods of heavy rainfall. For silt with $k_0 = 10^{-14} \text{ m}^2$, the hydraulic conductivity $K_0 \sim 10^{-7} \text{ m s}^{-1}$ or 3 m y^{-1} , while average rainfall in England, for example, is $\leq 1 \text{ m y}^{-1}$. Thus *on average* $q^* \leq 1$ for such soils, but during storms we can expect $q^* \gg 1$. When ponding does occur, the pond depth is determined by the balance between precipitation, infiltration, and surface run-off.

2.3.3 Snow melting

An application of the unsaturated flow model occurs in the study of melting snow. In particular, it is found that pollutants which may be uniformly distributed in snow (e. g. sulphate SO_4^{2-} from sulphur emissions via acid rain) can be concentrated in melt water run-off, with a consequent enhanced detrimental effect on stream pollution. The question then arises, why this should be so? We shall find that uniform surface melting of a dry snowpack can lead to a meltwater spike at depth.

Suppose we have a snow pack of depth l . Snow is a porous aggregate of ice crystals, and meltwater formed at the surface can percolate through the snow pack to the base, where run-off occurs. (We ignore effects of re-freezing of meltwater.) The model (2.132) is appropriate, and to be specific, we will also take

$$k_r = S^3, \quad \psi(S) = \frac{1}{S} - S, \quad (2.135)$$

based on typical experimental results.

Suitable boundary conditions in a melting event might be to prescribe the melt flux q_0 at the surface, thus

$$k_r \left(\varepsilon \frac{\partial \psi}{\partial \zeta} + 1 \right) = q^* = \frac{q_0}{K_0} \quad \text{at} \quad \zeta = 0. \quad (2.136)$$

If the base is impermeable, then

$$k_r \left(\varepsilon \frac{\partial \psi}{\partial \zeta} + 1 \right) = 0 \quad \text{at} \quad \zeta = 1. \quad (2.137)$$

This is certainly not realistic if S reaches 1 at the base, since then ponding must occur and presumably melt drainage will occur via a sub-horizontal flow under the snowpack, but we will examine the initial stages of the flow using (2.137) before that

happens. Finally, we suppose $S = 0$ at $t = 0$. Again, this is not realistic in the model (it implies infinite capillary suction) but it is a feasible approximation to make.

Simplification of this model now leads to the dimensionless Richards equation in the form

$$\frac{\partial S}{\partial t} + 3S^2 \frac{\partial S}{\partial \zeta} = \varepsilon \frac{\partial}{\partial \zeta} \left[S(1 + S^2) \frac{\partial S}{\partial \zeta} \right]. \quad (2.138)$$

If we choose $\gamma = 70 \text{ mN m}^{-1}$, $d_p = 0.1 \text{ mm}$, $\rho = 10^3 \text{ kg m}^{-3}$, $g = 10 \text{ m s}^{-2}$, $l = 1 \text{ m}$ as before, then again $\varepsilon = 0.07$. It follows that (2.138) has a propensity to form shocks, these being diffused by the term in ε over a distance $O(\varepsilon)$ (by analogy with the shock structure for the Burgers equation).

We want to solve (2.138) with the initial condition

$$S = 0 \quad \text{at} \quad t = 0, \quad (2.139)$$

and the boundary conditions

$$S^3 - \varepsilon S(1 + S^2) \frac{\partial S}{\partial \zeta} = q^* \quad \text{on} \quad \zeta = 0, \quad (2.140)$$

and

$$S^3 - \varepsilon S(1 + S^2) \frac{\partial S}{\partial \zeta} = 0 \quad \text{at} \quad \zeta = 1. \quad (2.141)$$

Roughly, for $\varepsilon \ll 1$, these are

$$\begin{aligned} S &= S_0 \quad \text{at} \quad \zeta = 0, \\ S &= 0 \quad \text{at} \quad \zeta = 1, \end{aligned} \quad (2.142)$$

where $S_0 = q^{*1/3}$, which we initially take to be $O(1)$ (and < 1 , so that surface ponding does not occur).

Neglecting ε , the solution is the step function

$$\begin{aligned} S &= S_0, & \zeta < \zeta_f, \\ S &= 0, & \zeta > \zeta_f, \end{aligned} \quad (2.143)$$

and the shock front at ζ_f advances at a rate $\dot{\zeta}_f$ given by the jump condition

$$\dot{\zeta}_f = \frac{[S^3]_{-}^{+}}{[S]_{-}^{+}} = S_0^2. \quad (2.144)$$

In dimensional terms, the shock front moves at speed $q_0/\phi S_0$, which is in fact obvious (given that it has constant S behind it).

The shock structure is similar to that of Burgers' equation. We put

$$\zeta = \zeta_f + \varepsilon Z, \quad (2.145)$$

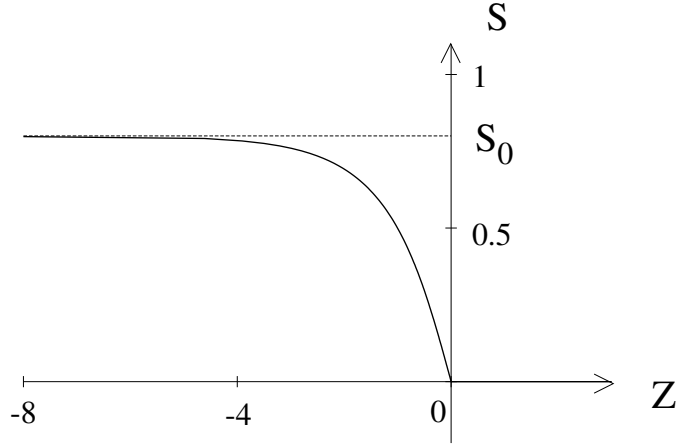


Figure 2.14: $S(Z)$ given by (2.150); the shock front terminates at the origin.

and S rapidly approaches the quasi-steady solution $S(Z)$ of

$$-cS' + 3S^2S' = [S(1 + S^2)S']', \quad (2.146)$$

where $c = \dot{\zeta}_f$; hence

$$S(1 + S^2)S' = -S(S_0^2 - S^2), \quad (2.147)$$

in order that $S \rightarrow S_0$ as $Z \rightarrow -\infty$, and where we have chosen

$$c = S_0^2, \quad (2.148)$$

(as $S_+ = 0$), thus reproducing (2.144). The solution is a quadrature,

$$\int^S \frac{(1 + S^2) dS}{(S_0^2 - S^2)} = -Z, \quad (2.149)$$

with an arbitrary added constant (amounting to an origin shift for Z). Hence

$$S - \frac{(1 + S_0^2)}{2S_0} \ln \left[\frac{S_0 + S}{S_0 - S} \right] = Z. \quad (2.150)$$

The shock structure is shown in figure 2.14; the profile terminates where $S = 0$ at $Z = 0$. In fact, (2.147) implies that $S = 0$ or (2.150) applies. Thus when S given by (2.150) reaches zero, the solution switches to $S = 0$. The fact that $\partial S/\partial Z$ is discontinuous is not a problem because the diffusivity $S(1 + S^2)$ goes to zero when $S = 0$. This degeneracy of the equation is a signpost for fronts with discontinuous derivatives: essentially, the profile can maintain discontinuous gradients at $S = 0$ because the diffusivity is zero there, and there is no mechanism to smooth the jump away.

Suppose now that $k_0 = 10^{-10} \text{ m}^2$ and $\mu/\rho = 10^{-6} \text{ m}^2 \text{ s}^{-1}$; then the saturated hydraulic conductivity $K_0 = k_0\rho g/\mu = 10^{-3} \text{ m s}^{-1}$. On the other hand, if a metre

thick snow pack melts in ten days, this implies $q_0 \sim 10^{-6} \text{ m s}^{-1}$. Thus $S_0^3 = q_0/K_0 \sim 10^{-3}$, and the approximation $S \approx S_0$ looks less realistic. With

$$S^3 - \varepsilon S(1 + S^2) \frac{\partial S}{\partial \zeta} = S_0^3, \quad (2.151)$$

and $S_0 \sim 10^{-1}$ and $\varepsilon \sim 10^{-1}$, it seems that one should assume $S \ll 1$. We define

$$S = \left(\frac{S_0^3}{\varepsilon} \right)^{1/2} s; \quad (2.152)$$

(2.151) becomes

$$\beta s^3 - s \left[1 + \frac{S_0^3}{\varepsilon} s^2 \right] \frac{\partial s}{\partial \zeta} = 1 \quad \text{on } \zeta = 0, \quad (2.153)$$

and we have $S_0^3/\varepsilon \sim 10^{-2}$, $\beta = (S_0/\varepsilon)^{3/2} \sim 1$.

We neglect the term in S_0^3/ε , so that

$$\beta s^3 - s \frac{\partial s}{\partial \zeta} \approx 1 \quad \text{on } \zeta = 0, \quad (2.154)$$

and substituting (2.152) into (2.138) leads to

$$\frac{\partial s}{\partial \tau} + 3\beta s^2 \frac{\partial s}{\partial \zeta} \approx \frac{\partial}{\partial \zeta} \left[s \frac{\partial s}{\partial \zeta} \right], \quad (2.155)$$

if we define $t = \tau / (\varepsilon S_0^3)^{1/2}$. A simple analytic solution is no longer possible, but the development of the solution will be similar. The flux condition (2.154) at $\zeta = 0$ allows the surface saturation to build up gradually, and a shock will only form if $\beta \gg 1$ (when the preceding solution becomes valid).

2.3.4 Similarity solutions

If, on the other hand, $\beta \ll 1$, then the saturation profile approximately satisfies

$$\begin{aligned} \frac{\partial s}{\partial \tau} &= \frac{\partial}{\partial \zeta} \left[s \frac{\partial s}{\partial \zeta} \right], \\ -s \frac{\partial s}{\partial \zeta} &= \begin{cases} 1 & \text{on } \zeta = 0, \\ 0 & \text{on } \zeta = 1. \end{cases} \end{aligned} \quad (2.156)$$

At least for small times, the model admits a similarity solution of the form

$$s = \tau^\alpha f(\eta), \quad \eta = \zeta / \tau^\beta, \quad (2.157)$$

where satisfaction of the equations and boundary conditions requires $2\alpha = \beta$ and $2\beta = 1 = \alpha$, whence $\alpha = \frac{1}{3}$, $\beta = \frac{2}{3}$, and f satisfies

$$(ff')' - \frac{1}{3}(f - 2\eta f') = 0, \quad (2.158)$$

with the condition at $\zeta = 0$ becoming

$$-ff' = 1 \quad \text{at} \quad \eta = 0. \quad (2.159)$$

The condition at $\zeta = 1$ can be satisfied for small enough τ , as we shall see, because the equation (2.158) is degenerate, and f reaches zero in a finite distance, η_0 , say, and $f = 0$ for $\eta > \eta_0$. As $\eta = 1/\tau^{2/3}$ at $\zeta = 1$, then this solution will satisfy the no flux condition at $\zeta = 1$ as long as $\tau < \eta_0^{-3/2}$, when the advancing front will reach $\zeta = 1$.

To see why f behaves in this way, integrate once to find

$$f(f' + \frac{2}{3}\eta) = -1 + \int_0^\eta f \, d\eta. \quad (2.160)$$

For small η , the right hand side is negative, and f is positive (to make physical sense), so f decreases (and in fact $f' < -\frac{2}{3}\eta$). For sufficiently small $f(0) = f_0$, f will reach zero at a finite distance $\eta = \eta_0$, and the solution must terminate. On the other hand, for sufficiently large f_0 , $\int_0^\eta f \, d\eta$ reaches 1 at $\eta = \eta_1$ while f is still positive (and $f' = -\frac{2}{3}\eta_1$ there). For $\eta > \eta_1$, then f remains positive and $f' > -\frac{2}{3}\eta$ (f cannot reach zero for $\eta > \eta_1$ since $\int_0^\eta f \, d\eta > 1$ for $\eta > \eta_1$). Eventually f must have a minimum and thereafter increase with η . This is also unphysical, so we require f to reach zero at $\eta = \eta_0$. This will occur for a range of f_0 , and we have to select f_0 in order that

$$\int_0^{\eta_0} f \, d\eta = 1, \quad (2.161)$$

which in fact represents global conservation of mass. Figure 2.15 shows the schematic form of solution both for $\beta \gg 1$ and $\beta \ll 1$. Evidently the solution for $\beta \sim 1$ will have a profile with a travelling front between these two end cases.

2.4 Immiscible two-phase flows

In some circumstances, the flow of more than one phase in a porous medium is important. For example, the flow of CO₂ in water (carbon sequestration), or the flow of oil and gas, or oil and water (or all three!) in a sedimentary basin, such as that beneath the North Sea. Suppose there are two phases; denote the phases by subscripts w and n , being the *wetting* and *non-wetting* fluids, and S_w, S_n are the saturations. It is assumed that together these two phases occupy all the pore space, such that $S_n + S_w = 1$. Note that the definition of which fluid is wetting and which is non-wetting relates to the size of the contact angle between the phases (i.e. if the angle is less than $\pi/2$, the fluid is known as wetting).

For each phase, there is an associated relative permeability function, which we denote $k_{rn}(S_n)$ and $k_{rw}(S_w)$. We write these in terms of the non-wetting saturation without loss of generality (since $S_w = 1 - S_n$). As discussed before, k_{rn} is a monotone

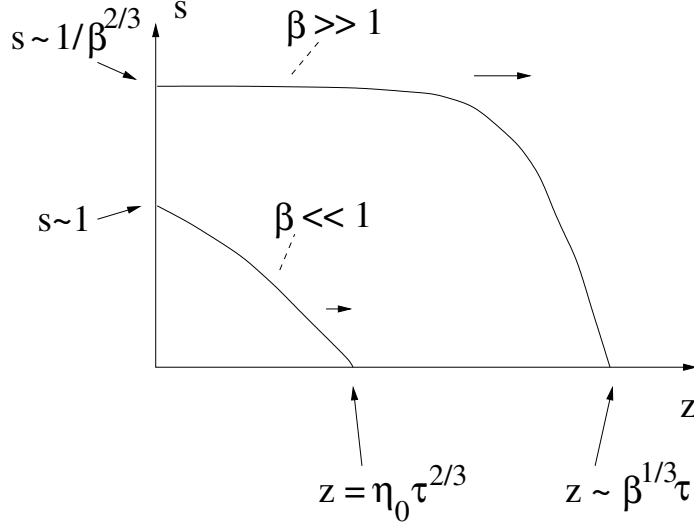


Figure 2.15: Schematic representation of the evolution of s in (2.155) for both large and small β .

increasing function of S_n , and for the same reasons k_{rw} is a decreasing function of S_n . They do not necessarily have a similar functional form. Furthermore, they typically display hysteresis phenomena. For example, it is easier (i.e. larger relative permeability) for CO_2 to invade a region of pore space than it is for it to withdraw from an existing area. This is the chief mechanism for capillary trapping during carbon sequestration.

The capillary (or suction) pressure $p_c = p_n - p_w$ is given by

$$p_c(S_n) = p_e \psi(S_n), \quad (2.162)$$

where p_e is the pore entry pressure, and ψ is a positive, monotonically increasing function of saturation S_n . The pore entry pressure is the minimum pressure required to fill the largest pore spaces of the rock with non-wetting phase. As the difference in pressure $p_n - p_w$ increases, smaller and smaller pore spaces can be occupied with non-wetting phase.

Mass conservation takes the form

$$\begin{aligned} \phi \frac{\partial S_n}{\partial t} + \nabla \cdot \mathbf{u}_n &= 0, \\ \phi \frac{\partial S_w}{\partial t} + \nabla \cdot \mathbf{u}_w &= 0, \end{aligned} \quad (2.163)$$

where ϕ is (constant) porosity, and Darcy's law for each phase is

$$\begin{aligned} \mathbf{u}_n &= -\frac{k_0}{\mu_n} k_{rn}(S_n) \left[\nabla p_n + \rho_n g \hat{\mathbf{k}} \right], \\ \mathbf{u}_w &= -\frac{k_0}{\mu_w} k_{rw}(S_n) \left[\nabla p_w + \rho_w g \hat{\mathbf{k}} \right]. \end{aligned} \quad (2.164)$$

2.4.1 Buckley-Leverett Flow

A canonical case of two-phase flow in porous media is the study of immiscible displacement in a long-thin aquifer, also known as Buckley-Leverett flow. To model this, we make the assumption that the flow is approximately one-dimensional, and the effects of gravity can be ignored. Such flows are relevant to geothermal energy production and carbon sequestration, but the problem formulation was originally employed to model hydrocarbon extraction in geological reservoirs.

We consider a constant injection of wetting and non-wetting phases at the aquifer inlet $x = 0$, and model the spatial and temporal development of the saturations S_n , S_w , downstream towards the aquifer outlet at $x = L$ (see figure 2.16). By conservation of mass (2.163) we have

$$u_n + u_w = U, \quad (2.165)$$

for some constant inlet velocity U . By inserting (2.164) (in one dimension) into (2.165) and substituting $p_w = p_n - p_c$, we get

$$-\frac{k_0}{\mu_w} \left[Mk_{rn} \frac{\partial p_n}{\partial x} + k_{rw} \left(\frac{\partial p_n}{\partial x} - \frac{\partial p_c}{\partial x} \right) \right] = U, \quad (2.166)$$

where $M = \mu_w/\mu_n$ is the viscosity ratio. Hence, we can re-arrange to get the non-wetting pressure gradient,

$$\frac{\partial p_n}{\partial x} = \frac{-\mu_w U/k_0}{Mk_{rn} + k_{rw}} + \frac{k_{rw}}{Mk_{rn} + k_{rw}} \frac{\partial p_c}{\partial x}. \quad (2.167)$$

By inserting this into (2.163) we get the governing equation for the saturation

$$\phi \frac{\partial S_n}{\partial t} + V(S_n) \frac{\partial S_n}{\partial x} = \frac{\partial}{\partial x} \left[D(S_n) \frac{\partial S_n}{\partial x} \right], \quad (2.168)$$

where the functions V , D are defined as

$$\begin{aligned} V(S_n) &= U \frac{\partial}{\partial S_n} \left[\frac{Mk_{rn}}{Mk_{rn} + k_{rw}} \right], \\ D(S_n) &= \frac{k_0 p_e}{\mu_w} \frac{Mk_{rn} k_{rw}}{Mk_{rn} + k_{rw}} \frac{\partial \psi}{\partial S_n}. \end{aligned} \quad (2.169)$$

The second term in (2.168) can therefore be interpreted as advection at speed $V = UJ'(S_n)$, where $J = Mk_{rn}/(Mk_{rn} + k_{rw})$ is the flow rate fraction. The third term is diffusive, indicating that the role of the capillary pressure is to smooth out gradients in the saturation S_n . It should be noted that a similar formulation can be achieved in terms of S_w , but here we stick with an S_n formulation without loss of generality.

It is interesting to measure the relative importance between each of these advective and diffusive effects. For this, we define a dimensionless Peclet number,

$$\text{Pe} = \frac{U \mu_w L}{k_0 p_e}. \quad (2.170)$$

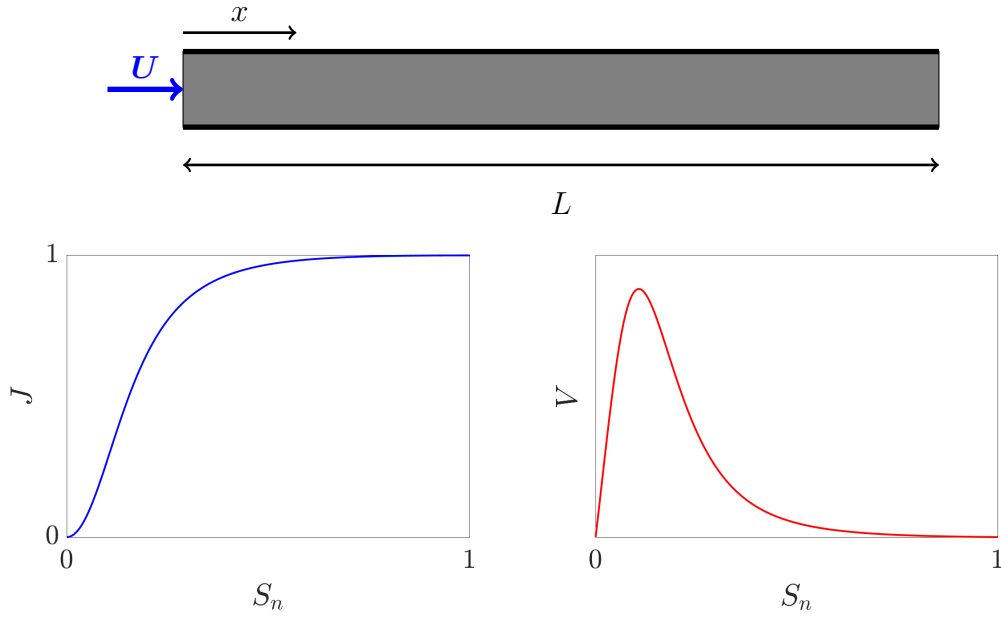


Figure 2.16: Schematic diagram and plots of the dimensionless flow rate fraction $J(S)$ and advection speed $V(S)$ as a function of non-wetting fluid saturation S_n (for the Buckley-Leverett problem). The viscosity ratio M is taken to be 30.

In many environmental scenarios, the above parameters lead to a large Peclet number $Pe \gg 1$, such that the effects of diffusion (and hence the third term in (2.168)) can be ignored to good approximation. This approximation breaks down, however, when there are sharp gradients of S_n , such as near a shock. In such scenarios where there are shocks, one can introduce a boundary layer near the shock front to address diffusive effects.

By non-dimensionalising the model according to

$$x \sim L, \quad t \sim \phi L/U, \quad V \sim U, \quad (2.171)$$

and by dropping the subscript $S = S_n$, we get the simple advection equation

$$S_t + V(S)S_x = 0. \quad (2.172)$$

Such equations can be solved using the method of characteristics

$$\frac{dx}{dt} = V(S), \quad (2.173)$$

given suitable inlet and initial conditions at $x = 0$ and $t = 0$. As an example we consider the initial/boundary conditions

$$\begin{aligned} S(0, t) &= 1, \\ S(x, 0) &= 0. \end{aligned} \quad (2.174)$$

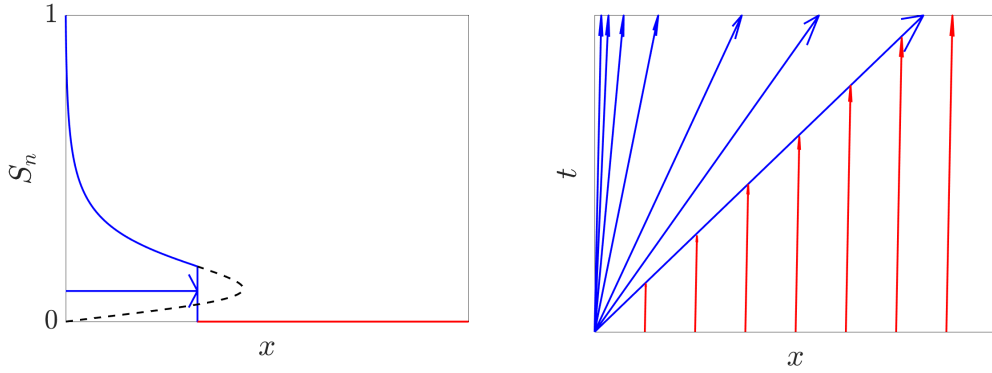


Figure 2.17: Illustration of a shock developing during Buckley-Leverett flow, as well as the corresponding characteristics in the $x - t$ plane. Blue curves indicate $S_n > S_s$ and red curves indicate $S_n = 0$.

This corresponds to an aquifer which is initially saturated with wetting phase, at which point pure non-wetting phase is injected at the inlet (e.g. CO_2 injected into a brine-filled aquifer).

To address this case, we first need to define expressions for the relative permeability functions in the advection term $V(S)$. For this we use the so-called ‘Corey’ model,

$$k_{rn} = S^\alpha, \quad k_{rw} = (1 - S)^\beta, \quad (2.175)$$

where $\alpha, \beta > 0$ are some empirical constants. In this case, plots of the flow rate fraction J and advection speed V are shown in figure 2.16 for illustration. In general, J is a monotone increasing function between 0 and 1 (reminiscent of a CDF for example), whereas V is a positive function with a unique maximum.

The non-monotone behaviour of V in conjunction with (2.173)-(2.174) indicate that a shock will develop to maintain a saturation S that is not multi-valued. To determine the saturation value at the shock, we employ the Rankine-Hugoniot jump condition, which takes the form

$$\frac{dx}{dt} = \frac{[Q]_-^+}{[P]_-^+}, \quad (2.176)$$

for a PDE of the form $P_t + Q_x = 0$. Hence, we have the shock condition

$$V(S_s)S_s = J(S_s), \quad (2.177)$$

which must be solved to find S_s .

A typical shock solution is displayed in figure 2.17 together with characteristics in the $x - t$ plane. Clearly the shock at $S = S_s$ causes the characteristics from $t = 0$ to collide with the dividing characteristic $X(t) = V(S_s)t$. As described earlier, diffusive effects due to the capillary pressure act to smooth out this shock front. This occurs over a boundary layer of width $\delta \propto (t/\text{Pe})^{1/2}$, located near the shock front $X(t)$.

2.4.2 Two-phase flow in heterogeneous media

Earlier we described how heterogeneities can affect the flow of a single phase within a porous medium. Here, we extend this analysis to account for multiphase effects between immiscible flows. In our earlier analysis, we discussed how heterogeneities are often characterised by variations in the pore size within a rock, manifesting in non-uniform porosity and permeability ϕ , k . However, variations in the pore size are also associated with different pore entry pressures p_e and therefore non-uniform capillary pressure p_c . In this section we describe how such variations modify the flow and distribution of the phase saturations S_n , S_w .

As before, it is useful to consider the most simple type of heterogeneity to gain a general understanding of the typical behaviour. To do so, we consider flow parallel to a system of two layers of equal thickness with permeability, porosity and pore entry pressure values k_i , ϕ_i , p_{e_i} , for $i = 1, 2$. The length and thickness of the medium is given by L , H , and the flow is predominantly horizontal, driven by an overarching pressure gradient $\Delta p/L$ (e.g. in the non-wetting phase).

It is useful to characterise the relative importance of viscous and capillary effects by the ratio

$$\frac{\partial p_n / \partial x}{\partial p_c / \partial z} \approx \frac{\Delta p / L}{\Delta p_e / H}, \quad (2.178)$$

where $\Delta p_e = p_{e_1} - p_{e_2}$. The above expression is the ratio between horizontal viscous pressure gradients and vertical gradients in the capillary pressure. We see this is analogous to the capillary number described earlier (remember $\text{Ca} \sim \mu U / \gamma$). Hence, we write

$$\text{Ca} = 1/\Gamma = \left| \frac{\Delta p H}{\Delta p_e L} \right|, \quad (2.179)$$

where a modulus sign is included to make sure the quantity is always positive, and Γ is introduced as a more intuitive alternative to the capillary number (since large Γ corresponds with large capillary effects).

The limit of large Γ is known as the ‘‘capillary limit’’. In this case the saturation of phases is dominated by capillary forces. Essentially, surface tension drives non-wetting phase into regions of larger pore space and away from smaller pore space (i.e. minimising surface energy). Comparatively the horizontal, viscous flow of phases is of lesser importance than the lateral rearrangement due to capillary effects.

By contrast, the limit of small Γ is known as the ‘‘viscous limit’’. In this case, the effect of capillary forces is negligible, and instead the flow is dominated by the flow-driving horizontal pressure gradients associated with viscous resistance. There is little saturation rearrangement due to surface tension, so the lateral saturation distribution remains close to the inlet conditions.

In general to account for the flow in such scenarios, we would have to solve the governing equations (2.163)-(2.164) for fixed Γ and suitable boundary conditions. However, in the limit of small and large Γ , we can make some simplifying assumptions to derive analytical solutions which give insight into the problem.

To start with we consider the case of steady flow in the viscous limit ($\Gamma \ll 1$). In this case, it can be shown (via asymptotic analysis) that the saturation is spatially uniform, e.g. $S_n = \bar{S}_n = S_n(x=0)$. In other words, the saturation of phases remains the same as imposed at the inlet $x=0$. Hence, the flow of non-wetting phase (for example) is

$$u_n = -\frac{k(z)}{\mu_n} k_{rn}(S_n) \frac{\partial p_n}{\partial x} = -\frac{k(z)}{\mu_n} k_{rn}(\bar{S}_n) \frac{\Delta p}{L}. \quad (2.180)$$

Hence, we can derive an effective property for the relative permeabilities in the viscous limit

$$\begin{aligned} k_{rn}^V(\bar{S}_n) &= \frac{\mu_n \bar{u}_n L}{-\Delta p \bar{k}} = k_{rn}(\bar{S}_n), \\ k_{rw}^V(\bar{S}_n) &= \frac{\mu_w \bar{u}_w L}{-\Delta p \bar{k}} = k_{rw}(\bar{S}_n), \end{aligned} \quad (2.181)$$

where bars indicate vertical averaging (e.g. $\bar{k} = (k_1 + k_2)/2$ for even thickness layers). These effective properties tell us how the mean flow \bar{u}_n, \bar{u}_w depends on the mean saturation, permeability, and viscous pressure gradient. Hence, if we know information about the heterogeneity, we can immediately describe the flow in the viscous limit without doing any intensive computations.

Similarly, in the capillary limit ($\Gamma \gg 1$) we can derive analogous effective properties. In this case, the flow is associated with very weak driving pressure gradients $\Delta p/L$. Hence, p_n and p_w are expected to be approximately constant. This leads to a capillary pressure

$$p_c = p_n - p_w \approx \gamma, \quad (2.182)$$

for some constant γ . The capillary pressure is related to the saturation according to (2.162), given some model for p_c . For this, we employ the commonly used Brooks-Corey model, which is

$$p_c(S_n) = p_e(z)(1 - S_n)^{-1/\lambda}, \quad (2.183)$$

where λ represents the pore size distribution (large/small values of λ correspond with a large/small distribution of pore sizes). Inverting this function we get

$$S_n(z) = 1 - \left(\frac{p_e(z)}{\gamma} \right)^\lambda. \quad (2.184)$$

This can be re-written in terms of the average (i.e. removing γ) as

$$S_n(z) = 1 - \frac{p_e(z)^\lambda}{p_e^\lambda} (1 - \bar{S}_n). \quad (2.185)$$

Hence, we can insert this into the Darcy equations and take the average, giving

$$\bar{u}_n = -\frac{1}{\mu_n} \overline{k(z) k_{rn}(S_n(z))} \frac{\Delta p}{L}. \quad (2.186)$$

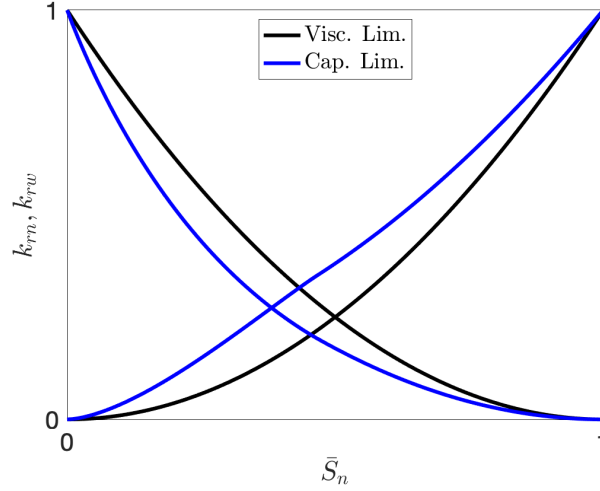


Figure 2.18: Effective relative permeabilities in the viscous and capillary limits in the case of flow parallel to a layered heterogeneous porous medium.

This (and a similar expression for the wetting phase) can be rearranged to derive expressions for effective relative permeabilities in the capillary limit, which are

$$\begin{aligned}
 k_{rn}^C(\bar{S}_n) &= \frac{\mu_n \bar{u}_n L}{-\Delta p \bar{k}} = \frac{\overline{k k_{rn}}}{\bar{k}}, \\
 k_{rw}^C(\bar{S}_n) &= \frac{\mu_w \bar{u}_w L}{-\Delta p \bar{k}} = \frac{\overline{k k_{rw}}}{\bar{k}}.
 \end{aligned} \tag{2.187}$$

Hence, we now have sufficient information to describe the bulk flow through a heterogeneous aquifer in the limit of small and large Γ without having to do any intensive computations. These two cases are the two end members (extreme scenarios) and therefore provide upper and lower bounds for the general case of $\Gamma = \mathcal{O}(1)$.

Due to the form of (2.184), capillary forces act to push non-wetting phase into regions of smaller p_e , which corresponds with larger pore space and larger values of k, ϕ . Hence, non-wetting phase is preferentially rearranged into less resistive channels of flow, enhancing \bar{u}_n and reducing \bar{u}_w . In this way, the effective relative permeabilities usually satisfy

$$k_{rn}^C > k_{rn}^V, \quad k_{rw}^C < k_{rw}^V. \tag{2.188}$$

In other words, heterogeneities act to enhance the flow of non-wetting phase and decrease the flow of wetting phase, which is in very good agreement with observations. An example of these effective properties is illustrated in figure 2.18. We will explore an example of such flows in Problem Sheet 3.

2.4.3 Heterogeneous Buckley-Leverett flows

The Buckley-Leverett flow studied earlier can be easily extended to account for heterogeneous systems. Whilst the flow formulation is in one-dimension, we can account for a vertical heterogeneity (i.e. sedimentary layers in two or three dimensions) by using effective properties for the relative permeabilities, either in the viscous or capillary limits. Hence, this models the vertical rearrangement of saturation due to capillary forces in a very long-thin aquifer in which the flow is predominantly one-dimensional.

As such, we can write down a dimensionless advection equation for the saturation of non-wetting phase

$$S_t + V(S)S_x = 0, \quad (2.189)$$

where the advection speed is given by either the capillary or viscous limits

$$V = \begin{cases} V^V(S), & \text{using } k_{rn}^V, k_{rw}^V : \Gamma \gg 1, \\ V^C(S), & \text{using } k_{rn}^C, k_{rw}^C : \Gamma \ll 1. \end{cases} \quad (2.190)$$

It should be noted that both the capillary and viscous limits have different shock saturation values S_s and consequently different advection speeds. Typically, since the flow of non-wetting phase is enhanced by heterogeneities, the capillary limit speed is usually faster than the viscous limit speed, such that $V^C(S_s) > V^V(S_s)$.

This class of approaches is sometimes referred to as ‘upscaling’, since the effects of the small-scale heterogeneities are incorporated into a model which describes the large-scale flow. Upscaling is useful in many environmental applications since it is much more computationally efficient than direct simulation, and also allows for ensemble predictions or best/worst case scenario estimates. Time-dependent simulation of a three-dimensional reservoir incorporating heterogeneities from the mm scale up to the km scale is not tractable. This is not only a result of computational limitations, but also due to a lack of existing heterogeneity data. For example, seismic surveys usually have a resolution of around ~ 1 m.

2.4.4 Incorporating gravity

Let’s consider the two-phase analogy of a gravity current spreading beneath an impermeable cap rock. For example, in the context of carbon sequestration, CO_2 is the non-wetting phase and salty brine is the wetting phase. As before, we assume that the flow has a long-thin aspect ratio. As a result, both the non-wetting and wetting phases satisfy a hydrostatic balance at leading order, such that

$$\begin{aligned} \frac{\partial p_n}{\partial z} &= \rho_n g, \\ \frac{\partial p_w}{\partial z} &= \rho_w g. \end{aligned} \quad (2.191)$$

This indicates that the capillary pressure satisfies

$$\frac{\partial p_c}{\partial z} = -\Delta \rho g. \quad (2.192)$$

Hence, in the absence of heterogeneity we have

$$p_c = p_e - \Delta\rho g(z - h), \quad (2.193)$$

where $z = h(x, t)$ is the gravity current thickness (measured downwards from the cap rock at $z = 0$). Hence, the capillary pressure can be inverted for the saturation of non-wetting phase,

$$S_n = 1 - (1 + \text{Bo}(h/L - z/L))^{-\lambda}, \quad (2.194)$$

where $\text{Bo} = \Delta\rho gL/p_e$ is the Bond number. The above expression is known as the ‘gravity-capillary’ balance. Hence, given a thickness h and Bond number, we can now calculate the vertical saturation distribution. In particular, S_n increases vertically, indicating that the non-wetting phase (which is assumed to be lighter than the wetting phase) preferentially rises towards the cap rock. The larger the effects of surface tension (i.e. small Bo) the more the capillary pressure acts to spread out the distribution of non-wetting phase.

2.5 Consolidation

Consolidation refers to the ability of a granular porous medium such as a soil to compact under its own weight, or by the imposition of an overburden pressure. The grains of the medium rearrange themselves under the pressure, thus reducing the porosity and in the process pore fluid is expelled. Since the porosity is no longer constant, we have to postulate a relation between the porosity ϕ and the pore pressure p . In practice, it is found that soils, when compressed, obey a (non-reversible) relation between ϕ and the *effective pressure*

$$p_{\text{eff}} = P - p, \quad (2.195)$$

where P is the overburden pressure.

The concept of effective pressure, or more generally effective stress, is an extremely important one. The idea is that the total imposed pressure (e.g., the overburden pressure due to the weight of the rock or soil) is borne by both the pore fluid and the porous medium. The pore fluid is typically at a lower pressure than the overburden, and the extra stress (the effective stress) is that which is applied through grain to grain contacts. Thus the effective pressure is that which is transmitted through the porous medium, and it is in consequence of this that the medium responds to the effective stress; in particular, the characteristic relation between ϕ and p_{eff} represents the nonlinear pseudo-elastic effect of compression.

The dependence of the effective pressure on porosity is non-trivial and involves hysteresis, as indicated in figure 2.19. Specifically, a soil follows the *normal consolidation line* providing consolidation is occurring, i.e. $\dot{p}_{\text{eff}} > 0$. However, if at some point the effective pressure is reduced, only a partial recovery of ϕ takes place. When p_{eff} is increased again, ϕ more or less retraces its (overconsolidated) path to the normal consolidation line, and then resumes its normal consolidation path. Here we will ignore effects of hysteresis, as in (3.147).

When modelling groundwater flow in a consolidating medium, we must take account also of deformation of the medium itself. In turn, this requires prescription of a constitutive rheology for the deformable matrix. This is often a complex matter, but luckily in one dimension, the issue does not arise, and a one-dimensional model is often what is of practical interest. We take z to point vertically upwards, and let v and w be the linear (or *phase-averaged*) velocities of liquid and solid, respectively. Then ϕv and $(1 - \phi)w$ are the respective fluxes, and conservation of mass of each phase requires

$$\begin{aligned} \frac{\partial \phi}{\partial t} + \frac{\partial(\phi v)}{\partial z} &= 0, \\ -\frac{\partial \phi}{\partial t} + \frac{\partial}{\partial z}\{(1 - \phi)w\} &= 0; \end{aligned} \quad (2.196)$$

Darcy's law is then

$$\phi(v - w) = -\frac{k}{\mu} \left[\frac{\partial p}{\partial z} + \rho_l g \right], \quad (2.197)$$

while the overburden pressure satisfies

$$\frac{\partial P}{\partial z} = -[\rho_s(1 - \phi) + \rho_l \phi]g, \quad P = P_0 \quad \text{on} \quad z = h; \quad (2.198)$$

here $z = h$ represents the ground surface and P_0 is the applied load. The effective pressure is just $-p_{\text{eff}} = P - p$.

Note that by adding the two mass conservation equations and integrating, we have

$$\phi v + (1 - \phi)w = q(t), \quad (2.199)$$

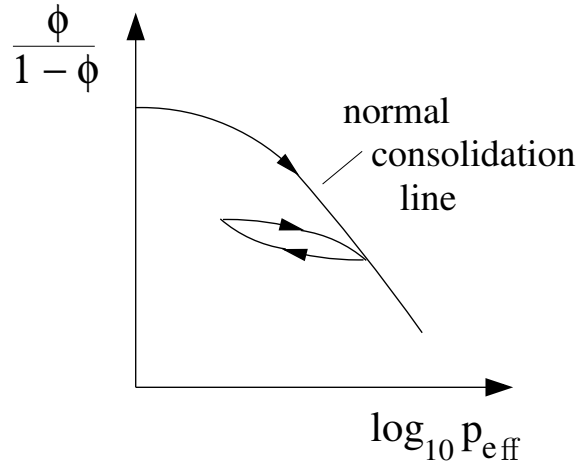


Figure 2.19: Form of the relationship between porosity and effective pressure. A hysteretic decompression-reconsolidation loop is indicated. In soil mechanics this relationship is often written in terms of the *void ratio* $e = \phi/(1 - \phi)$, and specifically $e = e_0 - C_c \log_{10} p_{\text{eff}}$, where C_c is the *compression index*.

which can be determined from the boundary conditions. In particular, if we assume an impermeable basement where $v = w = 0$, then $q = 0$ and

$$w = -\frac{\phi v}{1 - \phi}, \quad \phi(v - w) = -w. \quad (2.200)$$

We use the definition of the effective pressure in (2.195), together with (2.198) and (2.199), to derive the equation

$$\frac{\partial \phi}{\partial t} = -\frac{\partial}{\partial z} \left[\frac{k}{\mu} (1 - \phi) \left\{ \frac{\partial p_{\text{eff}}}{\partial z} + \Delta \rho (1 - \phi) g \right\} \right], \quad (2.201)$$

where $\Delta \rho = \rho_s - \rho_l$, and since $p_{\text{eff}}(\phi)$ is a monotonically decreasing function, this brings us back to the Richards equation (2.125). Specifically, we can write (2.201) in the form

$$\phi_t + V_z = [D \phi_z]_z, \quad (2.202)$$

where

$$V(\phi) = \frac{k(\phi) \Delta \rho g}{\mu} (1 - \phi)^2, \quad D = -\frac{k(\phi)}{\mu} (1 - \phi) p'_{\text{eff}}(\phi), \quad (2.203)$$

and this can be compared to (2.125).

A commonly used expression in soil mechanics for the relationship between effective pressure and porosity is a logarithmic dependence of the *void ratio* $\phi/(1 - \phi)$ on p_{eff} , as mentioned in figure 2.19. The *normal consolidation line* for a soil is that part of the yield surface on which the shear stress vanishes, and we may take

$$\frac{\phi}{1 - \phi} = e_0 - C_c \log_{10} \left(\frac{p_{\text{eff}}}{p_0^{\text{eff}}} \right); \quad (2.204)$$

the quantity C_c is called the *compression index*. Note that this prescription will not be valid at small effective pressure, since as $p_{\text{eff}} \rightarrow 0$, the porosity will tend to its value at loose packing, which we denote as ϕ_0 . This gives p_{eff} as a monotonically decreasing function of ϕ for $0 < \phi < 1$, and in particular,

$$p'_{\text{eff}}(\phi) = -\frac{0.43 p_{\text{eff}}}{C_c (1 - \phi)^2}, \quad (2.205)$$

where $0.43 \approx \ln 10$. In this case,

$$D = \frac{0.43 k(\phi) p_{\text{eff}}}{\mu C_c (1 - \phi)}. \quad (2.206)$$

The diffusion coefficient D is sometimes written as c_v , and is known as the *coefficient of consolidation*. If we use values $\mu = 10^{-3}$ Pa s, $p_{\text{eff}} = 10^4$ Pa, $k = 10^{-14}$ m² (for silt), $C_c = 0.1$ and $\phi = 0.4$, then $D \sim 10^{-6}$ m² s⁻¹. Of course this value depends strongly on the permeability, or equivalently the hydraulic conductivity $K = \frac{k \rho g}{\mu}$. For the silt permeability, $K \sim 3$ m y⁻¹, whereas actual soils (with organic matter, worm burrows,

etc.), typically have hydraulic conductivities $\sim 1 \text{ m d}^{-1}$, which is about a hundred times larger, and would give a corresponding diffusion coefficient of $D \sim 10^{-4} \text{ m}^2 \text{ s}^{-1}$.

We suppose these equations apply in a vertical column $0 < z < h$, for which suitable boundary conditions are (with an impermeable basement and no surface load)

$$\begin{aligned} v = w = 0 & \quad \text{at } z = 0, \\ \phi = \phi_0, \dot{h} = w & \quad \text{at } z = h, \end{aligned} \quad (2.207)$$

and with an initial condition for ϕ . Note that by comparing (2.196)₁ and (2.202), and using (2.200),

$$w = -\frac{(V - D\phi_z)}{1 - \phi}. \quad (2.208)$$

Therefore the boundary conditions in (2.207) collapse to

$$\begin{aligned} V - D\phi_z = 0 & \quad \text{at } z = 0, \\ \phi = \phi_0, \dot{h} = -\frac{(V - D\phi_z)}{1 - \phi} & \quad \text{at } z = h. \end{aligned} \quad (2.209)$$

In the steady state, it follows that $V - D\phi_z = 0$, and thus

$$\int_{\phi}^{\phi_0} \frac{D(\phi) d\phi}{V(\phi)} = h - z. \quad (2.210)$$

If C_c is small (and typical values are in the range $C_c \leq 0.1$) then ϕ varies little, and we can suppose V and D are approximately constant. In this case, the consolidation equation takes the simpler form

$$\phi_t = D\phi_{zz}, \quad (2.211)$$

together with (2.209), and the steady solution (2.210) is just

$$\phi = \phi_0 - \frac{V}{D}(h_0 - z). \quad (2.212)$$

We now consider settlement of the ground after imposition of a surface load pressure ΔP . We suppose the final steady state has depth h_∞ , so that the final steady solution (with D and V being constant) is

$$\phi^* = \phi_\infty - \frac{V}{D}(h_\infty - z), \quad (2.213)$$

and $\phi_\infty = \phi(p_{\text{eff}}^\infty)$, where p_{eff}^∞ is the applied surface effective pressure. With no initial surface load, $p_{\text{eff}}^\infty = \Delta P$, the prescribed surface load, and so (for small changes in ϕ)

$$\phi_\infty \approx \phi_0 - |\phi'(0)|\Delta P. \quad (2.214)$$

We perturb the system by writing

$$\phi = \phi^*(z) + \Phi, \quad h = h_\infty + \eta, \quad (2.215)$$

and then linearising the equation and boundary conditions. This leads to

$$\begin{aligned} \Phi_t &= D\Phi_{zz}, \\ \Phi_z &= 0 \quad \text{on} \quad z = 0, \\ \frac{V}{D}\eta + \Phi &= 0, \quad \eta_t = \frac{D\Phi_z}{1 - \phi_\infty} \quad \text{on} \quad z = h_\infty. \end{aligned} \quad (2.216)$$

Eliminating η from the surface boundary condition gives

$$\Phi_t + \frac{V\Phi_z}{1 - \phi_\infty} = 0 \quad \text{on} \quad z = h_\infty. \quad (2.217)$$

Subtracting the initial condition from the final condition, we find

$$\Phi = \phi_0 - \phi_\infty - \frac{V}{D}(h_0 - h_\infty), \quad \eta = h_0 - h_\infty \quad \text{at} \quad t = 0. \quad (2.218)$$

At this point we realise that the initial depth h is unconstrained. It is in fact determined by the volume of solids in the domain (which, unlike the volume of water which is squeezed out the top, is conserved). Thus we require

$$\int_0^{h_\infty + \eta} [1 - (\phi^* + \Phi)] dz = \int_0^{h_\infty} (1 - \phi^*) dz, \quad (2.219)$$

and linearising this leads to the normalising condition

$$\int_0^{h_\infty} \Phi dz = (1 - \phi_\infty)\eta. \quad (2.220)$$

This is consistent with (2.216) (as it must be), and it provides the necessary relation between h_0 and h_∞ , which is, using (2.214),

$$\frac{h_0 - h_\infty}{h_\infty} = \frac{|\phi'(0)|\Delta P}{1 - \phi_\infty + \frac{Vh_\infty}{D}}, \quad (2.221)$$

and this is the (relative) settlement due to a given load.

The other quantity of interest is the settlement time. The normal mode solutions of (2.216) are

$$\Phi = e^{-Ds^2t} \cos sz, \quad (2.222)$$

where

$$\tan \kappa = -\frac{\kappa}{Pe}, \quad \kappa = sh_\infty, \quad Pe = \frac{h_\infty V}{D(1 - \phi_\infty)}; \quad (2.223)$$

here Pe is a suitable Péclet number for the flow, and s is the wavenumber (normally one uses k , but that is already taken for the permeability). It is graphically straightforward to see that there is an infinite number of values of $\kappa_1, \kappa_2, \dots$ (positive, without loss of generality) satisfying (2.223), with $(n - \frac{1}{2})\pi < \kappa_n < n\pi$. The settlement or consolidation time scale t_c is essentially determined by κ_1 , and is thus

$$t_c \sim \frac{h_\infty^2}{D\kappa_1^2}, \quad (2.224)$$

where κ_1 lies between $\frac{1}{2}\pi$ and π . It depends primarily on the permeability k . If we use (2.206), and take $k \sim 10^{-14} \text{ m}^2$ (silt), $C_c = 0.1$, $\phi = 0.3$, $\mu = 10^{-3} \text{ Pa s}$, $P_0 = 10^5 \text{ Pa}$ (a small house), then $D \sim 0.6 \times 10^{-5} \text{ m}^2 \text{ s}^{-1}$. Similarly, with $\Delta\rho = 2 \times 10^3 \text{ kg m}^{-3}$, we find $V \sim 10^{-7} \text{ m s}^{-1}$, and so, if we take $h_\infty = 10 \text{ m}$, the Péclet number is $Pe \sim 0.23$; not extremely small, but small enough to use the approximation of small Pe in (2.223). When Pe is small, $\kappa \approx \frac{1}{2}\pi$, and so 14.82

$$t_c \sim \frac{4h_\infty^2}{\pi^2 D}, \quad (2.225)$$

which gives $t_c \sim 3$ months.

Exercises

- 2.1 Show that for a porous medium idealised as a cubical network of tubes, the permeability is given (approximately) by $k = d_p^2 \phi^2 / 72\pi$, where d_p is the grain size. How is the result modified if the pore space is taken to consist of planar sheets between identical cubical blocks? (The volume flux per unit width between two parallel plates a distance h apart is $-h^3 p' / 12\mu$, where p' is the pressure gradient.)
- 2.2 Groundwater flows between an impermeable basement at $z = h_b(x, y, t)$ and a phreatic surface at $z = z_p(x, y, t)$. Write down the equations governing the flow, and by using the Dupuit approximation, show that the saturated depth h satisfies

$$\phi h_t = \frac{k\rho g}{\mu} \nabla \cdot [h \nabla z_p],$$

where $\nabla = (\partial/\partial x, \partial/\partial y)$. Deduce that a suitable time scale for flows in an aquifer of typical depth h_0 and extent l is $t_{gw} = \phi\mu l^2 / k\rho gh_0$.

I live a kilometer from the river, on top of a layer of sediments 100 m thick (below which is impermeable basement). What sort of sediments would those need to be if the river responds to rainfall at my house within a day; within a year?

- 2.3 A two-dimensional earth dam with vertical sides at $x = 0$ and $x = l$ has a reservoir on one side ($x < 0$) where the water depth is h_0 , and horizontal dry

land on the other side, in $x > l$. The dam is underlain by an impermeable basement at $z = 0$.

Write down the equations describing the saturated groundwater flow, and show that they can be written in the dimensionless form

$$u = -p_x, \quad \varepsilon^2 w = -(p_z + 1),$$

$$p_{zz} + \varepsilon^2 p_{xx} = 0,$$

and define the parameter ε . Write down suitable boundary conditions on the impermeable basement, and on the phreatic surface $z = h(x, t)$.

Assuming $\varepsilon \ll 1$, derive the Dupuit-Forchheimer approximation for h ,

$$h_t = (hh_x)_x \quad \text{in } 0 < x < 1.$$

Show that a suitable boundary condition for h at $x = 0$ (the dam end) is

$$h = 1 \quad \text{at } x = 0.$$

Now define the quantity

$$U = \int_0^h p \, dz,$$

and show that the horizontal flux

$$q = \int_0^h u \, dz = -\frac{\partial U}{\partial x}.$$

Hence show that the conditions of hydrostatic pressure at $x = 0$ and constant (atmospheric) pressure at $x = 1$ (the seepage face) imply that

$$\int_0^1 q \, dx = \frac{1}{2}.$$

Deduce that, if the Dupuit approximation for the flux is valid all the way to the toe of the dam at $x = 1$, then $h = 0$ at $x = 1$, and show that in the steady state, the (dimensional) discharge at the seepage face is

$$q_D = \frac{k\rho gh_0^2}{2\mu l}.$$

Supposing the above description of the solution away from the toe to be valid, show that a possible boundary layer structure near $x = 1$ can be described by writing

$$x = 1 - \varepsilon^2 X, \quad h = \varepsilon H, \quad z = \varepsilon Z, \quad p = \varepsilon P,$$

and write down the resulting leading order boundary value problem for P .

2.4 I get my water supply from a well in my garden. The well is of depth h_0 (relative to the height of the water table a large distance away) and radius r_0 . Show that the Dupuit approximation for the water table height h is

$$\phi \frac{\partial h}{\partial t} = \frac{k\rho g}{\mu} \frac{1}{r} \frac{\partial}{\partial r} \left(rh \frac{\partial h}{\partial r} \right).$$

If my well is supplied from a reservoir at $r = l$, where $h = h_0$, and I withdraw a constant water flux q_0 , find a steady solution for h , and deduce that my well will run dry if

$$q_0 > \frac{\pi k \rho g h_0^2}{\mu \ln[l/r_0]}.$$

Use plausible values to estimate the maximum yield (gallons per day) I can use if my well is drilled through sand, silt or clay, respectively.

2.5 A volume V of effluent is released into the ground at a point ($r = 0$) at time t . Use the Dupuit approximation to motivate the model

$$\phi \frac{\partial h}{\partial t} = \frac{k\rho g}{\mu} \frac{1}{r} \frac{\partial}{\partial r} \left(rh \frac{\partial h}{\partial r} \right),$$

$$h = h_0 \quad \text{at } t = 0, \quad r > 0,$$

$$\int_0^\infty r(h - h_0) dr = V/2\pi, \quad t > 0,$$

where h_0 is the initial height of the water table above an impermeable basement. Find suitable similarity solutions in the two cases (i) $h_0 = 0$ (ii) $h_0 > 0$, $h - h_0 \ll h_0$, and comment on the differences you find.

2.6 Rain falls steadily at a rate q (volume per unit area per unit time) on a soil of saturated hydraulic conductivity K_0 ($= k_0 \rho_w g / \mu$, where k_0 is the saturated permeability). By plotting the relative permeability k_r and suction characteristic $\sigma\psi/d$ as functions of S (assuming a residual liquid saturation S_0), show that a reasonable form to choose for $k_r(\psi)$ is $k_r = e^{-c\psi}$. If the water table is at depth h , show that, in a steady state, ψ is given as a function of the dimensionless depth $z^* = z/z_c$, where $z_c = \sigma/\rho_w g d$ (σ is the surface tension, d the grain size) by

$$h^* - z^* = \frac{1}{2}\psi - \frac{1}{c} \ln \left[\frac{\sinh\{\frac{1}{2}(\ln \frac{1}{q^*} - c\psi)\}}{\sinh\{\frac{1}{2} \ln \frac{1}{q^*}\}} \right],$$

where $h^* = h/z_c$, providing $q^* = q/K_0 < 1$. Deduce that if $h \gg z_c$, then $\psi \approx \frac{1}{c} \ln \frac{1}{q^*}$ near the surface. What happens if $q > K_0$?

2.7 Derive the Richards equation

$$\phi \frac{\partial S}{\partial t} = - \frac{\partial}{\partial z} \left[\frac{k_0}{\mu} k_r(S) \left\{ \frac{\partial p_c}{\partial z} + \rho_w g \right\} \right]$$

for one-dimensional infiltration of water into a dry soil, explaining the meaning of the terms, and giving suitable boundary conditions when the surface flux q is prescribed. Show that if the surface flux is large compared with $k_0\rho_w g/\mu$, where k_0 is the saturated permeability, then the Richards equation can be approximated, in suitable non-dimensional form, by a nonlinear diffusion equation of the form

$$\frac{\partial S}{\partial t} = \frac{\partial}{\partial z} \left[D \frac{\partial S}{\partial z} \right].$$

Show that, if $D = S^m$, a similarity solution exists in the form

$$S = t^\alpha F(\eta), \quad \eta = z/t^\beta,$$

where $\alpha = \frac{1}{m+2}$, $\beta = \frac{m+1}{m+2}$, and F satisfies

$$(F^m F')' = \alpha F - \beta \eta F', \quad F^m F' = -1 \text{ at } \eta = 0, \quad F \rightarrow 0 \text{ as } \eta \rightarrow \infty.$$

Deduce that

$$F^m F' = -(\alpha + \beta) \int_\eta^{\eta_0} F d\eta - \beta \eta F,$$

where η_0 (which may be ∞) is where F first reaches zero. Deduce that $F' < 0$, and hence that η_0 must be finite, and is determined by

$$\int_0^{\eta_0} F d\eta = \frac{1}{\alpha + \beta}.$$

What happens for $t > F(0)^{-1/\alpha}$?

- 2.8 Write down the equations describing one-dimensional consolidation of wet sediments in terms of the variables $\phi, v, w, p, p_{\text{eff}}$, these being the porosity, solid and liquid (linear) velocities, and the pore and effective pressures. Neglect the effect of gravity.

Saturated sediments of depth h lie on a rigid but permeable (to water) basement, through which a water flux W is removed. Show that

$$w = \frac{k}{\mu} \frac{\partial p}{\partial z} - W,$$

and deduce that ϕ satisfies the equation

$$\frac{\partial \phi}{\partial t} = \frac{\partial}{\partial z} \left[(1 - \phi) \left\{ \frac{k}{\mu} \frac{\partial p}{\partial z} - W \right\} \right].$$

If the sediments are overlain by water, so that $p = \text{constant}$ (take $p = 0$) at $z = h$, and if $\phi = \phi_0 + p/K$, where the compressibility K is large (so $\phi \approx \phi_0$), show that a suitable reduction of the model is

$$\frac{\partial p}{\partial t} - W \frac{\partial p}{\partial z} = c \frac{\partial^2 p}{\partial z^2},$$

where $c = K(1 - \phi_0)k/\mu$, and $p = 0$ on $z = h$, $p_z = \mu W/k$. Non-dimensionalise the model using the length scale h , time scale h^2/c , and pressure scale $\mu Wh/k$. Hence describe the solution if the parameter $\varepsilon = \mu Wh/k$ is small, and find the rate of surface subsidence. What has this to do with Venice?

- 2.9 Write down a model for vertical flow of two immiscible fluids in a porous medium. Deduce that the saturation S of the wetting phase satisfies the equation

$$\phi \frac{\partial S}{\partial t} + \frac{\partial}{\partial z} \left[M_{\text{eff}} \left\{ \frac{q}{M_{nw}} + g\Delta\rho \right\} \right] = - \frac{\partial}{\partial z} \left[M_{\text{eff}} \frac{\partial p_c}{\partial z} \right],$$

where z is a coordinate pointing *downwards*,

$$p_c = p_{nw} - p_w, \quad \Delta\rho = \rho_w - \rho_{nw}, \quad M_{\text{eff}}^{-1} = (M_w^{-1} + M_{nw}^{-1}),$$

q is the total downward flux, and the suffixes w and nw refer to the wetting and non-wetting fluid respectively. Define the phase mobilities M_i . Give a criterion on the capillary suction p_c which allows the Buckley-Leverett approximation to be made, and show that for $q = 0$ and $\mu_w \gg \mu_{nw}$, waves typically propagate downwards and form shocks. What happens if $q \neq 0$? Is the Buckley-Leverett approximation realistic — e.g. for air and water in soil? (Assume $p_c \sim 2\gamma/r_p$, where $\gamma = 70 \text{ mN m}^{-1}$, and r_p is the pore radius: for clay, silt and sand, take $r_p = 1 \mu, 10 \mu, 100 \mu$, respectively.)

- 2.10 A model for snow melt run-off is given by the following equations:

$$\begin{aligned} u &= \frac{k}{\mu} \left[\frac{\partial p_c}{\partial z} + \rho_l g \right], \\ k &= k_0 S^3, \\ \phi \frac{\partial S}{\partial t} + \frac{\partial u}{\partial z} &= 0, \\ p_c &= p_0 \left(\frac{1}{S} - S \right). \end{aligned}$$

Explain the meaning of the terms in these equations, and describe the assumptions of the model.

The intrinsic permeability k_0 is given by

$$k_0 = 0.077 d^2 \exp[-7.8 \rho_s/\rho_l],$$

where ρ_s and ρ_l are snow and water densities, and d is grain size. Take $d = 1 \text{ mm}$, $\rho_s = 300 \text{ kg m}^{-3}$, $\rho_l = 10^3 \text{ kg m}^{-3}$, $p_0 = 1 \text{ kPa}$, $\phi = 0.4$, $\mu = 1.8 \times 10^{-3} \text{ Pa s}$, $g = 10 \text{ m s}^{-2}$, and derive a non-dimensional model for melting of a one metre thick snow pack at a rate (i.e. u at the top surface $z = 0$) of 10^{-6} m s^{-1} . Determine whether capillary effects are small; describe the nature of the model equation, and find an approximate solution for the melting of an initially dry snowpack. What is the (meltwater flux) run-off curve?

2.11 Consider the following model, which represents the release of a unit quantity of groundwater at $t = 0$ in an aquifer $-\infty < x < \infty$, when the Dupuit approximation is used:

$$\begin{aligned} h_t &= (hh_x)_x, \\ h &= 0 \text{ at } t = 0, x \neq 0, \\ \int_{-\infty}^{\infty} h dx &= 1 \end{aligned}$$

(i. e., $h = \delta(x)$ at $t = 0$). Show that a similarity solution to this problem exists in the form

$$h = t^{-1/3}g(\xi), \quad \xi = x/t^{1/3},$$

and find the equation and boundary conditions satisfied by g . Show that the water body spreads at a finite rate, and calculate what this is.

Formulate the equivalent problem in three dimensions, and write down the equation satisfied by the similarity form of the solution, assuming cylindrical symmetry. Does this solution have the same properties as the one-dimensional solution?

Chapter 3

Convection

Convection is the fluid motion induced by buoyancy; buoyancy is the property of a fluid whereby its density depends on external properties. The most common form of convection is *thermal convection*, which occurs due to the dependence of density on temperature: warm fluid is light, and therefore rises. Everyday examples of this are the circulation induced by a convector heater, or the motion which can be seen in a saucepan of oil when it is heated. (In the latter case, one can see convection rolls in the fluid, regular but time-dependent.) Another common form of convection is *compositional convection*, which is induced by density changes dependent on composition. An example of this occurs during the formation of sea ice in the polar regions. As salty sea water freezes, it rejects the salt (the ice is almost pure water substance), and the resulting salty water is denser than the sea water from which it forms, and thus induces a convective motion below the ice. Below, we discuss three geophysical examples from convection, but convection is everywhere: it drives the oceanic circulation, it drives the atmospheric circulation, it causes thunderstorms, it occurs in glass manufacture, in a settling pint of Guinness, in back boilers, in solar panels. And, it has formed the thematic core of the subject of geophysical fluid dynamics for almost a century.

3.1 Mantle convection

Most people have heard of continental drift, the process whereby the Earth's continents drift apart relative to each other. The Atlantic Ocean is widening at the rate of several centimetres a year, the crashing of India into Asia over the last 50 My (fifty million years) has caused the continuing uplift of the Himalayas, Scotland used to be joined to Newfoundland. The continents ride, like rafts of debris, on the tectonic plates of the Earth, which separate at mid-ocean ridges and converge at subduction zones. The theory of plate tectonics, which originated with the work of Wegener and Holmes in the early part of the twentieth century, and which was finally accepted by geophysicists in the 'plate tectonics revolution' of the 1960's, describes the surface of the Earth as being split up into some thirteen major tectonic plates: see figure

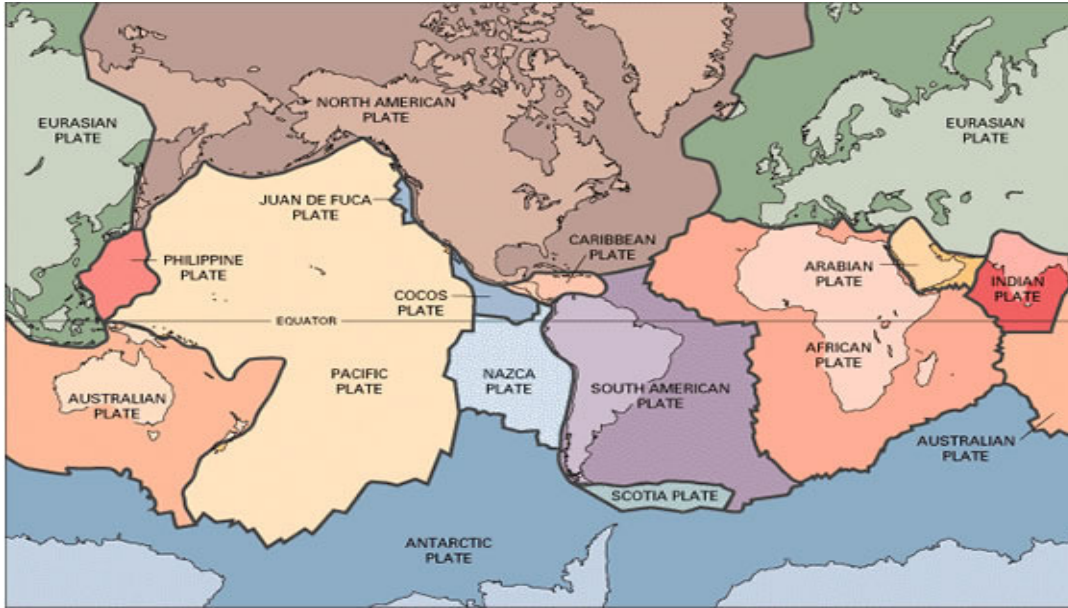


Figure 3.1: The tectonic plates of the Earth.

3.1. These plates move relative to each other across the surface, and this motion is the surface manifestation of a convective motion in the Earth's *mantle*, which is the part of the Earth from the surface to a depth of about 3,000 kilometres, and which consists of an assemblage of polycrystalline silicate rocks. Upwelling occurs at mid-ocean ridges, for example the mid-Atlantic ridge which passes through Iceland, and the East Pacific Rise off the coast of South America, which passes through the Galapagos Islands. The plates sink into the mantle at subduction zones, which adjoin continental boundaries, and which are associated with the presence of oceanic trenches.

The plates are so called because they are conceived of as moving quasi-rigidly. They are in fact the cold upper thermal boundary layers of the convective motion, in-

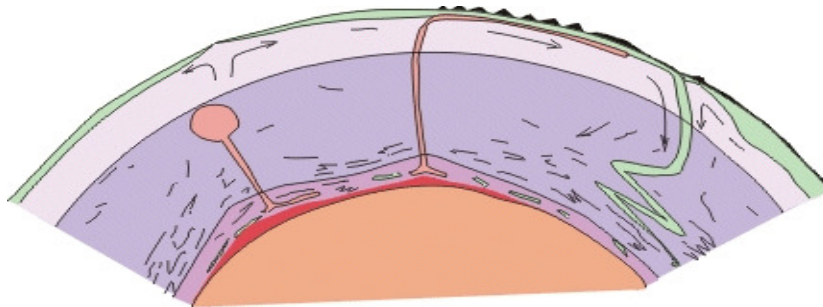


Figure 3.2: A cartoon of mantle convection. We see plumes, mid-ocean ridges, subducting slabs.

licated schematically in figure 3.2, and are plate-like because the strong temperature dependence of mantle viscosity renders these relatively cold rocks extremely viscous. One may wonder how the mantle moves at all, consisting as it does of mostly solid polycrystalline rocks. In fact, solids will deform just as fluids do when subjected to stress. The deformation is enabled by the migration of dislocations within the crystalline lattice of the solid grains of the rock. The effective viscosity of the Earth's mantle is a whopping 10^{21} Pa s; this is about eight orders of magnitude greater than the viscosity of ice, and twenty-four orders greater than the viscosity of water.

The reason that the mantle convects is that the Earth is cooling. The primordial heat of formation has gradually been lost over the Earth's history, but the central core of the planet is still very hot; some six thousand degrees Celsius at the centre of the Earth. This heat from the core is instrumental in heating the mantle from below, and driving the convective flow. Radioactive heating also contributes to an extent which is not certain, but which is thought to be significant.

3.2 The Earth's core

Part of the heat which drives mantle convection is derived from cooling the Earth's core. The core is the part of the Earth which lies between its centre and the mantle. Like the mantle, it is also some three thousand kilometres deep, and consists of a molten outer core of iron, alloyed with some lighter element, usually thought to be sulphur or oxygen, in a concentration of some 10%. The inner core is solid (pure) iron, of radius 1,000 km. It is generally thought that the core was initially molten throughout, and that the inner core has gradually solidified from the outer core over the course of geological time. It is the consequent release of latent heat which, at least partly, powers mantle convection.

One may wonder how the outer core can be liquid, and the inner core solid, if the inner core is hotter (as it must be). The reason for this is that the solidification temperature (actually the liquidus temperature, see below) depends on pressure, through the Clapeyron effect. This is the effect whereby a pressure cooker works: the boiling temperature increases with pressure, and similarly, the solidification temperature of the outer core iron alloy increases with pressure, and thus also depth. Thus, the inner core can be below the solidification temperature because of the greater pressure there.

The convection in the outer core is partly due to the dependence of density on temperature, but the primary dependence is, as often the case when composition varies, due to the dependence of density on the concentration of sulphur (or oxygen). In order to understand how the solidification of the inner core leads to convection, we need to understand the general thermodynamic way in which melting and solidification occur in multi-component materials. This is illustrated in figure 3.3, which indicates how the solidification temperatures vary with composition in a two-component melt. At a given temperature, there are two curves which describe the concentrations of the solid and liquid, when these are in thermodynamic equilibrium with each other. These two curves are called the solidus and liquidus, respectively. Often there are two sets of

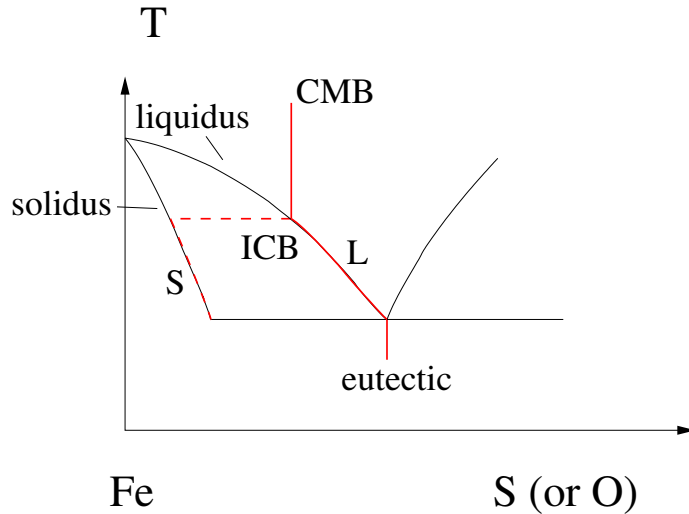


Figure 3.3: Typical phase diagram for a two-component alloy with a eutectic point. When the liquid reaches the liquidus (L), the resulting solid has the concentration of the solidus (S). When the liquid reaches the eutectic point, two solids, iron-rich and sulphur-rich respectively, will be formed.

solidus and liquidus curves, and they meet at a point called the eutectic point. The way in which a liquid alloy solidifies is then indicated by the red line in figure 3.3. In the outer core, the composition is relatively constant, but the temperature decreases (relative to the liquidus) from the core-mantle boundary (CMB) to the inner core boundary (ICB), where solidification occurs. (The phase diagram is indicated as if at constant pressure; in reality, the curves will also vary with pressure.)

At this temperature, the solid which crystallises has the solidus concentration, which is richer in iron than the liquid, and so as the temperature cools during freezing, the liquid concentration of sulphur or oxygen increases because of its rejection at the freezing interface. It is this source of buoyancy which provides the driving force for compositional convection.

Actually, it is typically the case that when alloys solidify, they do not form a solid with a clear interface. Rather, such a situation is typically *morphologically unstable*, and a dendritic mush consisting of a solid-liquid mixture is formed, as shown in figure 3.4. The convection caused by the release of light fluid now occurs throughout the mush, and leads to the formation of narrow ‘chimneys’, from which plumes emerge.

In the Earth’s core, it is this convection which forms the magnetic field. Convection in an electrically conducting fluid causes a magnetic field to grow, providing the magnetic diffusivity is sufficiently small, through the action of the Lorentz force. The study of such instabilities is a central part of the subject of magnetohydrodynamics.



Figure 3.4: A dendritic mush in the solidification of ammonium chloride in the laboratory. Convection occurs within the mush, leading to the formation of ‘chimneys’ which act as sources of plumes in the residual melt. Photo courtesy of Grae Worster.

3.3 Magma chambers

Our final example of convection arises in the formation and cooling of magma chambers. When mantle rock upwells, either at mid-ocean ridges, or in isolated thermal plumes such as that below Hawaii, the slight excess temperature causes the rock to partially melt. It is thought that the melt fraction can then ascend through the residual porous matrix, forming rivulets and channels which allow the escape of the magma through the lithosphere to the crust.¹ As the magma ascends into the crust, it can typically encounter unconformities, where the rock types alter, and where the density may be less than that of the magma. In that case, the magma will stop rising, but will spread laterally, simultaneously uplifting the overlying strata. Thus forms the *laccolith*, a magmatic intrusion, and over the course of time such intrusions, or magma chambers, will solidify, forming huge cauldrons of rock which may later be exposed at the Earth’s surface.

Convection undoubtedly occurs in such chambers, which may be tens of kilometres in extent. The hot magma is continuously chilled at the roof and sides of the chamber, and this leads to convective currents continually draining towards the floor of the chamber. There they will accumulate, leading to a cold, crystal-rich layer ly-

¹The *lithosphere* is the cold surface boundary layer of the convecting mantle, of depth some 100 km in the oceanic mantle, somewhat greater beneath continents; the crust is a relatively thin layer of rocks near the surface, formed through partial melting of the mantle and the resulting volcanism.



Figure 3.5: Graded layering in the Skaergaard intrusion. Photograph courtesy of Kurt Hollocher.

ing stagnant below the convecting upper portion. This is essentially the filling box mechanism which is discussed further below.

Magmas are multi-component alloys, and their convective solidification can lead to various exotic phenomena. The phase diagram of the type in figure 3.3 causes chemical differentiation on the large scale (in metal alloy castings this is called macrosegregation). For example, in an olivine–plagioclase magma, the heavy olivine will crystallise out first, and the crystals may settle to the base of the chamber. The residual liquid is then plagioclase-rich and lighter. So the end result would be a chamber having two distinct layers. Successive injections of magma may then lead to a sequence of such layers, as is seen in the Scottish island of Rum, and this has been suggested as an explanation for these particular layers.

Other magma chambers show layering at a much finer scale, and the origin of these layers is a mystery. An example is shown in figure 3.5. The layers are reminiscent of double-diffusive layering, which we discuss in section 3.6.2, but efforts to build a theory round this idea, or indeed any other, have so far not met with success.

3.4 Rayleigh–Bénard convection

The simplest model of convection is the classical Rayleigh–Bénard model in which a layer of fluid is heated from below, by application of a prescribed temperature

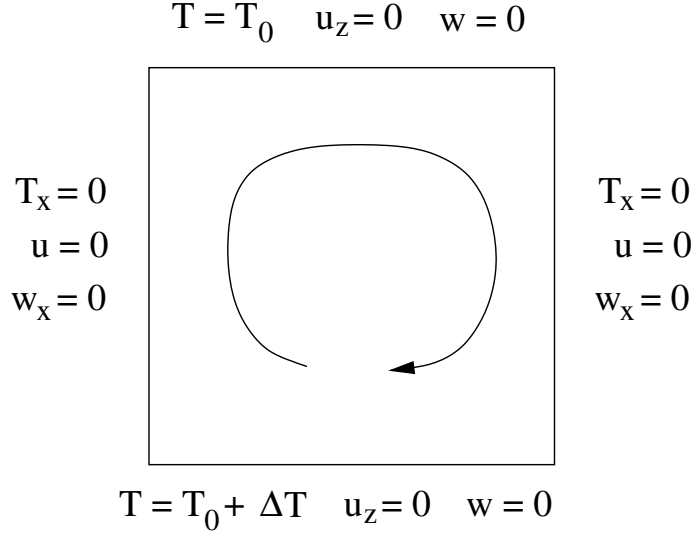


Figure 3.6: Geometry of a convection cell.

difference across the layer. Depending on the nature of the boundaries, one may have a no slip condition or a no shear stress condition applied at the bounding surfaces. For the case of mantle convection, one conceives of both the oceans (or atmosphere) and the underlying fluid outer core as exerting no stress on the extremely viscous mantle, so that no stress conditions are appropriate, and in fact it turns out that this is the simplest case to consider. The geometry of the flow we consider is shown in figure 3.6. It is convenient to assume lateral boundaries, although in a wide layer, these simply represent the convection cell walls, and can be an arbitrary distance apart.

The equations describing the flow are the Navier-Stokes equations, allied with the energy equation and an equation of state, and can be written in the form

$$\begin{aligned}
 \rho_t + \nabla \cdot (\rho \mathbf{u}) &= 0, \\
 \rho[\mathbf{u}_t + (\mathbf{u} \cdot \nabla) \mathbf{u}] &= -\nabla p - \rho g \mathbf{k} + \mu \nabla^2 \mathbf{u}, \\
 \rho c_p [T_t + \mathbf{u} \cdot \nabla T] &= k \nabla^2 T, \\
 \rho &= \rho_0 [1 - \alpha(T - T_0)];
 \end{aligned} \tag{3.1}$$

in these equations, ρ is the density, \mathbf{u} is the velocity, p is the pressure, g is the acceleration due to gravity, \mathbf{k} is the unit upwards vector, μ is viscosity, c_p is the specific heat, T is temperature, k is thermal conductivity, ρ_0 is the density at the reference temperature T_0 at the surface of the fluid layer, and α is the thermal expansion coefficient. The boundary conditions for the flow are indicated in figure 3.6, and correspond to prescribed temperature at top and bottom, no flow through the boundaries, and no shear stress at the boundaries. The lateral boundaries represent stress free ‘walls’, but as mentioned above, these simply indicate the boundaries of the convection cells

(across which there is no heat transport, hence the no flux condition for temperature).

To proceed, we non-dimensionalise the variables as follows. We use the convective time scale, and a thermally related velocity scale, and use the depth of the box d as the length scale:

$$\begin{aligned} \mathbf{u} &\sim \frac{\kappa}{d}, & \kappa &= \frac{k}{\rho_0 c_p}, & t &\sim \frac{d^2}{\kappa}, & \mathbf{x} &\sim d, \\ p - [p_0 + \rho_0 g(d - z)] &\sim \frac{\mu \kappa}{d^2}, & T - T_0 &\sim \Delta T. \end{aligned} \quad (3.2)$$

Here p_0 is the (prescribed) pressure at the surface, which we take as constant. We would also scale $\rho \sim \rho_0$, but in the scaled equations below, the density has been algebraically eliminated. The scaled equations take the form

$$\begin{aligned} -BT_t + \nabla \cdot [(1 - BT)\mathbf{u}] &= 0, \\ \frac{1}{Pr}[1 - BT][\mathbf{u}_t + (\mathbf{u} \cdot \nabla)\mathbf{u}] &= -\nabla p + Ra T \hat{\mathbf{k}} + \nabla^2 \mathbf{u}, \\ (1 - BT)(T_t + \mathbf{u} \cdot \nabla T) &= \nabla^2 T, \end{aligned} \quad (3.3)$$

and the dimensionless parameters are defined as

$$B = \alpha \Delta T, \quad Pr = \frac{\mu}{\rho_0 \kappa}, \quad Ra = \frac{\alpha \rho_0 \Delta T g d^3}{\mu \kappa}; \quad (3.4)$$

the parameters Ra and Pr are known as the Rayleigh and Prandtl numbers, respectively. The Prandtl number is a property of the fluid; for air it is 0.7, and for water it is 7. The Rayleigh number is a measure of the strength of the heating. As we shall see, convective motion occurs if the Rayleigh number is large enough, and it becomes vigorous if the Rayleigh number is large. The parameter B might be termed a Boussinesq number, although this is not common usage.

Suppose we think of values typical for a layer of water in a saucepan. We take $d = 0.1$ m, $\mu = 2 \times 10^{-3}$ Pa s, $\Delta T = 100$ K, $\alpha = 3 \times 10^{-5}$ K⁻¹, $\rho_0 = 10^3$ kg m⁻³, $\kappa = 0.3 \times 10^{-6}$ m² s⁻¹, $g = 9.8$ m s⁻². Then we have $Pr \approx 7$, $B \approx 3 \times 10^{-3}$, and $Ra \approx 5 \times 10^7$. In this case, we have that $B \ll 1$ and $Ra \gg 1$. This is typically the case. We now make the Boussinesq approximation, which says that $B \ll 1$, and we ignore the terms in B in (3.3). In words, we assume that the density is constant, except in the buoyancy term. The mathematical reason for this exception is that, although $Ra \propto B$ (and so $Ra \rightarrow 0$ as $B \rightarrow 0$), the actual numerical sizes of the two parameters are typically very different. The adoption of the Boussinesq approximation leads to what are called the Boussinesq equations of thermal convection:

$$\begin{aligned} \nabla \cdot \mathbf{u} &= 0, \\ \frac{1}{Pr}[\mathbf{u}_t + (\mathbf{u} \cdot \nabla)\mathbf{u}] &= -\nabla p + \nabla^2 \mathbf{u} + Ra T \hat{\mathbf{k}}, \\ T_t + \mathbf{u} \cdot \nabla T &= \nabla^2 T, \end{aligned} \quad (3.5)$$

with associated boundary conditions for free slip:

$$\begin{aligned} T = 1, \quad \mathbf{u} \cdot \mathbf{n} = \tau_{nt} = 0 \quad \text{on } z = 0, \\ T = 0, \quad \mathbf{u} \cdot \mathbf{n} = \tau_{nt} = 0 \quad \text{on } z = 1, \end{aligned} \quad (3.6)$$

where τ_{nt} represents the shear stress.

3.4.1 Linear stability

It is convenient to study the problem of the onset of convection in two dimensions (x, z) . In this case we can define a stream function ψ which satisfies

$$u = -\psi_z, \quad w = \psi_x. \quad (3.7)$$

(The sign is opposite to the usual convention; for $\psi > 0$ this describes a clockwise circulation.) We eliminate the pressure by taking the curl of the momentum equation (3.5)₂, which leads, after some algebra (see also question 3.2), to the pair of equations for ψ and T :

$$\begin{aligned} \frac{1}{Pr} [\nabla^2 \psi_t + \psi_x \nabla^2 \psi_z - \psi_z \nabla^2 \psi_x] &= Ra T_x + \nabla^4 \psi, \\ T_t + \psi_x T_z - \psi_z T_x &= \nabla^2 T, \end{aligned} \quad (3.8)$$

with the associated boundary conditions

$$\begin{aligned} \psi = \nabla^2 \psi = 0 \quad \text{at } z = 0, 1, \\ T = 0 \quad \text{at } z = 1, \\ T = 1 \quad \text{at } z = 0. \end{aligned} \quad (3.9)$$

In the absence of motion, $\mathbf{u} = \mathbf{0}$, the steady state temperature profile is linear,

$$T = 1 - z, \quad (3.10)$$

and the lithostatic pressure is modified by the addition of

$$p = -\frac{Ra}{2}(1 - z)^2. \quad (3.11)$$

(Even if Ra is large, this represents a small correction to the lithostatic pressure, of relative size $O(B)$.) The stream function is just

$$\psi = 0. \quad (3.12)$$

We define the temperature perturbation θ by

$$T = 1 - z + \theta. \quad (3.13)$$

This yields

$$\begin{aligned} \frac{1}{Pr} [\nabla^2 \psi_t + \psi_x \nabla^2 \psi_z - \psi_z \nabla^2 \psi_x] &= \nabla^4 \psi + Ra \theta_x, \\ \theta_t - \psi_x + \psi_x \theta_z - \psi_z \theta_x &= \nabla^2 \theta, \end{aligned} \quad (3.14)$$

and the boundary conditions are

$$\psi_{zz} = \psi = \theta = 0 \quad \text{on } z = 0, 1. \quad (3.15)$$

In the Earth's mantle, the Prandtl number is large, and we will now simplify the algebra by putting $Pr = \infty$. This assumption does not in fact affect the result which is obtained for the critical Rayleigh number at the onset of convection. The linear stability of the basic state is determined by neglecting the nonlinear advective terms in the heat equation. We then seek normal modes of wave number k in the form

$$\begin{aligned} \psi &= f(z)e^{\sigma t + ikx}, \\ \theta &= g(z)e^{\sigma t + ikx}, \end{aligned} \quad (3.16)$$

whence f and g satisfy (putting $Pr = \infty$)

$$\begin{aligned} (D^2 - k^2)^2 f + ikRa g &= 0, \\ \sigma g - ikf &= (D^2 - k^2)g, \end{aligned} \quad (3.17)$$

where $D = d/dz$, and

$$f = f'' = g = 0 \quad \text{on } z = 0, 1. \quad (3.18)$$

By inspection, solutions are

$$f = \sin m\pi z, \quad g = b \sin m\pi z, \quad (3.19)$$

($n = 1, 2, \dots$) providing

$$\sigma = \frac{k^2 Ra}{(m^2 \pi^2 + k^2)^2} - (m^2 \pi^2 + k^2), \quad (3.20)$$

which determines the growth rate for the m -th mode of wave number k .

Since σ is real, instability is characterised by a positive value of σ . We can see that σ decreases as m increases; therefore the value $m = 1$ gives the most unstable value of σ . Also, σ is negative for $k \rightarrow 0$ or $k \rightarrow \infty$, and has a single maximum. Since σ increases with Ra , we see that $\sigma > 0$ (for $m = 1$) if $Ra > Ra_{ck}$, where

$$Ra_{ck} = \frac{(\pi^2 + k^2)^3}{k^2}. \quad (3.21)$$

In turn, this value of the Rayleigh number depends on the selected wave number k . Since an arbitrary disturbance will excite all wave numbers, it is the minimum

value of Ra_{ck} which determines the absolute threshold for stability. The minimum is obtained when

$$k = \frac{\pi}{\sqrt{2}}, \quad (3.22)$$

and the resulting critical value of the Rayleigh number is

$$Ra_c = \frac{27\pi^4}{4} \approx 657.5; \quad (3.23)$$

That is, the steady state is linearly unstable if $Ra > Ra_c$.

For other boundary conditions, the solutions are still exponentials, but the coefficients, and hence also the growth rate, must be found numerically. The resultant critical value of the Rayleigh number is higher for no slip boundary conditions, for example, (it is about 1707), and in general, thermal convection is initiated at values of $Ra \gtrsim O(10^3)$.

3.5 High Rayleigh number convection

We have seen that convection occurs if the Rayleigh number is larger than $O(10^3)$ in general, depending on the precise boundary conditions which apply. In the Earth's mantle, suitable values of the constituent parameters are $\alpha = 3 \times 10^{-5} \text{ K}^{-1}$, $\Delta T = 3000 \text{ K}$, $\rho_0 = 3 \times 10^3 \text{ kg m}^{-3}$, $g = 10 \text{ m s}^{-2}$, $d = 3000 \text{ km}$, $\eta_0 = 10^{21} \text{ Pa s}$, $\kappa_0 = 10^{-6} \text{ m}^2 \text{ s}^{-1}$, and for these values, the Rayleigh number is slightly less than 10^8 . Thus the Rayleigh number is much larger than the critical value, and as a consequence we can expect the convection to be vigorous (if velocities of centimetres per year can be said to be vigorous).

There are various intuitive ways in which we can get a sense of the likely behaviour of the convective solutions of the Boussinesq equations when $Ra \gg 1$. Since Ra multiplies the buoyancy term, any $O(1)$ lateral temperature gradient will cause enormous velocities. One might thus expect the flow to organise itself so that either horizontal temperature gradients are small, or they are confined to thin regions, or both. Since $O(1)$ temperature variations are enforced by the boundary conditions, the latter is more plausible, and thus we have the idea of the *thermal plume*, a localised upwelling of hot fluid which will be instantly familiar to glider pilots and seabirds.

A mathematically intuitive way of inferring the same behaviour follows from the expectation that increasing Ra drives increasing velocities; then large Ra should imply large velocity, and the conduction term in the heat equation $\mathbf{u} \cdot \nabla T = \nabla^2 T$ is correspondingly small. Since the conduction term represents the highest derivative in the equation, its neglect would imply a reduction of order, and correspondingly we would expect *thermal boundary layers* to exist at the boundaries of the convecting cell. This is in fact what we will find: a hot thermal boundary layer adjoins the lower boundary, and a cold one adjoins the upper boundary, and a rapid circulation in the interior of the cell detaches these as upwelling and downwelling plumes. The general structure of the resulting flow is shown in figure 3.7. We analyse this structure in the following sections.

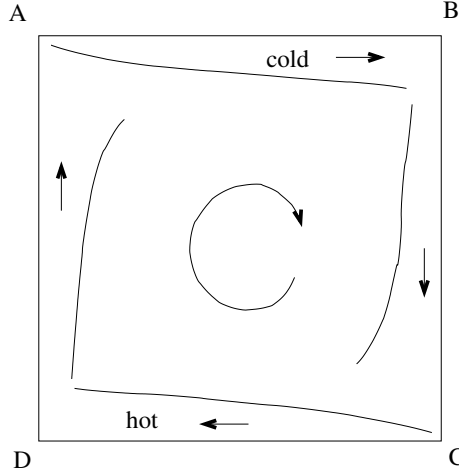


Figure 3.7: Schematic representation of boundary layer convection

3.5.1 Boundary layer theory

We now consider a convection cell in a finite box, as shown in figure 3.7, with (dimensionless) top and bottom boundaries at $z = 0, 1$, and side walls at $x = 0, a$. The Boussinesq equations describing thermal convection are written in the following dimensionless form:

$$\begin{aligned}\nabla \cdot \mathbf{u} &= 0, \\ \frac{1}{Pr} \frac{d\mathbf{u}}{dt} &= -\nabla p + \nabla^2 \mathbf{u} + Ra T \mathbf{k}, \\ \frac{dT}{dt} &= \nabla^2 T,\end{aligned}\tag{3.24}$$

where \mathbf{u} is velocity, p is pressure, T is temperature, and the Rayleigh and Prandtl numbers are defined in (3.4).

By considering only two-dimensional motion in the (x, z) plane, we define the stream function ψ by

$$u = -\psi_z, \quad w = \psi_x;\tag{3.25}$$

the vorticity is then $(0, \omega, 0)$, where $\omega = -\nabla^2 \psi$. Taking the curl of the momentum equation, we derive the set

$$\begin{aligned}\omega &= -\nabla^2 \psi, \\ \frac{dT}{dt} &= T_t + \psi_x T_z - \psi_z T_x = \nabla^2 T, \\ \frac{1}{Pr} \frac{d\omega}{dt} &= -Ra T_x + \nabla^2 \omega,\end{aligned}\tag{3.26}$$

which are supplemented by the boundary conditions

$$\begin{aligned}
\psi, \omega &= 0 \quad \text{on } x = 0, a, z = 0, 1, \\
T &= \frac{1}{2} \quad \text{on } z = 0, \\
T &= -\frac{1}{2} \quad \text{on } z = 1, \\
T_x &= 0 \quad \text{on } x = 0, a;
\end{aligned} \tag{3.27}$$

here a is the aspect ratio, and we have chosen free slip (no stress) conditions at the cell boundaries. Note that we have chosen that we have changed the reference temperature for the scaled temperature from T_0 to $T_0 - \frac{1}{2}\Delta T$; this is purely a matter of convenience, as the resultant symmetry of the thermal boundary conditions is more natural.

Rescaling

The idea is that when $Ra \gg 1$, thermal boundary layers of thickness $\delta \ll 1$ will form at the edges of the flow, and both ψ and ω will be $\gg 1$ in the flow. To scale the equations properly, we rescale the variables as

$$\psi, \omega \sim \frac{1}{\delta^2}, \tag{3.28}$$

and define

$$\delta = Ra^{-1/3}. \tag{3.29}$$

Rescaled, the equations are thus, in the steady state,

$$\begin{aligned}
\omega &= -\nabla^2 \psi, \\
\psi_x T_z - \psi_z T_x &= \delta^2 \nabla^2 T, \\
\nabla^2 \omega &= \frac{1}{\delta} T_x + \frac{1}{Pr \delta^2} \frac{d\omega}{dt}.
\end{aligned} \tag{3.30}$$

In order that the inertia terms be unimportant, we require $Pr \delta^2 \gg 1$, i. e., $Pr \gg Ra^{2/3}$. This assumption is easily satisfied in the Earth's mantle, but is difficult to achieve in the laboratory. Nevertheless, we assume this henceforth.

As in any singular perturbation procedure, we now examine the flow region by region, introducing special rescalings in regions where boundary conditions cannot be satisfied. Before doing so, note that the statement of the flow problem is symmetric, and we will therefore take the solution to be symmetric also.

Core flow

The temperature equation is linear in T , and implies $T = T_0(\psi) + O(\delta^2)$. For a flow with closed streamlines, the Prandtl-Batchelor theorem then implies $T_0 = \text{constant}$

(this follows from the exact integral $\oint_C \frac{\partial T}{\partial n} ds = 0$, where the integral is around a streamline, whence $T'_0(\psi) \oint_C \frac{\partial \psi}{\partial n} ds = 0$); it then follows that T is constant to all (algebraic) orders of δ , and is in fact zero by the symmetry of the flow. Thus

$$\begin{aligned} T &= 0, \\ \nabla^4 \psi &= 0, \end{aligned} \tag{3.31}$$

and clearly the core flow cannot have $\psi = \omega = 0$ at the boundaries, for non-zero ψ . In fact, ω jumps at the side-walls where the plume buoyancy generates a non-zero vorticity. We examine the plumes next.

Plumes

Near $x = 0$, for example, we rescale the variables as

$$x = \delta X, \quad \psi = \delta \Psi, \tag{3.32}$$

so that to leading order, we have

$$\Psi_{XX} \approx 0, \tag{3.33}$$

whence $\Psi \approx w_p(z)X$, and to match to the core flow, we define $w_p = \psi_x|_{x=0}$ as the core velocity at $x = 0$. Also

$$\begin{aligned} \Psi_X T_z - \Psi_z T_X &\approx T_{XX}, \\ \omega_{XX} &\approx T_X, \end{aligned} \tag{3.34}$$

the latter of which integrates to give

$$\omega = \int_0^X T dX, \quad \omega_p = \int_0^\infty T dX, \tag{3.35}$$

where matching requires ω_p to be the core vorticity at $x = 0$. Integration of (3.34)₁ gives

$$\int_0^\infty T d\Psi = C, \tag{3.36}$$

where C is constant, and it follows that the core flow must satisfy the boundary condition $\omega \psi_x = C$ on $x = 0$ (and therefore, by symmetry, $-C$ at $x = a$). In summary, the effective boundary conditions for the core flow are

$$\begin{aligned} \psi &= 0 \quad \text{on} \quad x = 0, a, \quad z = 0, 1, \\ \psi_{zz} &= 0 \quad \text{on} \quad z = 0, 1, \\ \psi_x \psi_{xx} &= -C \quad \text{on} \quad x = 0, \quad \psi_x \psi_{xx} = C \quad \text{on} \quad x = a, \end{aligned} \tag{3.37}$$

and the solution can be found as the *canonical solution*

$$\psi = C^{1/2} \hat{\psi}(x, z), \quad (3.38)$$

where $\hat{\psi}$ must be determined numerically. It thus remains to determine C . This requires consideration of the thermal boundary layers. Thermal boundary layers are necessary at the top and bottom because the core temperature ($T = 0$) does not satisfy the boundary conditions there.

Thermal boundary layers

Near the top surface, for example, we rescale the variables by writing

$$z = 1 - \delta Z, \quad \psi = \delta \Psi, \quad \omega = \delta \Omega, \quad (3.39)$$

to find the leading order rescaled equation for Ψ to be simply

$$\Psi_{ZZ} \approx 0, \quad (3.40)$$

whence $\Psi \sim u_s(x)Z$, and u_s is the core value of the surface velocity $-\psi_z|_{z=1}$. Then $\Omega_{ZZ} \approx T_x$ determines Ω (with $\Omega = 0$ on $Z = 0$, and $\Omega \sim \omega_s(x)Z$ as $Z \rightarrow \infty$, where ω_s is the core value of the surface vorticity), and T satisfies

$$\Psi_Z T_x - \Psi_x T_Z \approx T_{ZZ}. \quad (3.41)$$

In Von Mises coordinates x, Ψ , the equation is

$$T_x \sim \frac{\partial}{\partial \Psi} \left[\Psi_Z \frac{\partial T}{\partial \Psi} \right], \quad (3.42)$$

and putting $\xi = \int_0^x u_s(x) dx$, this is just the diffusion equation

$$T_\xi = T_{\Psi\Psi}, \quad (3.43)$$

with

$$T = -\frac{1}{2} \quad \text{on} \quad \Psi = 0, \quad T \rightarrow 0 \quad \text{as} \quad \Psi \rightarrow \infty. \quad (3.44)$$

Note that the same Von Mises transformation (but from (z, X) to (z, Ψ)) can be used in the plume equation (3.34)₁, which can thus also be written in the diffusion equation form (3.43), where ξ is extended as $\int^z w_p(z) dz$.

A quantity of interest is the Nusselt number, defined as

$$Nu = - \int_0^1 \frac{\partial T}{\partial z}(x, 1) dx, \quad (3.45)$$

and from the above, this can be written as

$$Nu \approx \left[\int_0^\infty -T d\Psi \right]_{x=0}^{x=a} Ra^{1/3}. \quad (3.46)$$

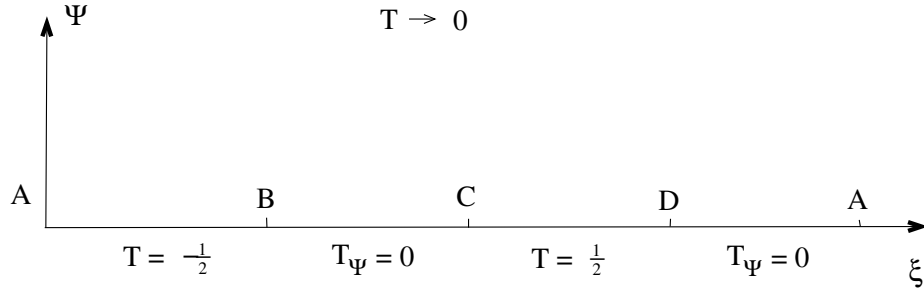


Figure 3.8: Boundary conditions for the thermal boundary layer solution of (3.49).

Corner flow

The core flow has a singularity in each corner, where (if r is distance from the corner), then $\psi \sim r^{3/2}$, $\omega \sim r^{-1/2}$, and (for the corner at $x = 0$, $z = 0$, for example) $x, z \sim r$. There must be a region where this singularity is alleviated by the incorporation of the buoyancy term. This requires $\omega/r^2 \sim 1/\delta r$, whence $r \sim \delta^{2/3}$. Rescaling the variables as indicated ($x, z \sim \delta^{2/3}$, $\psi \sim \delta$, $\omega \sim \delta^{-1/3}$) then gives the temperature equation as

$$\Psi_X T_Z - \Psi_Z T_X \sim \delta \nabla^2 T, \quad (3.47)$$

which shows that (since the ψ scale, δ , is the same as that of the boundary layers adjoining the corner) the boundary layer temperature field is carried through the corner region without change (to leading order). The corner flow thus has $T \approx T(\Psi)$, so that

$$\nabla^4 \Psi + T'(\Psi) \Psi_X = 0, \quad (3.48)$$

with appropriate matching conditions. The main point of this is to show that in solving the thermal boundary layer equations round the perimeter of the box, the transverse profile (in Ψ) can be taken to be continuous when the boundary conditions change at the corners.

Solution strategy

The Von Mises transformation shows that the temperature in the thermal boundary layers and the thermal plumes satisfies the diffusion equation

$$T_\xi = T_{\Psi\Psi}, \quad (3.49)$$

where we define

$$\xi = \int_0^s U(s) ds, \quad (3.50)$$

and we define s to be arc length around the perimeter of the box (starting for example at the point A in figure 3.7, and $U(s)$ is the (core-determined) tangential velocity on the perimeter. The temperature equation must be solved in the four regions

corresponding to the boundary layer at $z = 1$, plume at $x = a$, boundary layer at $z = 0$, and plume at $x = 0$, representing the four edges AB , BC , CD , DA indicated in figure 3.7, with T being continuous at each junction point (corner), and

$$\begin{aligned}
T &\rightarrow 0 \quad \text{as } \Psi \rightarrow \infty, \\
T &= -\frac{1}{2} \quad \text{on } \Psi = 0 \quad [z = 1, \text{ top } AB], \\
T_\Psi &= 0 \quad \text{on } \Psi = 0 \quad [x = a, \text{ right } BC], \\
T &= \frac{1}{2} \quad \text{on } \Psi = 0 \quad [z = 0, \text{ bottom } CD], \\
T_\Psi &= 0 \quad \text{on } \Psi = 0 \quad [x = 0, \text{ left } DA],
\end{aligned} \tag{3.51}$$

as indicated in figure 3.8.

What of the initial condition? The novelty here is that prescription of an initial condition is supplanted by the necessary requirement that the solution be periodic in ξ . Beginning from $x = 0$, $z = 1$, we may denote the values of ξ at the corners as ξ_A ($x = 0$, $z = 1$), ξ_B ($x = a$, $z = 1$), ξ_C ($x = a$, $z = 0$), ξ_D ($x = 0$, $z = 0$). Now from the definition of ξ , we have $\xi_k = C^{1/2}\hat{\xi}_k$, where the values of $\hat{\xi}_k$ are independent of C (because they are determined by the canonical solution in (3.38)). Putting

$$\xi = C^{1/2}\hat{\xi}, \quad \Psi = C^{1/4}\hat{\Psi}, \quad T(\xi, \Psi) = \hat{T}(\hat{\xi}, \hat{\Psi}), \tag{3.52}$$

we see that the problem for $\hat{T}(\hat{\xi}, \hat{\Psi})$ is independent of C .

Just as for the flow in the core, this problem must be solved numerically for $\hat{T}(\hat{\xi}, \hat{\Psi})$. Assuming this is done, then

$$\int_0^\infty T(\xi, \Psi) d\Psi = C^{1/4} \int_0^\infty \hat{T}(\hat{\xi}, \hat{\Psi}) d\hat{\Psi}. \tag{3.53}$$

If, for example, we evaluate both quantities at $\xi = 0$ (i. e., the point A), then it follows from (3.36) that

$$C = \int_0^\infty T(0, \Psi) d\Psi = C^{1/4} \int_0^\infty \hat{T}(0, \hat{\Psi}) d\hat{\Psi}, \tag{3.54}$$

and this determines C as

$$C = \left[\int_0^\infty \hat{T}(0, \hat{\Psi}) d\hat{\Psi} \right]^{4/3}. \tag{3.55}$$

Given this, the Nusselt number is then given from (3.46) as

$$Nu \approx C^{1/4} \left[- \int_0^\infty \hat{T} d\hat{\Psi} \right]_0^{\hat{\xi}_A} Ra^{1/3}. \tag{3.56}$$

No-slip boundary conditions

For no slip boundary conditions, the necessary preliminary rescaling is $\psi \sim 1/\delta^3$, $\omega \sim 1/\delta^3$, where $\delta = Ra^{-1/5}$. Thus the Nusselt number $Nu \sim Ra^{1/5}$. There is no longer parity between the thermal boundary layers and plumes, as the former are slowed down by the no slip conditions. The rescaled equations are

$$\begin{aligned}\omega &= -\nabla^2\psi, \\ \psi_x T_z - \psi_z T_x &= \delta^3 \nabla^2 T, \\ \nabla^2 \omega &= \frac{1}{\delta^2} T_x.\end{aligned}\tag{3.57}$$

The core flow is as before; the thermal boundary layers have $\psi \sim \delta^2$, $\omega \sim 1$, $z \sim \delta$, so that vorticity balances buoyancy), and all three equations are necessary to solve for T ; it is still the case that $\int T d\psi$ is conserved at corners, but now in the plume, $x \sim \delta^{3/2}$, $\psi \sim \delta^{3/2}$, and $T \sim \delta^{1/2}$. The initial plume profile is effectively a delta function, and the plume temperature is just the resultant similarity solution. The remainder of the structure must be computed numerically.

3.6 Double-diffusive convection

Double-diffusive convection refers to the motion which is generated by buoyancy, when the density depends on two diffusible substances or quantities. The simplest examples occur when salt solutions are heated; then the two diffusing quantities are heat and salt. Double-diffusive processes occur in sea water and in lakes, for example. Other simple examples occur in multi-component fluids containing more than one dissolved species; convection in magma chambers is one such.

The guiding principle behind double-diffusive convection is still that light fluid rises, and convection occurs in the normal way (the direct mode) when the steady state is statically unstable (i. e., when the density increases with height), but confounding factors arise when, as normally the case, the two substances diffuse at different rates. Particularly when we are concerned with temperature and salt, the ratio of thermal to solutal diffusivity is large, and in this case different modes of convection occur near the statically neutral buoyancy state: the cells can take the form of long thin ‘fingers’, or the onset of convection can be oscillatory. In practice, fingers are seen, but oscillations are not.

A further variant on Rayleigh-Bénard convection arises in the form of convective layering. This is a long-lived transient form of convection, in which separately convecting layers form, and is associated partly with the high diffusivity ratio, and partly with the usual occurrence of no flux boundary conditions for diffusing chemical species.

We pose a model for double-diffusive convection based on a density which is related linearly to temperature T and salt composition c in the form

$$\rho = \rho_0[1 - \alpha(T - T_0) + \beta(c - c_0)],\tag{3.58}$$

where we take α and β to be positive constants; thus the presence of salt makes the fluid heavier. The equation that then needs to be added to (3.1) is that for convective diffusion of salt:

$$c_t + \mathbf{u} \cdot \nabla c = D \nabla^2 c, \quad (3.59)$$

where D is the solutal diffusion coefficient, assuming a dilute solution. We adopt the same scaling of the variables as before, with the extra choice

$$c - c_0 \sim \Delta c, \quad (3.60)$$

where Δc is a relevant salinity scale (in our stability analysis, it will be the prescribed salinity difference between the lower and upper surfaces of the fluid layer). The Boussinesq form of the scaled equations, based on the assumptions that $\alpha \Delta T \ll 1$ and $\beta \Delta c \ll 1$, are then

$$\begin{aligned} \nabla \cdot \mathbf{u} &= 0, \\ \frac{1}{Pr} [\mathbf{u}_t + (\mathbf{u} \cdot \nabla) \mathbf{u}] &= -\nabla p + \nabla^2 \mathbf{u} + Ra T \hat{\mathbf{k}} - Rs c \hat{\mathbf{k}}, \\ T_t + \mathbf{u} \cdot \nabla T &= \nabla^2 T, \\ c_t + \mathbf{u} \cdot \nabla c &= \frac{1}{Le} \nabla^2 c. \end{aligned} \quad (3.61)$$

The Rayleigh number Ra and the Prandtl number Pr are defined as before, and the solutal Rayleigh number Rs and the Lewis number Le are defined by

$$Rs = \frac{\beta \rho_0 \Delta c g d^3}{\mu \kappa}, \quad Le = \frac{\kappa}{D}. \quad (3.62)$$

Note that in the absence of temperature gradients, the quantity $-Rs Le$ would be the effective Rayleigh number determining convection.

3.6.1 Linear stability

Now we study the linear stability of a steady state maintained by prescribed temperature and salinity differences ΔT and Δc across a stress-free fluid layer. In dimensionless terms, we pose the boundary conditions

$$\begin{aligned} \psi = \nabla^2 \psi = 0 &\quad \text{at } z = 0, 1, \\ T = c = 0 &\quad \text{at } z = 1, \\ T = c = 1 &\quad \text{at } z = 0, \end{aligned} \quad (3.63)$$

where as before, we restrict attention to two dimensions, and adopt a stream function ψ . The steady state is

$$c = 1 - z, \quad T = 1 - z, \quad \psi = 0, \quad (3.64)$$

and we perturb it by writing

$$c = 1 - z + C, \quad T = 1 - z + \theta, \quad (3.65)$$

and then linearising the equations on the basis that $C, \theta, \psi \ll 1$. This leads to

$$\begin{aligned} \frac{1}{Pr} \nabla^2 \psi_t &\approx Ra \theta_x - Rs C_x + \nabla^4 \psi, \\ \theta_t - \psi_x &\approx \nabla^2 \theta, \\ C_t - \psi_x &\approx \frac{1}{Le} \nabla^2 C, \end{aligned} \quad (3.66)$$

with

$$C = \psi = \psi_{zz} = \theta = 0 \quad \text{on} \quad z = 0, 1. \quad (3.67)$$

By inspection, solutions satisfying the temperature and salinity equations are

$$\begin{aligned} \psi &= \exp(ikx + \sigma t) \sin m\pi z, \\ \theta &= \frac{ik}{\sigma + K^2} \exp(ikx + \sigma t) \sin m\pi z, \\ C &= \frac{ik}{\sigma + \frac{K^2}{Le}} \exp(ikx + \sigma t) \sin m\pi z, \end{aligned} \quad (3.68)$$

where we have written

$$K^2 = k^2 + m^2\pi^2. \quad (3.69)$$

Substituting these into the momentum equation leads to the dispersion relation determining σ in terms of k :

$$(\sigma + K^2 Pr)(\sigma + K^2) \left(\sigma + \frac{K^2}{Le} \right) + k^2 Pr \left[\frac{(Rs - Ra)\sigma}{K^2} + Rs - \frac{Ra}{Le} \right] = 0. \quad (3.70)$$

This is a cubic in σ , which can be written in the form

$$\sigma^3 + a\sigma^2 + b\sigma + c = 0, \quad (3.71)$$

where

$$\begin{aligned} a &= K^2 \left(Pr + 1 + \frac{1}{Le} \right), \\ b &= K^4 \left(Pr + \frac{1}{Le} + \frac{Pr}{Le} \right) + \frac{k^2}{K^2} Pr (Rs - Ra), \\ c &= \frac{K^6}{Le} Pr + k^2 Pr \left(Rs - \frac{Ra}{Le} \right). \end{aligned} \quad (3.72)$$

Instability occurs if any one of the three roots of (3.71) has positive real part. Since Le and Pr are properties of the fluid, we take them as fixed, and study the

effect of varying Ra and Rs on the stability boundaries where $\text{Re } \sigma = 0$. Firstly, if $Ra < 0$ and $Rs > 0$, then a , b and c are all positive. We can then show (see question 3.3) that $\text{Re } \sigma < 0$ for all three roots providing $ab > c$, and this is certainly the case if $Le > 1$, which is always true for heat and salt diffusion. Thus when both temperature and salinity fields are stabilising, the state of no motion is linearly stable.

To find regions of instability in the (Rs, Ra) plane, it thus suffices to locate the curves where $\text{Re } \sigma = 0$. There are two possibilities. The first is referred to as exchange of stability, or the direct mode, and occurs when $\sigma = 0$. From (3.71), this is when $c = 0$, or $Rs = \frac{Ra}{Le} - \frac{K^6}{k^2 Le}$. This is a single curve (for each k), and since we know that $\text{Re } \sigma < 0$ in $Ra < 0$ and $Rs > 0$, this immediately tells us that a direct instability occurs if

$$Ra - Le Rs > R_c = \min_k \frac{K^6}{k^2} = \frac{27\pi^4}{4}. \quad (3.73)$$

This direct transition is the counterpart of the onset of Rayleigh-Bénard convection, and shows that $Ra - Le Rs$ is the effective Rayleigh number. This is consistent with the remark just after (3.62).

The other possibility is that there is a Hopf bifurcation, i. e., a pair of complex conjugate values of σ cross the imaginary axis at $\pm i\Omega$, say. The condition for this is $ab = c$, which is again a single curve, and one can show (see question 3.4) that oscillatory instability occurs for

$$Ra > \frac{\left(Pr + \frac{1}{Le}\right) Rs}{1 + Pr} + \frac{\left(1 + \frac{1}{Le}\right) \left(Pr + \frac{1}{Le}\right)}{Pr} R_c. \quad (3.74)$$

Direct instability occurs along the line XZ in figure 3.9, while oscillatory instability occurs at the line XW . Between XW and the continuation XU of XZ , there are two roots with positive real part and one with negative real part. As Ra increases above XW , it is possible that the two complex roots coalesce on the real axis, so that the oscillatory instability is converted to a direct mode. One can show (see question 3.5) that the criterion for this is that $b < 0$ and

$$c = \frac{1}{9} \left[ab + \frac{(a^2 - 6b)}{3} \{-a + (a^2 - 3b)^{1/2}\} \right]. \quad (3.75)$$

For large Rs , this becomes (for $k^2 = \frac{\pi^2}{2}$)

$$Ra \approx Rs + \frac{3R_c^{1/3} Rs^{2/3}}{2^{2/3} Pr^{1/3}}, \quad (3.76)$$

and is shown as the line XW in figure 3.9. Thus the onset of convection is oscillatory only between the lines XW and XV , and beyond (above) XV it is direct. In practice, oscillations are rarely seen.

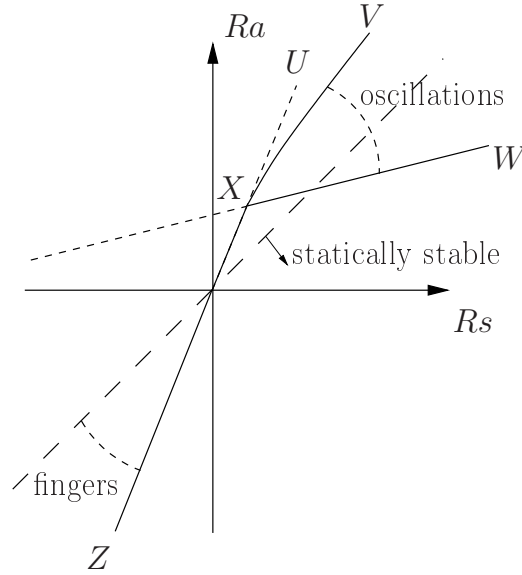


Figure 3.9: Stability diagram for double-diffusive convection.

Fingers

If we return to the cubic in the form (3.70), and consider the behaviour of the roots in the third quadrant as $Ra, Rs \rightarrow -\infty$, it is easy to see that one root is

$$\sigma \approx \frac{K^2 \left[\frac{Ra}{Le} - Rs \right]}{Rs - Ra}, \quad (3.77)$$

while the other two are oscillatorily stable (see question 3.6). Thus this growth rate is positive when $Le Rs < Ra < Rs$ and grows unboundedly with the wave number k (since $K^2 = k^2 + \pi^2$ when $m = 1$). This is an indication of ill-posedness, and in fact we anticipate that σ will become negative at large k . To see when this occurs, inspection of (3.70) shows that the neglected terms in the approximation (3.77) become important when $k \sim |Ra|^{1/4}$, where σ is maximum (of $O|Ra|^{1/2}$), and then $\sigma \sim -O(k^2)$ for larger k .² Thus in the ‘finger’ régime sector indicated in figure 3.9, the most rapidly growing wavelengths are short, and the resulting waveforms are tall and thin. This is what is seen in practice, and the narrow cells are known as fingers. An example is shown in figure 3.10.

3.6.2 Layered convection

The linear stability analysis we have given above is only partially relevant to double diffusive convection. It is helpful in the understanding of the finger régime, but

²In the common case where $Pr, Le > 1$, one finds $\sigma \approx -\frac{k^2}{Le}$.

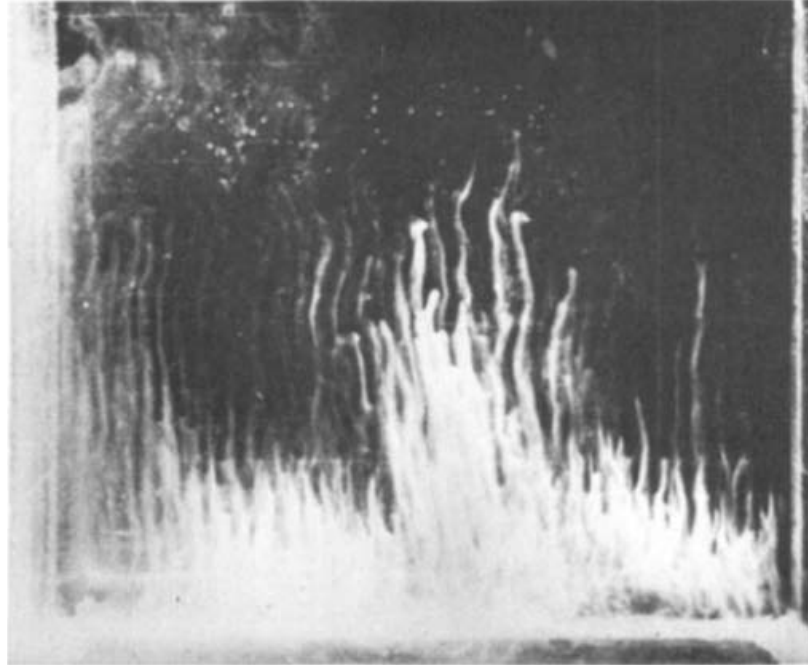


Figure 3.10: Finger convection (Turner 1974).

the oscillatory mode of convection is not particularly relevant. The other principal phenomenon which double diffusive systems exhibit is that of layering. This is a transient, but long-term, phenomenon associated often with the heating of a stable salinity gradient, and arises because in normal circumstances, more appropriate boundary conditions for salt concentration are to suppose that there is no flux at the bounding surfaces.

In pure thermal convection, the heating of an initially stably thermally stratified fluid will lead to the formation of a layer of convecting fluid below the stable region. This (single) convecting layer will grow in thickness until it fills the entire layer. This is essentially the ‘filling box’. Suppose now we have a stable salinity gradient which is heated from below. Again a convecting layer forms, which mixes the temperature and concentration fields so that they are uniform within the layer. At the top of the convecting layer, there will be a step down ΔT in temperature, and a step down Δc in salinity. It is found experimentally that $\alpha\Delta T = \beta\Delta c$, that is, the *boundary layer*³ is neutrally stable. However, the disparity in diffusivities (typically $Le \gg 1$) means that there is a thicker thermal conductive layer ahead of the interface. In effect, the stable salinity gradient above the convecting layer is heated by the layer itself, and a second, and then a third, layer forms. In this way, the entire fluid depth can fill up with a sequence of long-lived, separately convecting layers. The layers will eventually merge and form a single convecting layer over a time scale controlled by the very slow transport of salinity between the convecting layers. Such layers are very suggestive

³For discussion of boundary layers, see section 3.5.1.

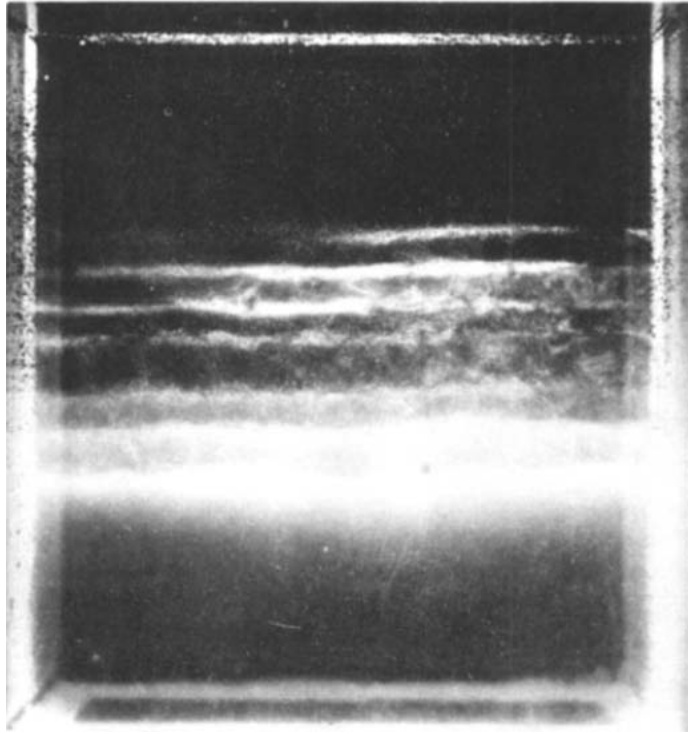


Figure 3.11: Layered convection (Turner 1974). A stable salt solution has been heated from below.

of some of the fossilised layering seen in magma chambers, as for example in figure 3.5, but the association may be a dangerous one. An experimental realisation of this form of layered convection is shown in figure 3.11.

A further example of some of the exotic behaviour which double diffusion can lead to is shown in figure 3.12, again taken from the review article by Turner (1974). In this experiment, the two diffusing substances were sugar and salt, and the fluid was initially set up with a top-heavy gradient of salt (which plays the rôle of temperature here as its diffusivity is larger) and a bottom-heavy gradient of sugar, such that the overall density gradient was statically stable. This is the analogue of cold/fresh above hot/salty, so in the ‘diffusive’ régime of the first quadrant in figure 3.9. The rôle of the Prandtl number is taken by the Schmidt number defined by

$$Sc = \frac{\nu}{D_l}, \quad (3.78)$$

where D_l is the diffusivity of salt and ν is the kinematic viscosity. (The ‘Lewis’ number is the ratio D_l/D_g , where D_g is the diffusivity of sugar. For salt and sugar, $Le \approx 3$.⁴) Now the Schmidt number for salt is around 10^6 , so the ‘Prandtl’ number is large, and the static stability limit in the diffusive régime is essentially the same as the

⁴Specifically, $D_l \approx 1.5 \times 10^{-9} \text{ m}^2 \text{ s}^{-1}$ (Vitagliano and Lyons 1956) and $D_g \approx 0.5 \times 10^{-9} \text{ m}^2 \text{ s}^{-1}$ (Ziegler *et al.* 1987).

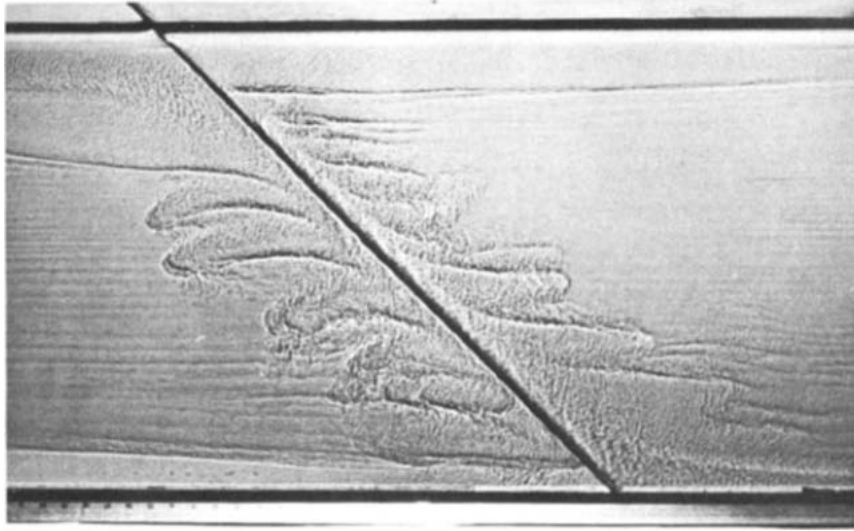


Figure 3.12: Sloping layered convection (Turner 1974).

dynamic stability limit: so nothing should happen. However, if a sloping boundary exists as shown, convection is initiated, and takes the layered form shown. We leave it as an exercise to explain why.

3.7 Turbulence

Many forms of convection involve turbulent flow, namely when the Reynolds number and the Rayleigh number are sufficiently large (i.e. for strong inertia). For example, the hot smoke rising from a flame can often be seen to transition from a smooth laminar regime to a chaotic turbulent regime as it accelerates due to buoyancy. Similarly, plumes arising from heat sources in buildings often transition to turbulence as they rise towards the ceiling, before cooling and recirculating. Hence, in this section we briefly outline some of the fundamentals of turbulent flows as well as common modelling techniques. Much of the following section has been taken from the introduction of (Benham, *DPhil thesis* (2018)). For further reading, see the books by Schlichting (1960), Jimenez (2000) and Pope (2000).

We start by reminding ourselves of the dimensionless Navier-Stokes equations (ignoring buoyancy for the moment), which are

$$\begin{aligned} \nabla \cdot \mathbf{u} &= 0, \\ \frac{\partial \mathbf{u}}{\partial t} + (\mathbf{u} \cdot \nabla) \mathbf{u} &= -\nabla p + \frac{1}{\text{Re}} \nabla^2 \mathbf{u}, \end{aligned} \quad (3.79)$$

where $\text{Re} = \rho U_0 L / \mu$ for some typical velocity and length scales U_0 , L . We consider high Reynolds number flows $\text{Re} \gg 1$ where inertia is important. In particular, for these flows, the non-linear inertial terms on the left hand side of the Navier-Stokes

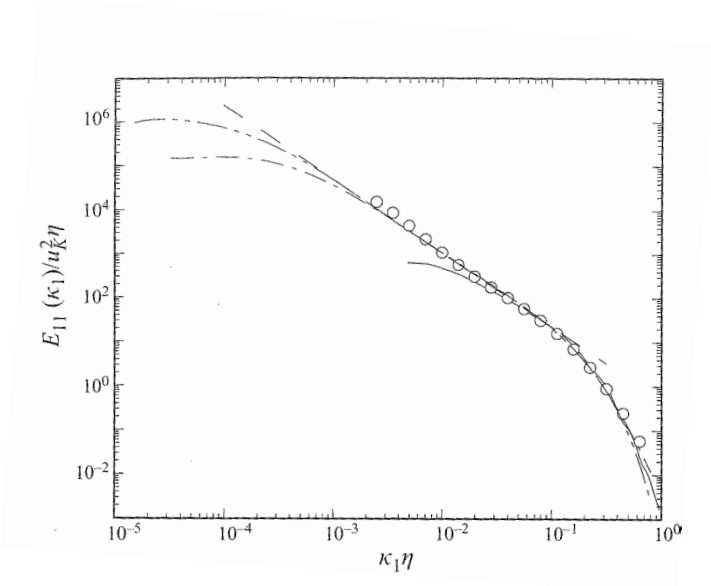


Figure 3.13: Dimensionless energy spectrum (one-dimensional) in terms of dimensionless wavenumber for turbulent flow. This image is taken from (Jimenez (2000)).

equations are responsible for complex flow behaviour, also known as turbulence, which is characteristic of the high Reynolds number regime.

One of the characteristic features of turbulent flows is the mechanism through which energy is transferred between eddies. Although at high Reynolds number viscous terms appear to be negligible (see (3.79)), turbulence is in fact dissipative. It does not, however, dissipate energy at the large scale, like laminar flows. Instead, energy is exchanged in an inviscid way between eddies of diminishing size. Energy is only dissipated (i.e. converted to heat) due to eddies which are so small that viscous effects become important. This critical size is called the Kolmogorov length scale and is given by

$$\eta = \left(\frac{\nu^3}{\varepsilon} \right)^{1/4}, \quad (3.80)$$

where ε is the turbulent energy dissipation and ν is the kinematic viscosity $\nu = \mu/\rho$. When modelling turbulence, it is necessary to account for many different length scales, from the Kolmogorov scale η up to the dominant length scale of the problem L , which can be problematic for computations. The energy spectrum for turbulent flow is shown in figure 3.13, illustrating how energy is transferred from small wavenumbers (large wavelengths) down to large wavenumbers (small wavelengths). This transfer of energy from the large to the small scale, also known as the *energy cascade*, was first described by Kolmogorov (1941). In this famous paper Kolmogorov derived a scaling relationship between the energy of the eddies and their wavenumber $E \propto \kappa^{-5/3}$, showing close agreement with experimental data.

Re	Spatial steps		Time steps	Total	
	2D	3D		2D	3D
10^3	3.2×10^4	5.6×10^6	1.8×10^2	5.6×10^6	1.0×10^9
10^4	1.0×10^6	1.0×10^9	1.0×10^3	1.0×10^9	1.0×10^{12}
10^5	3.2×10^7	1.8×10^{11}	5.6×10^3	1.8×10^{11}	1.0×10^{15}
10^6	1.0×10^9	3.2×10^{13}	3.2×10^4	3.2×10^{13}	1.0×10^{18}

Table 3.1: Minimum number of spatial and time steps for DNS in two and three-dimensional flows at different Reynolds numbers.

In order to solve (3.79) numerically (with suitable boundary conditions), which is known as Direct Numerical Simulation (DNS), the domain is discretised spatially with step size Δx . Let us assume that there are N elements along each dimension of the domain, such that

$$N\Delta x = L. \quad (3.81)$$

Making sure that the smallest eddies are resolved, we must choose $\Delta x \leq \eta$. According to an equilibrium-based scaling law, the energy dissipation obeys the self-similar relationship (i.e. across scales)

$$\varepsilon \approx \frac{u_L^3}{L} \approx \frac{\tilde{u}^3}{\eta}, \quad (3.82)$$

where u_L , \tilde{u} are the velocity scales associated with the largest and smallest (Kolmogorov) eddies. Therefore, if we redefine the Reynolds number in terms of u_L , the Kolmogorov length scale is written in dimensionless form as $\eta/L = \text{Re}^{-3/4}$. Hence, the number of spatial steps must be

$$N \geq \text{Re}^{3/4}. \quad (3.83)$$

Therefore, the number of steps for a two dimensional domain scales like $N^2 \sim \text{Re}^{3/2}$, and like $N^3 \sim \text{Re}^{9/4}$ for a three-dimensional domain. To make things worse, we must also consider the number of discretisation points in time. Since memory storage requirements (due to spatial discretisation) are very large at high Reynolds numbers, integration of the solution in time is usually performed using an explicit method. For explicit methods with time step Δt , the Courant-Friedrichs-Lewy (CFL) condition

$$\frac{u_L \Delta t}{\Delta x} < 1, \quad (3.84)$$

must hold in order to achieve stability. If we take $\tau = L/u_L$ as the timescale of interest for the flow, then the number of time steps N_t is given by

$$N_t \Delta t = \frac{L}{u_L}. \quad (3.85)$$

Hence, the CFL condition (3.84) implies

$$N_t \geq \text{Re}^{3/4}. \quad (3.86)$$

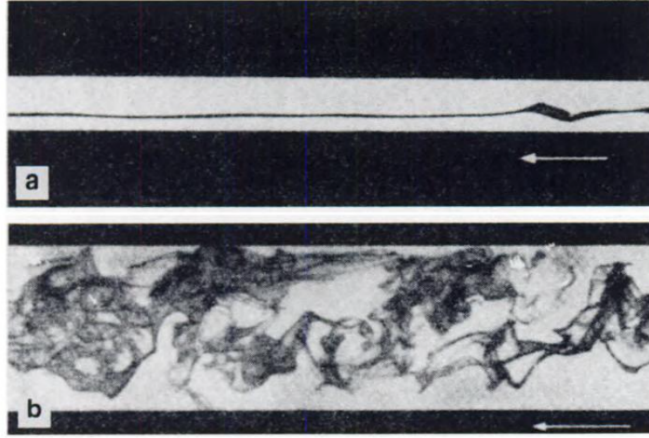


Figure 3.14: Illustration of the difference between laminar flow (a) at Reynolds number $Re = 1150$ and turbulent flow (b) at Reynolds number $Re = 2520$. This image is taken from Dubs (1939), which describes the coloured filament experiments of Reynolds (1883).

In Table 3.1 we display the minimum number of spatial and time steps necessary to perform DNS at Reynolds numbers between $Re = 10^3$ and $Re = 10^6$. It is clear that DNS becomes incredibly computationally intensive at even moderately high Reynolds numbers for both two and three-dimensional problems, though three-dimensional problems are much worse. For example, if we cap the number of degrees of freedom at 10^{10} , which is still a very computationally demanding procedure, then $Re > 2.8 \times 10^4$ becomes intractable for two-dimensional flows and $Re > 2.2 \times 10^3$ for three-dimensional flows.

Reynolds exhibited the disruptive and chaotic qualities of turbulence in 1883 with a coloured dye experiment (see Figure 3.14). He concluded that it would be almost impossible to model flow characteristics exactly and introduced the idea of averaging the Navier-Stokes equations over time. Such approaches are known as Reynolds-averaged Navier-Stokes (RANS) modelling. Let us define the time-averaging of a function f as

$$\bar{f} = \lim_{T \rightarrow \infty} \frac{1}{T} \int_0^T f(t) dt. \quad (3.87)$$

We split all variables into a time-dependant part, which corresponds to turbulent fluctuations, and a time-averaged part, such that

$$\begin{aligned} u_i &= U_i(x, y, z) + u'_i(x, y, z, t), \quad i = 1, 2, 3, \\ p &= P(x, y, z) + p'(x, y, z, t), \end{aligned} \quad (3.88)$$

where subscripts 1, 2, 3 correspond to coordinate directions x, y, z . We define the

fluctuating parts to have zero mean, such that

$$\begin{aligned}\overline{u'_i} &= 0, \quad i = 1, 2, 3, \\ \overline{p'_i} &= 0.\end{aligned}\tag{3.89}$$

This decomposition into mean and fluctuating parts is known as the Reynolds decomposition.

By inserting (3.88) into the continuity equation and averaging, we see that this equation is preserved for both the mean and fluctuating parts of the velocity

$$\begin{aligned}\frac{\partial U_i}{\partial x_i} &= 0, \\ \frac{\partial u'_i}{\partial x_i} &= 0,\end{aligned}\tag{3.90}$$

where we sum over the indices using Einstein notation. Similarly, by inserting (3.88) into the dimensional momentum equation and averaging, we get

$$\rho U_j \frac{\partial U_i}{\partial x_j} = -\frac{\partial P}{\partial x_i} + \mu \frac{\partial^2 U_i}{\partial x_j \partial x_j} - \overline{\rho u'_j \frac{\partial u'_i}{\partial x_j}},\tag{3.91}$$

where the final term on the right hand side is an inertial term due to the turbulent fluctuations. We keep it on the right hand side, together with the viscous stress term, because it represents a stress contribution due to the turbulent fluctuations. Hence, it is known as the Reynolds stress term. It should be noted that

$$\overline{\rho u'_j \frac{\partial u'_i}{\partial x_j}} = \frac{\partial}{\partial x_j} [\overline{\rho u'_i u'_j}],\tag{3.92}$$

due to (3.90). The Reynolds stress is typically written in terms of an ‘eddy viscosity’ μ_t and gradients in the mean velocity, such that

$$-\overline{\rho u'_i u'_j} = \mu_t \left[\frac{\partial U_i}{\partial x_j} + \frac{\partial U_j}{\partial x_i} \right].\tag{3.93}$$

Considering (3.93), the momentum equation (3.91) can be rewritten as

$$\rho U_j \frac{\partial U_i}{\partial x_j} = -\frac{\partial P}{\partial x_i} + \frac{\partial}{\partial x_j} \left((\mu + \mu_t) \left(\frac{\partial U_i}{\partial x_j} + \frac{\partial U_j}{\partial x_i} \right) \right).\tag{3.94}$$

The eddy viscosity plays an important role in turbulence modelling. Whilst in laminar flows, viscous stresses are responsible for the diffusion of momentum, in turbulent flows, it is the eddies and the turbulent fluctuations which are responsible. Therefore, we represent the Reynolds stress as a diffusive term on the right hand side of (3.94), where the diffusion coefficient is the non-linear eddy viscosity.

Equations (3.90a) and (3.94) together are by no means complete. The non-uniqueness of the Reynolds decomposition results in a so-called ‘closure problem’,

where we are left with too few equations for too many unknowns. Some approaches involve finding higher *moments* of the governing equations. For example, the turbulent kinetic energy is defined as

$$k = \frac{1}{2} \overline{u'_i u'_i}, \quad (3.95)$$

for which a governing equation can be derived by multiplying the Navier-Stokes equations by u'_i and averaging. However, since new variables are introduced, the system remains unclosed, requiring higher and higher moments (an unending process). Typically, turbulence models make an empirical hypothesis for μ_t (and/or k) to close the system. In the next section we discuss one such turbulence closure assumption.

3.7.1 Prandtl mixing length theory

There are a vast number of different turbulence closure models that have been proposed in the literature. These models are largely classified into three different types. The most basic type, known as algebraic models, do not model the turbulent kinetic energy k , but instead use an eddy viscosity μ_t , which is a function of the mean velocity U_i and its gradients alone. In these models, (3.90a) and (3.94) form a complete system of equations. Next we summarise the assumptions of one of these models, known as Prandtl mixing length theory.

In the early 20th century Ludwig Prandtl suggested a very simple algebraic model for the eddy viscosity which is based on simple scaling laws (Prandtl (1925)). Prandtl mixing length theory states that the kinematic eddy viscosity $\nu_T = \mu_t/\rho$ is proportional to a velocity scale via a mixing length ℓ , such that

$$\nu_T = \ell U_0, \quad (3.96)$$

where in simple shear flows the velocity scale is locally determined by the mean velocity gradient

$$U_0 = \ell \left| \frac{\partial U}{\partial y} \right|. \quad (3.97)$$

Therefore, the eddy viscosity is written as

$$\nu_T = \ell^2 \left| \frac{\partial U}{\partial y} \right|. \quad (3.98)$$

The mixing length ℓ can be interpreted as the approximate distance it takes for a parcel of fluid to move before it becomes blended into its surroundings due to turbulent mixing. The mixing length is considered as a variable and it is modelled differently depending on the problem. For example, in wall bounded flows the mixing length may be taken as the distance to the wall. For flow in a mixing layer, the mixing length may be taken as proportional to the width of the mixing layer.

This model provides a good approximation for simple turbulent flows, such as a boundary layer on a flat plate, or a free mixing layer, though may be less accurate for more complicated turbulent flows. Nevertheless, it is one of the few turbulence models which yields simple and useful analytical results. Later we use Prandtl mixing length theory to derive a model for the growth of a turbulent mixing layer.

3.7.2 Turbulent boundary layer equations

Next we discuss the boundary layer approximation to the RANS equations (3.90a) and (3.94), restricting our attention to two-dimensional flows. We scale the variables according to

$$x \sim L, \quad y \sim L\text{Re}^{-1/2}, \quad U \sim U_0, \quad V \sim U_0\text{Re}^{-1/2}, \quad P \sim \rho U_0^2. \quad (3.99)$$

Therefore, to leading order the two-dimensional turbulent boundary layer equations (reverting the variables back to lower case for convenience) are

$$\begin{aligned} \frac{\partial u}{\partial x} + \frac{\partial v}{\partial y} &= 0, \\ u \frac{\partial u}{\partial x} + v \frac{\partial u}{\partial y} &= -\frac{1}{\rho} \frac{\partial p}{\partial x} + \frac{\partial}{\partial y} \left((\nu + \nu_T) \frac{\partial u}{\partial y} \right), \\ 0 &= -\frac{\partial p}{\partial y}. \end{aligned} \quad (3.100)$$

For axisymmetric flows, we follow the above steps, except starting with the Navier-Stokes equations in cylindrical coordinates (r, θ, z) . The corresponding time-averaged velocities are (U_r, U_θ, W) . Since the flow is axisymmetric, we ignore all derivatives in θ and we assume zero swirl ($U_\theta = 0$). The corresponding scalings for the variables are

$$z \sim L, \quad r \sim L\text{Re}^{-1/2}, \quad U_r \sim U_0\text{Re}^{-1/2}, \quad W \sim U_0, \quad P \sim \rho U_0^2. \quad (3.101)$$

Therefore, in dimensional form and reverting the variables back to lower case for convenience, the cylindrical turbulent boundary layer equations are

$$\begin{aligned} \frac{1}{r} \frac{\partial}{\partial r} (ru_r) + \frac{\partial w}{\partial z} &= 0, \\ 0 &= -\frac{1}{\rho} \frac{\partial p}{\partial r}, \\ u_r \frac{\partial w}{\partial r} + w \frac{\partial w}{\partial z} &= -\frac{1}{\rho} \frac{\partial p}{\partial z} + \frac{1}{r} \frac{\partial}{\partial r} \left((\nu + \nu_T) r \frac{\partial w}{\partial r} \right). \end{aligned} \quad (3.102)$$

3.7.3 A mixing layer model for unconfined parallel flows

Mixing layers, where two parallel flows undergo turbulent mixing, are a common feature in convection. For laterally unconfined flows, mixing layers can be described using a simple analytical model, which is derived from the turbulent boundary layer equations and Prandtl mixing length theory. In this section we derive this simple model in the absence of buoyancy (i.e. where the flow is momentum-driven rather than density-driven). However, the components of this model will be used later in Section 3.8 when considering convective plumes.

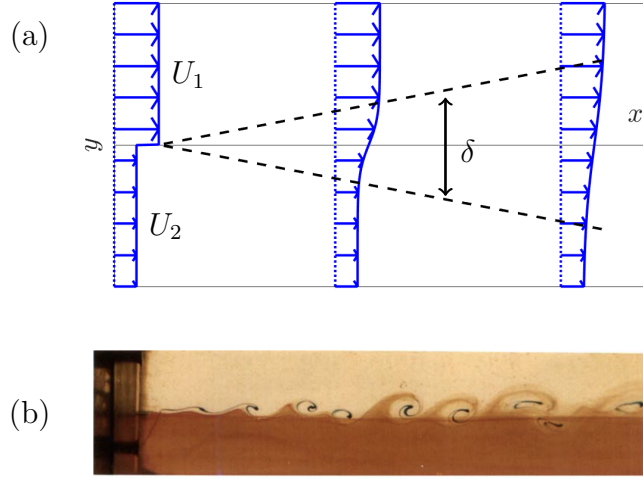


Figure 3.15: (a) Schematic diagram of a mixing layer between parallel flows. (b) Kelvin-Helmholtz vortices in a mixing layer experiment (taken from Lasheras and Choi (1988)).

The flow situation we consider is illustrated in Figure 3.15, in which we illustrate our chosen coordinate system (x, y) . A flow with velocity U_1 in the x direction meets a second, parallel flow with velocity $U_2 < U_1$. Due to the Kelvin-Helmholtz instability, the flow profile is unstable to perturbations. The discontinuous jump in velocity between U_2 and U_1 generates a vortex sheet which rolls up downstream into discrete vortical structures. These structures pair and merge forming larger vortical structures. In this way a region of flow forms between the parallel flows which undergoes intense mixing, and which grows downstream, entraining fluid from either side. The time-averaged velocity in the layer is a smoothed quasi-linear profile which increases from U_2 to U_1 over an approximate width $\delta(x)$. The layer is known as a *mixing layer* due to the intense mixing.

The mixing layer region is long and thin, such that the two-dimensional boundary layer approximation applies (3.100). However, since the flow is unconfined it is expected that pressure gradients in the x direction are negligible. Furthermore, we ignore the viscous stress term in (3.100) since we expect $\nu \ll \nu_T$ within the mixing layer. Therefore, the governing equations, defined for $0 \leq x < \infty$ and $-\infty < y < \infty$, are

$$\begin{aligned} \frac{\partial u}{\partial x} + \frac{\partial v}{\partial y} &= 0, \\ u \frac{\partial u}{\partial x} + v \frac{\partial u}{\partial y} &= \frac{\partial}{\partial y} \left(\nu_T \frac{\partial u}{\partial y} \right). \end{aligned} \quad (3.103)$$

The boundary conditions for the streamwise velocity u correspond to matching with

the free stream velocities

$$\begin{aligned} u(x, \infty) &= U_1, \\ u(x, -\infty) &= U_2, \end{aligned} \quad (3.104)$$

and the inflow condition

$$u(0, y) = U_c + \frac{\Delta U}{2} \operatorname{sgn}(y), \quad (3.105)$$

where $U_c = (U_1 + U_2)/2$ is the average velocity and $\Delta U = U_1 - U_2$ is the velocity difference. We also need a boundary condition for v , but we leave this for later discussion.

We rewrite the velocity u in terms of a similarity variable $\zeta = y/\delta(x)$ that depends on the width of the mixing layer, such that

$$u = U_c + \Delta U \frac{d\mathcal{U}}{d\zeta}, \quad (3.106)$$

where $\mathcal{U} = \mathcal{U}(\zeta)$ is an unknown function. From (3.103) the transverse velocity v must take the form

$$v = \Delta U \frac{d\delta}{dx} \left(\zeta \frac{d\mathcal{U}}{d\zeta} - \mathcal{U} \right). \quad (3.107)$$

We use the Prandtl mixing length model (3.98) for the eddy viscosity, where we approximate the velocity gradient by

$$\left| \frac{\partial u}{\partial y} \right| \approx \frac{\Delta U}{\delta}, \quad (3.108)$$

and we use a mixing length proportional to the width of the mixing layer $\ell = C\delta$, such that

$$\nu_T = C^2 \delta \Delta U. \quad (3.109)$$

Inserting (3.106), (3.107) and (3.109) into the momentum equation (3.103), we get

$$\frac{d\delta}{dx} \frac{U_c}{\Delta U} \left(\frac{\Delta U}{U_c} \mathcal{U} + \zeta \right) \frac{d^2 \mathcal{U}}{d\zeta^2} + C^2 \frac{d^3 \mathcal{U}}{d\zeta^3} = 0. \quad (3.110)$$

Similarity solutions to (3.110) are only possible if

$$\frac{d\delta}{dx} \frac{U_c}{\Delta U} = S, \quad (3.111)$$

where S is a constant known as the spreading parameter, and whose value has been determined by experiments, finding $S = 0.06 - 0.11$. Equation (3.111) is often written in terms of the free stream velocities U_1 and U_2 , such that

$$\frac{d\delta}{dx} = 2S \frac{U_1 - U_2}{U_1 + U_2}. \quad (3.112)$$

The mixing layer growth rate (3.112) increases with velocity difference, indicating that more non-uniform mixing layers entrain fluid faster.

We simplify (3.110) by introducing rescaled variables

$$\xi = \frac{\sqrt{S}}{C}\zeta, \quad F(\xi) = \frac{\Delta U \sqrt{S}}{U_c C} \mathcal{U} \left(\frac{C\xi}{\sqrt{S}} \right). \quad (3.113)$$

In terms of these new variables (3.110) becomes

$$(\xi + F) \frac{d^2 F}{d\xi^2} + \frac{d^3 F}{d\xi^3} = 0, \quad (3.114)$$

and the boundary condition (3.104) becomes

$$\frac{dF}{d\xi}(\pm\infty) = \pm\gamma, \quad (3.115)$$

where $\gamma = (U_1 - U_2)/(U_1 + U_2)$.

In the case of a weak mixing layer $\gamma \ll 1$, we rescale $F \sim \gamma$ and the governing equations and boundary conditions simplify to

$$\begin{aligned} \xi \frac{d^2 F}{d\xi^2} + \frac{d^3 F}{d\xi^3} &= 0, \\ \frac{dF}{d\xi}(\pm\infty) &= \pm 1. \end{aligned} \quad (3.116)$$

This system can be solved explicitly, such that

$$\begin{aligned} \frac{dF}{d\xi} &= \operatorname{erf}(\xi/\sqrt{2}), \\ F &= \sqrt{2/\pi} e^{-\xi^2/2} + \xi \operatorname{erf}(\xi/\sqrt{2}) + D, \end{aligned} \quad (3.117)$$

where D is a constant of integration. This is determined by considering the transverse velocity

$$\lim_{\xi \rightarrow \infty} \left(\xi \frac{dF}{d\xi} - F \right) = -D = \lim_{\xi \rightarrow -\infty} \left(\xi \frac{dF}{d\xi} - F \right). \quad (3.118)$$

Hence, we set $D = 0$ to avoid a net mean transverse flow (which is unphysical).

In the case where γ is not small, the transverse boundary condition requires more careful attention. Schlichting (1960) suggested the boundary condition

$$v(x, \infty) = -\frac{U_2}{U_1} v(x, -\infty), \quad (3.119)$$

which is based on a global momentum balance. The condition (3.119) indicates that there is greater entrainment from the slower stream than the faster stream. Hence the dividing streamline, along which $v = 0$, is inclined downwards from the x -axis.

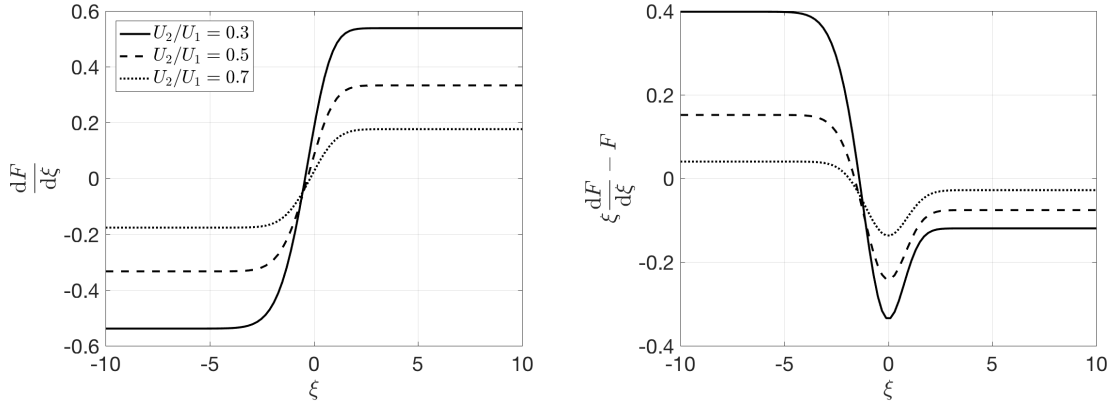


Figure 3.16: Solution to (3.114) for different values of U_2/U_1 . (a) Streamwise velocity (3.106) (rescaled). (b) Transverse velocity (3.107) (rescaled).

This is in accordance with experimental observations. In dimensionless terms, this takes the form

$$\lim_{\xi \rightarrow \infty} \left(\xi \frac{dF}{d\xi} - F \right) = - \left(\frac{U_2}{U_1} \right) \lim_{\xi \rightarrow -\infty} \left(\xi \frac{dF}{d\xi} - F \right). \quad (3.120)$$

Given a value for U_2/U_1 , or equivalently γ , we can solve Equation (3.114), with boundary conditions (3.115) & (3.120), for the function $F(\xi)$. In Figure 3.16 the numerical solution is plotted using three different values of $U_2/U_1 = 0.3, 0.5, 0.7$ (corresponding to $\gamma = 1.08, 0.67, 0.35$).

We can see that the streamwise velocity (a) within the mixing layer is approximately linear. The transverse velocity (b) indicates that there is greater entrainment when the velocity difference is larger, which is consistent with (3.112). However, entrainment is always greater (in magnitude) at the slower stream.

3.8 Parameterised convection

The boundary layer theory described in section 3.5 applies to steady state solutions at high Rayleigh number, but in fact real convection becomes time-varying at such parameter values. The behaviour becomes first oscillatory, and then becomes increasingly irregular, so that at very high Rayleigh numbers, the cellular structure of convection in a fluid layer breaks down. The upwelling and downwelling plumes of the boundary layer theory still exist, but their detachment is sporadic and irregular. In these circumstances, the theoretical description of convection may become, paradoxically, easier. Just as for turbulent shear flows at high Reynolds numbers, one uses empirically-based measures of the fluxes at boundaries to describe the flow. Turbulence mixes the fluid, so that, as in the boundary layer theory, the interior of a convecting cell is taken to be isothermal. In this section, we describe one particular



Figure 3.17: On the left, a sub-oceanic black smoker issuing from a vent at the ocean floor; image from <http://oceanexplorer.noaa.gov>. On the right, a laboratory plume; image courtesy of Andy Woods.

example of turbulent convection to illustrate these ideas. The example is that of the turbulent convective plume.

3.8.1 Plumes

A plume is an isolated convective upwelling. Examples are the rise of smoke from an industrial chimney, the formation of cumulus clouds over oceans, ‘black smokers’ at mid-ocean rise vents, and explosive volcanic eruptions. In these examples, a source of buoyancy at (essentially) a point drives a convective flow in the fluid above. As suggested in figure 3.17, the plume forms a turbulent, approximately conical region, with a fairly sharp (but time-varying) boundary. The turbulence causes rapid convective mixing, and allows us to conceptualise the plume as a relatively homogeneous cloud of density $\rho = \rho_0 - \Delta\rho$ rising through an ambient medium of density ρ_0 . If ρ_0 depends on height z , then the medium is called a stratified medium, and it is stably stratified if $\rho'_0(z) < 0$.

Mathematical model

The simplest mathematical model is of a steady⁵ cylindrically symmetric plume of radius $r = b(z)$, in which we use cylindrical coordinates (r, z) , with corresponding velocity components (u, w) (thus the upwards fluid velocity is w). The plume rises through a medium of density $\rho_0(z)$. We will make the Boussinesq approximation, which is that variations in density are neglected, except in the buoyancy term of the momentum equation, and in the ‘buoyancy’ equation itself. This requires variations of the density from that of the ambient density to be small, and also that the variation of ρ_0 with height (if any) is small. We also make the assumption that the plume has a long and thin aspect ratio, such that the boundary layer approximation (3.102) applies. The basic model is then given by

$$\begin{aligned} \frac{1}{r}(ru)_r + w_z &= 0, \\ 0 &= -\frac{1}{\rho_0}p_r, \\ uw_r + ww_z &= -\frac{1}{\rho_0}p_z - \frac{\rho}{\rho_0}g + \frac{1}{r}\frac{\partial}{\partial r}\left[\nu_T r \frac{\partial w}{\partial r}\right], \\ u\rho_r + w\rho_z &= +\frac{1}{r}\frac{\partial}{\partial r}\left[\nu_T r \frac{\partial \rho}{\partial r}\right]. \end{aligned} \tag{3.121}$$

These equations represent respectively conservation of mass, momentum (horizontal and vertical), and buoyancy; p is the pressure, ρ the density, ρ_0 the reference density, and g is the acceleration due to gravity. We have included radial diffusion terms which represent the effects of turbulent mixing. We define the density deficit $\Delta\rho$ in the plume to be

$$\Delta\rho = \rho_0 - \rho. \tag{3.122}$$

The Boussinesq approximation is based on the assumption that $\Delta\rho$ is small, $\Delta\rho \ll \rho_0$.

The rather odd-looking final equation in (3.121) requires some comment. It caters for the fact that the density deficit in plumes may arise because of temperature, dissolved concentrations or particulate load, or a combination. But in all such cases, the turbulent conservation field for the relevant variable is simply that advection is zero; for example we would have $T_t + \mathbf{u} \cdot \nabla T = \nabla \cdot [\nu_T \nabla T]$ for temperature, and similarly for particulate or solute concentrations. Thus the buoyancy conservation equation simply represents this fact, together with the assumption that the density is an algebraic function of the conserved quantities. In certain circumstance, the veracity of this assumption may need to be examined further. For example, in a volcanic ash-laden plume, the eruption column has a density which is dependent on both temperature and ash concentration, and it rises through a surrounding stratified atmosphere whose stratification is itself determined by the relation of density to temperature and pressure. In such circumstance, (3.121)₄ may warrant further consideration, but such issues will be ignored here.

⁵The turbulent time variation is averaged out.

The boundary layer approximation implies that radial pressure gradients are negligible, and hence that the pressure is that of the surrounding ambient fluid,

$$p_z \approx -\rho_0 g. \quad (3.123)$$

This allows us to write the remaining three equations in terms of the *reduced gravity*, which is defined to be

$$g' = \frac{g\Delta\rho}{\rho_0}. \quad (3.124)$$

The equations (3.121) then take the simple form

$$\begin{aligned} (ru)_r + rw_z &= 0, \\ uw_r + ww_z &= g' + \frac{1}{r} \frac{\partial}{\partial r} \left[\nu_T r \frac{\partial w}{\partial r} \right], \\ N^2 w + ug'_r + wg'_z &= \frac{1}{r} \frac{\partial}{\partial r} \left[\nu_T r \frac{\partial g'}{\partial r} \right], \end{aligned} \quad (3.125)$$

where N is the Brunt-Väisälä frequency, defined as

$$N = \left(-\frac{g\rho'_0}{\rho_0} \right)^{1/2}, \quad (3.126)$$

and we have put a pre-factor of $1 - \frac{\Delta\rho}{\rho_0}$ equal to one in the N^2 term.

It is fairly evident in figure 3.17 that the plume has a fairly well-defined edge, and we will assume this. The boundary of the plume is taken to be at $r = b(z)$. The question then arises as to what, if any, boundary conditions should be applied there. Since the ambient fluid outside the plume has $w = g' = 0$, these are natural conditions to apply, at least when the diffusion terms are included. We therefore pose the conditions

$$w = g' = 0 \quad \text{at} \quad r = b(z). \quad (3.127)$$

One might suppose that also $u = 0$ would be appropriate, but in fact this is found not to be the case. The turbulent eddies of the plume incorporate the ambient fluid, and dramatically increase the plume volume flux. If the entrainment velocity (inwards) at the edge of the plume is u_e , then we have that

$$u = -u_e \quad \text{at} \quad r = b. \quad (3.128)$$

The entrainment velocity needs to be constituted, and a common assumption is to suppose that

$$u_e = \alpha \bar{w}, \quad (3.129)$$

where \bar{w} is the cross-sectionally averaged vertical velocity, and the value of α is found experimentally to be approximately 0.1. We note that the plume boundary $r = b(z)$ is indeterminate, so that an extra condition to determine it is apparently necessary. If $b = \infty$, this issue does not arise.

The case $\nu_T = 0$

We now ignore the radial diffusion terms in (3.125) by putting $\nu_T = 0$. The resulting equations are given by

$$\begin{aligned}(ru)_r + rw_z &= 0, \\ ww_r + ww_z &= g', \\ ug'_r + wg'_z &= -N^2w,\end{aligned}\tag{3.130}$$

and are hyperbolic, and suitable boundary conditions to consider are (3.127) and (3.128) at the plume boundary; in addition, for a plume emanating from a vent of radius a at $z = 0$, we might pose

$$w = w_0, \quad u = 0, \quad g' = g'_0 \quad \text{at} \quad z = 0, \quad 0 < r < a.\tag{3.131}$$

Whether all these conditions can be applied depends on the characteristic directions of the hyperbolic set (3.130). This is examined in question 3.8. If we define the Stokes stream function by $ru = \psi_z$, $rw = -\psi_r$, then the characteristics are just the streamlines, and follow the direction of flow. Therefore the characteristics point inwards from all parts of the boundary, and all the boundary conditions can be applied.

Without writing an analytical solution for the flow, what happens is fairly clear (we assume positive vent buoyancy, $g'_0 > 0$). On the streamlines from the vent which form the central part of the plume, $g' \equiv g'_0$, and w increases upwards, thus the vent streamlines shrink radially. Equally, the prescription of $g' = 0$ on the plume boundary $r = b$ ensures that $g' = w = 0$ on all characteristics that begin there, so that $g' = 0$ everywhere outside the vent characteristics; the characteristics are horizontal. In fact, there is no reason to define the plume outside the central core, since there is no buoyancy there.

It is fairly clear what the matter is: the diffusion terms in (3.125) can not be ignored. Their effect is precisely to broaden the spike of buoyancy which emerges from the vent. We can go further. A typical prescription for the eddy viscosity is to take (in the present situation)

$$\nu_T = \varepsilon_T bw,\tag{3.132}$$

where ε_T is relatively small, perhaps $\sim 10^{-2}$. The point is that with this assumption, the eddy viscosity tends to zero at the plume edge, which suggests as with other examples of such degenerate diffusion that no extra condition is necessary to determine it (and that its location is at a finite distance).

Moment equations

In order to progress with the solution of the equations (3.125), we integrate them from the centre to the edge of the plume, the second and third after multiplying by

r . With our assumption that $\nu_T = 0$ when $w = 0$, the two diffusion integrals vanish, and we are left with three evolution equations for the three quantities

$$\begin{aligned} Q &= 2\pi \int_0^b r w \, dr, \\ M &= 2\pi \int_0^b r w^2 \, dr, \\ B &= 2\pi \int_0^b r w g' \, dr, \end{aligned} \tag{3.133}$$

which are the volume flux, the momentum flux and the buoyancy flux, respectively. Bearing in mind that $w = g' = 0$ at $r = b$, we find, noting also (3.128) and (3.129),

$$\begin{aligned} \frac{dQ}{dz} &= 2\pi\alpha b \bar{w}, \\ \frac{dM}{dz} &= 2\pi \int_0^b r g' \, dr, \\ \frac{dB}{dz} &= -N^2 Q. \end{aligned} \tag{3.134}$$

We note also that

$$Q = \pi b^2 \bar{w}, \tag{3.135}$$

so that these are almost self-contained. In order to proceed, some further simplifications must be made. We consider first the case of an unstratified environment.

Unstratified environment

In the case that the ambient fluid is unstratified, the Brunt-Väisälä frequency N is zero, and the buoyancy flux B is constant. In practice it is sufficient to consider the release of buoyant material from a point source, as this effectively is the common situation of interest. If in addition we suppose that the volume flux (and hence also the momentum flux) is zero at the source, then there is no intrinsic length scale in the problem, and a similarity solution is suggested. Indeed, the only dimensional quantities in the problem are the buoyancy flux B with units of $\text{m}^4 \text{s}^{-3}$ and the lengths r and z . So the similarity variable must be

$$\eta = \frac{r}{z}, \tag{3.136}$$

and the solution must have the form, by dimensional reasoning,

$$b = \beta z, \quad w = B^{1/3} z^{-1/3} W(\eta), \quad g' = B^{2/3} z^{-5/3} G(\eta), \tag{3.137}$$

with u being determined by quadrature. It seems that these expressions fit well to experiments, with the functions W and G being approximately Gaussians.

The question then arises, can we actually find the functions W and G by solving the model (3.125)? As we might expect, the equations without the diffusion terms admit a similarity form of solution, although as discussed above this is of little use. What is (perhaps) surprising is that the equations (3.125) *including* the diffusion terms, have a similarity solution of the form

$$w = z^\nu W(\eta), \quad u = z^\nu U(\eta), \quad g' = z^{2\nu-1} G(\eta), \quad \eta = \frac{r}{z}, \quad b = \beta z, \quad \nu = -\frac{1}{3}, \quad (3.138)$$

providing we choose the eddy viscosity to be given by (3.132), and then U , W and G satisfy the equations

$$\begin{aligned} (\eta U)' + \eta(\nu W - \eta W') &= 0, \\ UW' + W(\nu W - \eta W') &= G + \frac{\varepsilon_T \beta}{\eta} (\eta W W')', \\ UG' + W\{(2\nu - 1)G - \eta G'\} &= \frac{\varepsilon_T \beta}{\eta} (\eta W G')', \end{aligned} \quad (3.139)$$

with such boundary conditions as we can muster:

$$W = G = 0, \quad U = -\frac{2\alpha}{\beta^2} \int_0^\beta \eta W d\eta \quad \text{at} \quad \eta = \beta. \quad (3.140)$$

There will be symmetry conditions at $\eta = 0$, but since the equations in (3.139) are degenerate at both end points (and β is not known), it is unclear just how many conditions are necessary. In addition we have the prescribed buoyancy flux B , which gives another condition via the presumed first integral

$$B = 2\pi \int_0^\beta \eta W G d\eta. \quad (3.141)$$

It remains to be seen whether the numerical solution of (3.139) gives solutions similar to observations.

Plumes in a stratified environment

If, as for example in the atmosphere, the ambient density decreases with height, then a similarity solution is no longer feasible because the stratification introduces a natural scale height. To derive a model for such a plume, we must assume some form for the cross-section profiles, which will allow closure expressions for the average fluxes B , Q and M in terms of the plume (average) velocity w and radius b . The simplest assumption to make is that the profiles of buoyancy and vertical velocity have ‘top hat’ profiles, that is to say they are uniform and then drop rapidly at the plume edges. Such profiles might be motivated by a particular choice of expression for the eddy viscosity in (3.125), for example. With this assumption, we find

$$B = \pi b^2 w g', \quad Q = \pi b^2 w, \quad M = \pi b^2 w^2; \quad (3.142)$$



Figure 3.18: An umbrella cloud resulting from the eruption of Mount Redoubt, Alaska, in 1991. Image from Huppert (2000).

in addition we have

$$2\pi \int_0^b r g' dr = \pi b^2 g'. \quad (3.143)$$

Eliminating w and b finally yields the equations

$$\begin{aligned} \frac{dB}{dz} &= -N^2 Q, \\ \frac{dM}{dz} &= \frac{BQ}{M}, \\ \frac{dQ}{dz} &= 2\pi^{1/2} \alpha M^{1/2}. \end{aligned} \quad (3.144)$$

We can see from this that the buoyancy flux continually decreases with height, while the volume flux increases. When $B = 0$, the plume reaches its level of neutral buoyancy, but continues to rise because of its momentum. With $B < 0$, M decreases, and will not rise any further when M reaches 0. According to the equations, the volume flux is still positive, but in fact the plume spreads out laterally, forming an *umbrella cloud* as shown in figure 3.18, and the one-dimensional description becomes irrelevant. Thus a plume in a stratified medium will level out at a height z_s which can be determined from (3.144) in the form (see question 3.11)

$$z_s = c B_0^{1/4} N^{-3/4}, \quad (3.145)$$

where B_0 is the buoyancy flux at $z = 0$, and N is assumed constant.

3.9 Turbulent convection

As the Rayleigh number increases in Rayleigh–Bénard convection, the convective rolls which can be seen at the onset of convection bifurcate to three-dimensional planforms, typically either square cells or hexagons. In a layer of large horizontal extent, convective rolls tend to be weakly chaotic, because the alignment in different parts of the layer is different, and thus defects or dislocations are formed in the cellular structure, and these migrate slowly, sometimes permanently. Three-dimensional cells tend to be more stable, because they are essentially confined, but at higher Rayleigh number, an oscillatory instability sets in. The thermal boundary layers which migrate across the base of the cells and detach at the cell boundaries start to prematurely thicken and then thin again before detachment, causing an oscillation which is a manifestation of budding plume development. Eventually, these budding plumes do begin to detach before reaching the cell walls, and at this point the convection becomes temporally and spatially disordered. Thermal boundary layers thicken and plumes detach irregularly, and a defined cellular structure disappears, being replaced by a host of upwelling and downwelling thermal plumes. In fact, a large scale circulation does come into existence, but this is on a much larger scale than the typical plume spacing.

A very famous but simple model of turbulent thermal convection was put forward by Lou Howard in 1964, at the International Congress of Mechanics in Munich. In his model, a quiescent thermal boundary layer grows into an isothermal core until it reaches a critical thickness, when it suddenly forms a plume and detaches, mixing the fluid and returning to isothermal conditions. The average heat flux is then determined by that during the quiescent, conductive phase. The conductive temperature in the growing boundary layer is given by the solution of

$$T_t = \kappa T_{zz}, \quad (3.146)$$

with

$$\begin{aligned} T &= \frac{1}{2}\Delta T \quad \text{on } z = 0, \\ T &\rightarrow 0 \quad \text{as } z \rightarrow \infty; \end{aligned} \quad (3.147)$$

here we imagine a convecting fluid layer of depth d , across which the prescribed temperature difference is ΔT (and thus half across the boundary layers on each surface). Starting from an isothermal state $T = 0$ (boundary layer of thickness zero), the solution is

$$T = \frac{1}{2}\Delta T \operatorname{erfc} \left(\frac{z}{2\sqrt{\kappa t}} \right), \quad (3.148)$$

and thus the average heat flux from the surface $z = 0$ is

$$F = \frac{1}{t_c} \int_0^{t_c} \left(-k \frac{\partial T}{\partial z} \right) \Big|_{z=0} dt, \quad (3.149)$$

where t_c is the time of detachment of the boundary layer. Using (3.148), we then find

$$F = \frac{k\Delta T}{2\sqrt{\kappa t_c}} = \frac{k\Delta T}{2d_c}, \quad (3.150)$$

where $d_c = \sqrt{\kappa t_c}$ is the thickness of the thermal boundary layer at detachment.

Howard hypothesised that detachment would occur when a locally defined Rayleigh number, using the boundary layer thickness as the depth scale, became critical, of order

$$Ra_c \sim 10^3; \quad (3.151)$$

thus we define the critical thickness d_c via the effective critical Rayleigh number condition

$$\frac{\alpha\rho_0gd_c^3\Delta T}{2\mu\kappa} = Ra_c, \quad (3.152)$$

where the factor 2 allows for the temperature drop of $\frac{1}{2}\Delta T$ across the boundary layer. In terms of the Rayleigh number of the fluid layer

$$Ra = \frac{\alpha\rho_0gd^3\Delta T}{\mu\kappa}, \quad (3.153)$$

we thus have the dimensionless heat flux, called the Nusselt number Nu , given by

$$Nu = \frac{F}{(k\Delta T/d)} = \frac{d}{d_c} = cRa^{1/3}, \quad (3.154)$$

where

$$c = (2Ra_c)^{-1/3} \approx 0.08. \quad (3.155)$$

Thus the heat flux can be parameterised as

$$F = c \left(\frac{\alpha g c_p}{\mu} \right)^{1/3} (\rho_0 k)^{2/3} \Delta T^{4/3}, \quad (3.156)$$

which is the famous four-thirds law for turbulent convection. It is reasonably consistent with experimental results.

3.10 Notes and references

The theory of continental drift was famously published by Alfred Wegener, a German meteorologist, in 1915. An English translation of his book was published later, see Wegener (1924). His ideas were scorned by the geophysical establishment, and in particular, in Britain, by the colossal figure of Harold Jeffreys. The blind ignorance with which he and other fellow geologists refuted Wegener's ideas should serve (but have not) as a lesson for scientists against the perils of treating science as religion, and hypothesis as dogma. A notable supporter of the thesis of continental drift was

Holmes (1978), who understood that mantle convection was the driving mechanism. A more modern treatment of geodynamics is the classic book by Turcotte and Schubert (1982), while Davies (1999) gives a readable but technically undemanding account.

The layered magma chamber known as the Skaergaard intrusion was the subject of a massive memoir by Wager and Brown (1968), who gave painstaking descriptions of the series of layered rocks. They made some attempts at a theoretical description, as did McBirney and Noyes (1979), based on analogous processes in chemical reaction-diffusion theory. Neither of these, nor any subsequent attempts at a theoretical model, have been altogether successful.

Baines and Gill (1969), Turner (1979)

Balmforth *et al.* (2001)

The basic description of boundary layer theory at high Rayleigh number and infinite Prandtl number was first done successfully by Turcotte and Oxburgh (1967). A more complete theory is due to Roberts (1979), although even this is not quite watertight.. The necessary numerical results to compute C in (3.37) are given by Roberts (1979) and Jimenez and Zufria (1987). The results are slightly different, with the latter paper considering Roberts' numerical results to be wrong. For $a = O(1)$, then $2C \approx 0.1$.

Jimenez and Zufria (1987) claim that the equivalent problem to (3.48) for the case of no-slip boundary conditions has no solution, but do not adduce details. Their inference is that the boundary layer approximation fails: this seems a hazardous conclusion.

Linden (2000), Morton *et al.* (1956).

The model of turbulent thermal convection described in section 3.9 is due to Howard (1966). Baines and Turner (1969).

Exercises

3.1 The Boussinesq equations of two-dimensional thermal convection can be written in the dimensionless form

$$\begin{aligned}\nabla \cdot \mathbf{u} &= 0, \\ \frac{1}{Pr} [\mathbf{u}_t + (\mathbf{u} \cdot \nabla) \mathbf{u}] &= -\nabla p + \nabla^2 \mathbf{u} + Ra T \hat{\mathbf{k}}, \\ T_t + \mathbf{u} \cdot \nabla T &= \nabla^2 T.\end{aligned}$$

Explain the meaning of these equations, and write down appropriate boundary conditions assuming stress-free boundaries.

By introducing a suitably defined stream function, show that these equations can be written in the form

$$\begin{aligned}\frac{1}{Pr} [\nabla^2 \psi_t + \psi_x \nabla^2 \psi_z - \psi_z \nabla^2 \psi_x] &= Ra T_x + \nabla^4 \psi, \\ T_t + \psi_x T_z - \psi_z T_x &= \nabla^2 T,\end{aligned}$$

with the associated boundary conditions

$$\begin{aligned}\psi = \nabla^2\psi = 0 & \quad \text{at } z = 0, 1, \\ T = 0 & \quad \text{at } z = 1, \\ T = 1 & \quad \text{at } z = 0,\end{aligned}$$

and write down the conductive steady state solution.

By linearising about this steady state, show that

$$\frac{1}{Pr} \left(\frac{\partial}{\partial t} - \nabla^2 \right) \nabla^2 \psi_t = \left(\frac{\partial}{\partial t} - \nabla^2 \right) \nabla^4 \psi + Ra \psi_{xx},$$

and deduce that solutions are $\psi = e^{\sigma t} \sin kx \sin m\pi z$, and thus that

$$(\sigma + K^2) \left(\frac{\sigma}{K^2 Pr} + 1 \right) - \frac{Ra k^2}{K^4} = 0, \quad K^2 = k^2 + m^2 \pi^2.$$

By considering the graph of this expression as a function of σ , show that oscillatory instabilities can not occur, and hence derive the critical Rayleigh number for the onset of convection.

3.2 A two-dimensional, incompressible fluid flow has velocity $\mathbf{u} = (u, 0, w)$, and depends only on the coordinates x and z . Show that there is a stream function ψ satisfying $u = -\psi_z$, $w = \psi_x$, and that the vorticity

$$\boldsymbol{\omega} = \nabla \times \mathbf{u} = -\nabla^2 \psi \mathbf{j},$$

and thus that

$$\mathbf{u} \times \boldsymbol{\omega} = (\psi_x \nabla^2 \psi, 0, \psi_z \nabla^2 \psi),$$

and hence

$$\nabla \times (\mathbf{u} \times \boldsymbol{\omega}) = (\psi_x \nabla^2 \psi_z - \psi_z \nabla^2 \psi_x) \mathbf{j}.$$

Use the vector identity $(\mathbf{u} \cdot \nabla) \mathbf{u} = \nabla(\frac{1}{2}u^2) - \mathbf{u} \times \boldsymbol{\omega}$ to show that

$$\nabla \times \frac{d\mathbf{u}}{dt} = [-\nabla^2 \psi_t - \psi_x \nabla^2 \psi_z + \psi_z \nabla^2 \psi_x] \mathbf{j}.$$

Show also that

$$\nabla \times \theta \mathbf{k} = -\theta_x \mathbf{j},$$

and use the Cartesian identity

$$\nabla^2 \equiv \text{grad div} - \text{curl curl}$$

to show that

$$\nabla \times \nabla^2 \mathbf{u} = -\nabla^4 \psi \mathbf{j},$$

and hence deduce that the momentum equation for Rayleigh–Bénard convection can be written in the form

$$\frac{1}{Pr} [\nabla^2 \psi_t + \psi_x \nabla^2 \psi_z - \psi_z \nabla^2 \psi_x] = Ra \theta_x + \nabla^4 \psi.$$

3.3 Suppose that σ satisfies

$$p(\sigma) \equiv \sigma^3 + a\sigma^2 + b\sigma + c = 0,$$

and that a , b and c are positive. Suppose, firstly, that the roots are all real. Show in this case that they are all negative.

Now suppose that one root (α) is real and the other two are complex conjugates $\beta \pm i\gamma$. Show that $\alpha < 0$. Show also that $\beta < 0$ if $a > \alpha$. Show that $a > \alpha$ if $p(-a) < 0$, and hence show that $\beta < 0$ if $c < ab$.

If

$$\begin{aligned} a &= K^2 \left(Pr + 1 + \frac{1}{Le} \right), \\ b &= K^4 \left(Pr + \frac{1}{Le} + \frac{Pr}{Le} \right) + \frac{k^2}{K^2} Pr(Rs - Ra), \\ c &= \frac{K^6}{Le} Pr + k^2 Pr \left(Rs - \frac{Ra}{Le} \right), \end{aligned}$$

show that $a, b, c > 0$ if $Ra < 0$, $Rs > 0$, and show that if $Le > 1$, then $c < ab$.

What does this tell you about the stability of a layer of fluid which is both thermally and salinely stably stratified?

3.4 Suppose that σ satisfies

$$p(\sigma) \equiv \sigma^3 + a\sigma^2 + b\sigma + c = 0,$$

and that all the roots have negative real part if $c < ab$. Show that the condition that there be two purely imaginary roots $\pm i\Omega$ is that $c = ab$, and deduce that there are two (complex) roots with positive real part if $c > ab$. With

$$\begin{aligned} a &= K^2 \left(Pr + 1 + \frac{1}{Le} \right), \\ b &= K^4 \left(Pr + \frac{1}{Le} + \frac{Pr}{Le} \right) + \frac{k^2}{K^2} Pr(Rs - Ra), \\ c &= \frac{K^6}{Le} Pr + k^2 Pr \left(Rs - \frac{Ra}{Le} \right), \end{aligned}$$

show that this condition reduces to

$$Ra > \frac{\left(Pr + \frac{1}{Le} \right) Rs}{1 + Pr} + \frac{\left(1 + \frac{1}{Le} \right) \left(Pr + \frac{1}{Le} \right) K^6}{Pr k^2}.$$

Assuming $K^2 = k^2 + m^2\pi^2$, where m is an integer, show that the minimum value of Ra where this condition is satisfied is when $m = 1$, and give the corresponding critical value Ra_{osc} .

3.5 On the line XV in figure 3.9, the cubic

$$p(\sigma) = \sigma^3 + a\sigma^2 + b\sigma + c$$

has two positive real roots β and one negative real root α . Show that the condition for this to be the case is that

$$a = \alpha - 2\beta, \quad b = \beta^2 - 2\alpha\beta, \quad c = \alpha\beta^2,$$

and deduce that

$$a\beta^2 + 2b\beta + 3c = 0. \quad (1)$$

Show also that at the double root β ,

$$3\beta^2 + 2a\beta + b = 0. \quad (2)$$

Deduce from (1) and (2) that

$$\beta = \frac{9c - ab}{a^2 - 6b},$$

and hence, using (2), that

$$\beta = \frac{1}{3} [-a + \{a^2 - 3b\}^{1/2}]. \quad (3)$$

Explain why the positive root is taken in (3), and why we can assume $b < 0$.

Use the definitions

$$\begin{aligned} a &= K^2 \left(Pr + 1 + \frac{1}{Le} \right), \\ b &= K^4 \left(Pr + \frac{1}{Le} + \frac{Pr}{Le} \right) + \frac{k^2}{K^2} Pr (Rs - Ra), \\ c &= \frac{K^6}{Le} Pr + k^2 Pr \left(Rs - \frac{Ra}{Le} \right), \end{aligned}$$

to show that if $Ra \sim Rs \gg 1$, $Ra - Rs \gg 1$ and $Le \gg 1$, then XV is approximately given by

$$Ra \approx Rs + \frac{3K^2 Rs^{2/3}}{(4k^2 Pr)^{2/3}}.$$

3.6 The growth rate σ for finger instabilities is given by

$$(\sigma + K^2 Pr)(\sigma + K^2) \left(\sigma + \frac{K^2}{Le} \right) + k^2 Pr \left[\frac{(Rs - Ra)\sigma}{K^2} + Rs - \frac{Ra}{Le} \right] = 0,$$

and $Ra, Rs < 0$ with $-Ra, -Rs \gg 1$; K is defined by $K^2 = k^2 + \pi^2$.

Define $Rs = Rar$, and consider the behaviour of the roots when $Ra \rightarrow -\infty$ with r fixed. Show that when k is $O(1)$, one root is given by

$$\sigma = \frac{\left(r - \frac{1}{Le}\right) K^2}{1 - r} + O\left(\frac{1}{|Ra|}\right), \quad (*)$$

and that this is positive if

$$\frac{1}{Le} < r < 1.$$

Show that the other two roots are of $O(|Ra|^{1/2})$, and by putting

$$\sigma = |Ra|^{1/2}\Sigma_0 + \Sigma_1 + \dots,$$

show that they are given by

$$\sigma = \pm i \frac{k}{K} \{Pr(Ra - Rs)\}^{1/2} - \frac{1}{2} K^2 \left(Pr + \frac{1 - \frac{1}{Le}}{1 - r} \right) + O\left(\frac{1}{|Ra|^{1/2}}\right),$$

and thus represent stable modes.

Show further that when k is large, an appropriate scaling when $(*)$ breaks down is given by

$$k = |Ra|^{1/4}\alpha, \quad \sigma = |Ra|^{1/2}\Sigma,$$

and write down the equation satisfied by Σ in this case. Show also that when α is large, the three roots are all negative, with $\Sigma \sim -\alpha^2 S$, and $S = Pr, 1$, or $\frac{1}{Le}$.

Deduce that the maximal growth rate for finger instability occurs when $k \sim |Ra|^{1/4}$.

- 3.7 The scaled Boussinesq equations for two-dimensional thermal convection at infinite Prandtl number and large Rayleigh number R in $0 < x < a$, $0 < z < 1$, can be written in the form

$$\begin{aligned} \omega &= -\nabla^2 \psi, \\ \nabla^2 \omega &= \frac{1}{\delta} T_x, \\ \psi_x T_z - \psi_z T_x &= \delta^2 \nabla^2 T, \end{aligned}$$

where $\delta = R^{-1/3}$. Explain what is meant by the Boussinesq approximation, and explain what the equations represent. Explain why suitable boundary conditions for these equations which represent convection in a box with stress free boundaries, as appropriate to convection in the Earth's mantle, are given by

$$\psi = 0, \quad \omega = 0, \quad \text{on } x = 0, a, \quad z = 0, 1,$$

$$T = \frac{1}{2} \quad \text{on} \quad z = 0, \quad T = -\frac{1}{2} \quad \text{on} \quad z = 1, \quad T_x = 0 \quad \text{on} \quad x = 0, \quad a.$$

Show that, if $\delta \ll 1$, there is an interior ‘core’ in which $T \approx 0$, $\nabla^4 \psi = 0$.

By writing $1 - z = \delta Z$, $\psi = \delta \Psi$ and $\omega = \delta \Omega$, show that $\Psi \approx u_s(x)Z$, and deduce that the temperature in the thermal boundary layer at the surface is described by the approximate equation

$$u_s T_x - Z u_s' T_Z \approx T_{ZZ},$$

with

$$T = -\frac{1}{2} \quad \text{on} \quad Z = 0, \quad T \rightarrow 0 \quad \text{as} \quad Z \rightarrow \infty.$$

If u_s is constant, find a similarity solution, and show that the scaled surface heat flux $q = \partial T / \partial Z|_{Z=0}$ is given by

$$q = \frac{1}{2} \sqrt{\frac{u_s}{\pi x}}.$$

3.8 The Boussinesq equations describing the rise of a cylindrical plume are, ignoring turbulent eddy viscosity,

$$\begin{aligned} (ru)_r + rw_z &= 0, \\ uw_r + ww_z &= g', \\ ug'_r + wg'_z &= 0, \end{aligned}$$

in which r and z are cylindrical coordinates, u and w are radial and vertical velocities, and g' is the reduced gravity. Explain the basis for the derivation of these equations, including a definition of what is meant by the ‘reduced gravity’.

Write the equations in the form

$$A\phi_r + B\phi_z = \mathbf{c},$$

and hence show that the characteristics $\frac{dr}{dz} = \lambda$ satisfying $\det(A - \lambda B) = 0$ are

$$\lambda = \frac{u}{w}, \frac{u}{w}, \infty.$$

What is meant by saying that the third characteristic is ∞ ? What might make it finite?

Define a suitable stream function ψ for the flow, and show that the characteristics are the streamlines.

Assuming the plume emerges from a chimney of finite radius a with uniform upwards speed w_0 and uniform buoyancy (reduced gravity) $g_0 > 0$, and that entrainment occurs at the plume edge, write down suitable boundary conditions

for the flow, and draw a sketch of the resulting characteristic diagram. (Assume that the plume boundary $b(z) > a$.)

By explicitly solving the characteristic equations, show that the edge of the central part of the plume is given by

$$r = \frac{a}{\left(1 + \frac{2g_0 z}{w_0^2}\right)^{1/4}}.$$

What happens if $g_0 < 0$? Explain this physically.

3.9 The equations describing the steady motion of a turbulent plume in $z > 0$ and $0 < r < b(z)$ (using cylindrical polar coordinates) are

$$\begin{aligned} (ru)_r + rw_z &= 0, \\ uw_r + ww_z &= g' + \frac{1}{r} \frac{\partial}{\partial r} \left[\nu_T r \frac{\partial w}{\partial r} \right], \\ N^2 w + ug'_r + wg'_z &= \frac{1}{r} \frac{\partial}{\partial r} \left[\nu_T r \frac{\partial g'}{\partial r} \right], \end{aligned}$$

where u and w are radial and vertical velocities, g' is the reduced gravity, N is the Brunt–Väisälä frequency, and the eddy viscosity is assumed to be

$$\nu_T = \varepsilon_T b w,$$

where $\varepsilon_T \ll 1$. Boundary conditions for the flow are

$$w = g' = 0, \quad u = -\alpha \bar{w} \quad \text{at} \quad r = b,$$

where \bar{w} is the cross-sectional average of w and α (≈ 0.1) is a positive constant, and

$$w = w_0, \quad g' = g_0 \equiv \frac{g \Delta \rho}{\rho_0} \quad \text{at} \quad z = 0, 0 < r < a,$$

where also $b(0) = a$.

Assuming a stratified atmosphere in which $-\frac{1}{\rho_0} \frac{\partial \rho_0}{\partial z} \sim \frac{1}{H}$ (H is the scale height) and that $w_0 \lesssim \sqrt{g_0 l}$, show how to non-dimensionalise the equations so that all the terms in each equation balance. Hence show that the plume aspect ratio is ε_T , and that the natural length scale is $l \sim \frac{H \Delta \rho}{\rho_0}$.

By defining a stream function ψ with $\psi = 0$ on $r = 0$ and $\psi > 0$ for $r > 0$, make a Von Mises transformation from variables z, r to z, ψ , and hence show that w and g' satisfy nonlinear diffusion-type equations.

3.10 An isolated turbulent cylindrical plume in a stratified medium of density $\rho_0(z)$ is described by the inviscid Boussinesq equations

$$\begin{aligned} uu_r + wu_z &= -\frac{1}{\rho_0}p_r, \\ uw_r + ww_z &= -\frac{1}{\rho_0}p_z - \frac{\rho}{\rho_0}g, \\ u\rho_r + w\rho_z &= 0, \\ \frac{1}{r}(ru)_r + w_z &= 0, \end{aligned}$$

where (r, z) are cylindrical coordinates, (u, w) the corresponding velocity components, p the pressure, ρ the density, ρ_0 the reference density, and g is the acceleration due to gravity. If $\rho = \rho_0 - \Delta\rho$, explain what is meant by the Boussinesq approximation.

Suppose the edge of the plume is at radius $r = b$, such that $w = 0$ there. Suppose also that the plume entrains ambient fluid, such that

$$(ru)|_b = -b\alpha\bar{w},$$

where \bar{w} denotes the cross-sectional average value of w . Deduce that the plume volume flux

$$Q = 2\pi \int_0^b rw \, dr$$

satisfies

$$\frac{dQ}{dz} = 2\pi\alpha b\bar{w}.$$

The momentum flux is defined by

$$M = 2\pi \int_0^b rw^2 \, dr.$$

Show that, assuming that

$$\frac{\partial p}{\partial z} = -\rho_0 g$$

throughout the plume, that

$$\frac{dM}{dz} = 2\pi \int_0^b rg' \, dr,$$

where

$$g' = \frac{g\Delta\rho}{\rho_0}.$$

Why would the hydrostatic approximation be appropriate?

The buoyancy flux is defined by

$$B = 2\pi \int_0^b r w g' dr;$$

assuming $g' = 0$ at $r = b$, show that

$$\frac{dB}{dz} = -N^2 Q,$$

where the Brunt–Väisälä frequency N is defined by

$$N = \left(-\frac{g\rho'_0(z)}{\rho_0} \right)^{1/2}.$$

3.11 The buoyancy flux B , momentum flux M , and mass flux Q of a turbulent plume in a stratified atmosphere satisfy the equations

$$\frac{dB}{dz} = -N^2 Q,$$

$$\frac{dM}{dz} = 2\pi \int_0^b r g' dr,$$

$$\frac{dQ}{dz} = 2\pi \alpha b w,$$

where w is the plume velocity, b is its radius, g' is the reduced gravity, N is the Brunt–Väisälä frequency, $\alpha \approx 0.1$ is an entrainment coefficient, and r and z are radial and axial coordinates. Assuming that

$$2\pi \int_0^b r A dr = \pi b^2 A$$

for any plume quantity, assumed to be approximated by a top hat profile, show that

$$\frac{dB}{dz} = -N^2 Q,$$

$$\frac{dM}{dz} = \frac{BQ}{M},$$

$$\frac{dQ}{dz} = 2\pi^{1/2} \alpha M^{1/2}.$$

Now suppose that $B = B_0$, $M = Q = 0$ at $z = 0$. By non-dimensionalising the equations appropriately, show that the level of neutral buoyancy where $B = 0$ is given by

$$z_s = \frac{\zeta_s}{(2\alpha\pi^{1/2})^{1/2}} \frac{B_0^{1/4}}{N^{3/4}},$$

where ζ_s is a numerical constant (it is approximately measured to be 1.5). Write down the equations and boundary conditions necessary to determine ζ_s , and by integrating them, show that

$$\zeta_s = \int_0^1 \frac{db}{\left[2 \int_b^1 (1 - \beta^2)^{1/4} d\beta\right]^{1/2}}.$$

If, instead, $w = w_0$ and $b = b_0$ at $z = 0$, show that the same model to determine z_s is valid provided w_0 and b_0 are small enough, and specifically if

$$w_0 \ll \frac{g'}{N}, \quad b_0^2 w_0 \ll \frac{g'^3}{N^5}.$$

Show that if the first inequality is satisfied, then the second is as well, provided

$$b_0 \lesssim \frac{g'}{N^2}.$$

If the scale height of the medium is h (i. e., $\rho'_0/\rho \sim 1/h$), show that these two inequalities take the form

$$w_0 \ll \frac{\Delta\rho}{\rho_0} \sqrt{gh}, \quad b_0 \lesssim \frac{\Delta\rho}{\rho_0} h.$$

References

- Baines, P. G. and A. E. Gill 1969 On thermohaline convection with linear gradients. *J. Fluid Mech.* **37**, 289-306.
- Baines, W. D. and J. S. Turner 1969 Turbulent buoyant convection from a source in a confined region. *J. Fluid Mech.* **37**, 51-80.
- Balmforth, N. J., A. Provenzale and J. A. Whitehead 2001 The language of pattern and form. In: *Geomorphological fluid mechanics*, eds. N. J. Balmforth and A. Provenzale, pp. 3-33. Springer-Verlag, Berlin.
- Barlow, P. M. 2003. *Ground water in freshwater-saltwater environments of the Atlantic coast* (Vol. 1262). Washington, DC, USA: US Department of the Interior, US Geological Survey.
- Batchelor, G. K. 1967 *An introduction to fluid dynamics*. C. U. P., Cambridge.
- Benham, G.P., 2018. *Mathematical modelling and optimisation of Venturi-enhanced hydropower* (Doctoral dissertation, University of Oxford).
- Benney, D., 1966 Long waves on liquid films. *J Math. and Phy.*, **45**(1-4), pp.150-155.
- Bui, M., Adjiman, C.S., Bardow, A., Anthony, E.J., Boston, A., Brown, S., Fennell, P.S., Fuss, S., Galindo, A., Hackett, L.A. and Hallett, J.P., 2018. Carbon capture and storage (CCS): the way forward. *Energy & Environmental Science*, **11**(5), pp.1062-1176.
- Davies, G. F. 1999 *Dynamic Earth: plates, plumes and mantle convection*. C. U. P., Cambridge.
- Dubs, W. 1939 Über den einfluß laminarer und turbulenter strömung auf das röntgenbild von wasser und nitrobenzol. Ein röntgenographischer Beitrag zum Turbulenzproblem. *Helv. phys. Acte*, **12**, pp.169-228.
- Holmes, A. 1978 *Principles of physical geology*. 3rd edition, revised by Doris Holmes. John Wiley and sons, New York.
- Howard, L. N. 1966 Convection at high Rayleigh number. *Proc. 11th Int. Cong. Appl. Mech.*, ed. H. Görtler, pp. 1109-1115. Springer, Berlin.
- Huppert, H. E. 2000 Geological fluid mechanics. In: Batchelor, G. K., H. K. Moffatt and M. G. Worster (eds.), *Perspectives in fluid dynamics*, pp. 447-506. C. U. P., Cambridge.
- Jimenez, J. and J. A. Zufiria 1987 A boundary layer analysis of Rayleigh-Bénard convection at large Rayleigh number. *J. Fluid Mech.* **178**, 53-71.

- Jimenez, J. 2000 Turbulence. In: Perspectives in fluid dynamics, eds. G. K. Batchelor, H. K. Moffatt and M. G. Worster, pp. 231-288. C. U. P., Cambridge.
- Krevor, S., Blunt, M.J., Benson, S.M., Pentland, C.H., Reynolds, C., Al-Menhali, A. and Niu, B., 2015. Capillary trapping for geologic carbon dioxide storage—From pore scale physics to field scale implications. *International Journal of Greenhouse Gas Control*, 40, pp.221-237.
- Kolmogorov, A.N., 1941. The local structure of turbulence in incompressible viscous fluid for very large Reynolds numbers. *Cr Acad. Sci. URSS*, 30, pp.301-305.
- Lasheras, J.C. and Choi, H., 1988. Three-dimensional instability of a plane free shear layer: an experimental study of the formation and evolution of streamwise vortices. *J. Fluid Mech.*, 189, pp.53-86.
- Linden, P.F. 2000 Convection in the environment. In: Perspectives in fluid dynamics, eds. G. K. Batchelor, H. K. Moffatt and M. G. Worster, pp. 289-345. C. U. P., Cambridge.
- McBirney, A. R. and R. M. Noyes 1979 Crystallisation and layering of the Skaergaard intrusion. *J. Petrol.* **20**, 487-554.
- Mondal, R., Benham, G., Christodoulides, P., Neokleous, N. and Kaouri, K. 2019 Modelling and optimisation of water management in sloping coastal aquifers with seepage, extraction and recharge. *J. Hydrol.* **571**, 471-484.
- Morton, B.R., G. Taylor and J. S. Turner 1956 Turbulent gravitational convection from maintained and instantaneous sources. *Proc. R. Soc. Lond.* **A234**, 1-23.
- Pope, S. B. 2000 Turbulent flows. Cambridge University Press.
- Prandtl, L. 1925 Bericht uber untersuchungen zur ausgebildeten turbulenz. *Zs. angew. Math. Mech.*, 5:136–139.
- Reynolds, O. 1883 An experimental investigation of the circumstances which determine whether the motion of water shall be direct or sinuous, and of the law of resistance in parallel channels. *Proc. R. Soc. Lond.*, 35(224-226), pp.84-99.
- Roberts, G.O. 1979 Fast viscous Bénard convection. *Geophys. Astrophys. Fluid Dynamics* **12**, 235-272.
- Schlichting, H., Gersten, K., Krause, E., Oertel, H. and Mayes, K. Boundary-layer theory, volume 7. Springer, 1960.
- Turcotte, D.L. and E.R. Oxburgh 1967 Finite amplitude convection cells and continental drift. *J. Fluid Mech.* **28**, 29-42.
- Turcotte, D.L. and G. Schubert 1982 Geodynamics: applications of continuum physics to geological problems. John Wiley, New York.

- Turner, J. S. 1974 Double-diffusive phenomena. *Ann. Rev. Fluid Mech.* **6**, 37-54.
- Turner, J. S. 1979 Buoyancy effects in fluids. C. U. P., Cambridge.
- Vitagliano, V. and P. A. Lyons 1956 Diffusion coefficients for aqueous solutions of sodium chloride and barium chloride. *J. Amer. Chem. Soc.* **78** (8), 1,549-1,552.
- Wager, L. R. and G. M. Brown 1968 Layered igneous rocks. Oliver and Boyd, Edinburgh.
- Wegener, A. L. 1924 The origin of continents and oceans. 3rd ed., trans. J. G. A. Skerl. Methuen, London.
- Ziegler, G. R., A. L. Benado and S. S. H. Rizvi 1987 Determination of mass diffusivity of simple sugars in water by the rotating disk method. *J. Food. Sci.* **52** (2), 501-502.
- Woods, A.W., 2015. Flow in porous rocks. Cambridge University Press.